FLUID-STRUCTURE INTERACTION DURING SEISMICALLY EXCITED SLOSHING WITHIN SHALLOW SKIRT SUPPORTED PRESSURE VESSELS

by

Bikramjit Singh Antaal

A dissertation submitted to the faculty of
The University of North Carolina at Charlotte
in partial fulfillment of the requirements
for the degree of Doctor of Philosophy in
Mechanical Engineering

Charlotte

2010

Approved by:

_____
Dr. Yogeshwar Hari

_____
Dr. Dennis K. Williams

_____
Dr. Russell G. Keanini

_____
Dr. Rajaram Janardhanam

_____
Dr. Shen-En Chen

ABSTRACT

BIKRAMJIT SINGH ANTAAL. Fluid-structure interaction during seismically excited sloshing within shallow skirt supported pressure vessels. (Under the direction of DR. YOGESHWAR HARI and DR. DENNIS K. WILLIAMS)

This dissertation describes the finite element considerations employed in a seismic response spectrum analysis of a skirt supported, liquid containing pressure vessel. Like many axisymmetric cylindrical vessels, the gross seismic response to an input response spectrum can be categorized by a simplified lump mass model that includes both the mass of the vessel proper in combination with the associated mass of multiple fluid levels. This simplified response may be utilized to determine the initial sizing of the supporting configuration, such as a skirt, but lacks the ability to properly address the fluid-structure interaction that creates sloshing loads on the vessel walls. The most obvious method to address the fluid-structure interaction when considering the finite element method is to build a three-dimensional model of the vessel proper, including, but not limited to the shell courses, the top and bottom heads (for a vertical vessel), and the support skirt. The inclusion of the fluid effects may now be incorporated with a "contained fluid" finite element, however, for vessels of any significant volume, the number of finite elements can easily exceed 100,0000 and the number of degrees of freedom can sore from as few as 300,0000 to as many as 500,0000 or more. While these types of finite element analysis problems can be solved with today's computer hardware and software, it is not desirable in any analysis to have that volume of information that has to be reviewed and approved in a highly regulated nuclear QA environment (if at all possible).

With these items in mind, the methodology described in this dissertation seeks to minimize the number of degrees of freedom associated with a response spectrum analysis of a liquid filled, skirt supported vertical pressure vessel. The input response spectra are almost always provided in Cartesian coordinates, while many, if not most liquid containing pressure vessels are almost always axisymmetric in geometry without having benefit of being subjected to an axisymmetric load (acceleration in this case) due to the specified seismic event. The use of harmonic finite elements for both the vessel structure and the contained fluid medium permit the efficiencies associated with an axisymmetric geometry to be leveraged when the seismic response spectrum is formulated in terms of a Fourier series and combined to regain the effects of the two orthogonal, horizontally applied accelerations as a function of frequency. The end result as discussed and shown in this dissertation is a finite element model that permits a dense mesh of both the fluid and the structure, while economizing on the number of simultaneous equations required to be solved by the chosen finite element analysis.

The method to obtain results at any chosen circumferential location is first developed for a simpler geometry utilizing a ground supported tank with flat heads. The results of the method developed herein are verified by comparison to published analytical results. The subject methodology is then applied to the skirt supported pressure vessel.

DEDICATION

To my loving parents and wife.

ACKNOWLEDGEMENTS

This dissertation arose in part out of a gradual research that has been done since I came to study at UNC at Charlotte. By this time, I have worked with a number of people whose contribution, in assorted ways to the research and the making of the dissertation, deserves special mention. It is a pleasure to convey my gratitude to them all in my humble acknowledgment.

First and foremost I offer my sincerest gratitude to my supervisor, Dr. Yogeshwar Hari, who has supported me throughout my dissertation with his knowledge of subject whilst allowing me the room to work in my own way. Above all and the most needed, he provided me unflinching encouragement and support in various ways. His truly professional intuition has made him as a constant oasis of ideas, which exceptionally inspire and enrich my growth as a student and as a researcher. I am indebted to him more than he knows.

I gratefully acknowledge Dr. Dennis K. Williams for introducing this problem to me. His valuable advice, supervision, and crucial contribution made him the backbone of this research and so to this dissertation. In all stages of my doctoral study, his profound expertise and knowledge provided crucial and key injection to the technical solutions. His involvement with his originality has triggered and nourished my intellectual maturity that I will benefit from, for a long time to come. I am grateful to him in every possible way and hope to keep learning from him in the future. I could never have embarked and finished my journey of doctoral study without the motivation and help of Dr. Hari and Dr. Williams.

I was fortunate in having Dr. Russell Keanini, Dr. Rajaram Janardhanam and Dr. Chen-En-Shen as the members of my Ph.D committee. Many thanks go to them for their indispensable help and constructive comments on this dissertation.

I am also grateful to the department of mechanical engineering, University of North Carolina at Charlotte for providing me an excellent work environment during the past three and half years. The financial support from the graduate school and department of mechanical engineering of The University of North Carolina at Charlotte is gratefully acknowledged.

Where would I be without my family? My father, Mr. Jagir Singh and my mother, Mrs. Shamsher Kaur deserve special mention for their inseparable support and prayers. My uncle Mr. Harnek Singh and my aunt Mrs. Jasvinder Kaur in the first place, are the persons who laid the foundation of my learning character, showing me the joy of intellectual pursuit ever since I was a child. Very special thanks to them all for their love and support. Words fail me to express my appreciation to my wife Rajbir whose love and persistent confidence in me, has taken the load off my shoulder.

Above all, I would thank God for showering his blessings on me.

TABLE OF CONTENTS

LIST OF FIGURES

LIST OF TABLES

LIST OF SYMBOLS

A	Amplitude of vibrations
Acc	Net ground acceleration
A_i	Mode coefficient (i^{th} mode)
A_{max_i}	Maximum value of mode coefficient
A_{ratio_i}	Mode coefficient ratio (i^{th} mode)
A_X	Radial acceleration
A_Y	Axial acceleration
A_Z	Circumferential acceleration
A_0	Fourier constant, axisymmetric portion
A_1	Fourier multiplier, asymmetric portion
[C]	Damping matrix
C_c	Convective coefficient
C_i	Impulsive coefficient
{D}	Spectral acceleration direction vector
E	Young's modulus of elasticity
{F(t)}	Forcing function vector
F(u,t)	Time varying forcing function
H	Height of fluid in tank or vessel
I	Identity matrix
[K]	Stiffness matrix
$[K_P]$	Principal stiffness matrix

$[M]$	Mass matrix
$[M_P]$	Principal mass matrix
M_{eff_i}	Effective mass (i^{th} mode)
M_o	Overturning moment
Q_b	Base shear
$\{Q\}_i$	Time varying arbitrary forcing function (i^{th} mode)
$\{Q\}_{Ni}$	Arbitrary forcing function normalized w.r.t. mass matrix
Q	Force (total)
R	Radius of tank or vessel
R_i	Response (i^{th} mode)
R_{total}	Total response
S_{ai}	Spectral acceleration corresponding to i^{th} mode
T_{con}	Time period of convective sloshing
T_{imp}	Time period of impulsive sloshing
$\{U\}$	Displacement vector
$\{\ddot{U}\}$	Acceleration vector
$\{U\}_p$	Generalize displacement vector
$\{\ddot{U}\}_p$	Generalized acceleration vector
d	Sloshing height
f	Fundamental natural frequency
f_i	Natural frequency (i^{th} mode)
g	Acceleration due to gravity
h	Total height of tank or vessel

h_c	Height of center of gravity of convective mass
h_i	Height of center of gravity of impulsive mass
h_r	Height of center of gravity of tank roof
h_w	Height of center of gravity of tank wall
k	Stiffness
m	Mass
m_c	Mass of convective fluid
m_i	Mass of impulsive fluid
m_r	Mass of tank or vessel roof
m_w	Mass of tank or vessel walls
q	Force per unit mass
q_{Ni}	Force per unit mass normalized w.r.t. mass matrix
t	Time
t_h	Wall thickness of tank or vessel
t’	Dummy time variable
u	Displacement (response)
ü	Acceleration
u_g	Ground displacement
$ü_g$	Ground acceleration
u_o	Initial displacement
F(θ)	Load as a function of circumferential coordinate
[Φ]	Modal matrix
$[\Phi_{Ni}]$	Modal matrix normalized w.r.t. mass matrix

$\{\Phi\}_i$	Eigen vector (i^{th} mode)
$\{\Phi\}_{Ni}$	Eigen vector normalized w.r.t mass matrix (i^{th} mode)
Ψ_i	Generalized Eigen vector (i^{th} mode)
Ω	Frequency of forced vibrations
β	Magnification factor
γ_i	Participation factor (i^{th} mode)
ρ	Density of tank or vessel material
ω_d	Frequency of damped vibration
ω_i	Circular frequency (i^{th} mode)
ω_i^2	Eigen value (i^{th} mode)

CHAPTER 1: INTRODUCTION

1.1 Purpose

The twofold purpose of this dissertation is to first, develop a robust, efficient and accurate finite element analysis (FEA) method to analyze fluid-structure interaction due to seismic loading (accelerations in case) by taking advantage of axisymmetric geometry of cylindrical tanks or vessels. Second, at the same time, the solution must economize on the total engineering effort in analyzing the fluid-structure interaction problem.

1.2 Introduction to Tanks and Vessels

Pressure vessels and tanks are leak proof containers used to store a variety of fluids for industrial processing, power generation, and a host of other domestic purposes. A container operating under a pressure of less than 15 psig is classified as a tank, and in case the operating pressure is more than 15 psig, the container is classified as a pressure vessel in accordance with the ASME Boiler and Pressure Vessel Code. Tanks are further classified as tall tanks if their height to radius ratio is more than one ($H/R > 1$) and broad tanks if height to radius ratio is less than or equal to 1 ($H/R \leq 1$). The contained fluid in a vessel exerts hydrostatic pressure on the vessel walls. The intensity of pressure on the walls of a vessel is due to the fluid at rest and is equal in all directions. The hydrostatic pressure at any point on the vessel wall depends on the height of the fluid above the particular point of interest. In case of a seismic event, due to the acceleration of the fluid in the horizontal direction, additional hydrodynamic pressures (hydrodynamic forces) act

on the vessel walls in addition to the already present hydrostatic pressure. Generally pressure vessels are designed taking into account the internal or external pressure, weight of the contents to be supported by the vessel (i.e., the live load), the self weight of vessel (i.e., the dead load), temperature gradient and thermal expansion, seismic loads, and wind loads. Pressure vessels can be spherical, rectangular, or cylindrical in shape. The majority of tanks and vessels are cylindrical in shape having flat, elliptical, conical, spherical, or torospherical heads. The selection of a head is based on the vessel design pressure and space restrictions. Hemispherical heads are best suited for high design pressures, whereas flat heads are not recommended at all for vessels operating at high pressures. Vessels or tanks may be ground supported or elevated above the ground. The elevated vessels may be supported by saddle or skirt supports. The skirt support permits radial growth of the vessel, due to temperature and pressure through bending of the shell wall of the skirt. The length of the skirt is chosen such that it permits bending to take place safely and to provide any required clearance for bottom mounted nozzles and appurtenances.

1.3 Axisymmetric Analysis Versus Full 3-D Analysis

A full 3-D finite element analysis is often favored by many analysts when using a commercially available analysis code in seeking a quick solution. For a medium to large capacity fluid filled tank, the number of nodes and the respective number of degrees of freedom (DOFs), when using a dense mesh of elements (required for accurate results), can easily extend into the millions. This extensive modeling can unnecessarily consume both man-hours and computational time to obtain the final solution. Apart from these aforementioned undesirables, it is practically impossible to verify the FEA results at each

node and element as part of any requisite QA program. To eliminate the aforementioned drawbacks, utilization of geometrically axisymmetric property of tanks allows the analyst to minimize the geometric model features (i.e., nodes and elements). Fig. 1.1 depicts a qualitative comparison of the number of elements used in a 3-D model versus an equivalent axisymmetric model. The axisymmetric model uses only a fraction of total number of elements as compared to a full 3-D model. It is a well known fact that as the number of elements increases for a FEA problem, the computational time increases rapidly and hence limits the use of a fine mesh. The use of an axisymmetric model overcomes this limitation by allowing the use of a fine mesh and at the same time, achieving a huge reduction in analysis and modeling time. The use of an axisymmetric model greatly reduces the total engineering effort as compared to that of an equivalent 3-D model, especially in case of the fluid-structure interaction problem due to the requirement for coupling the fluid and structural nodes in the direction normal to the interface through appropriate coupling equations. The coupling at critical interfaces allows the fluid in contact with the structure to move freely and yet be contained within the structure. Furthermore, fluid elements including both 2-D four node axisymmetric harmonic and 3-D eight node brick elements, are not expected to give sufficiently good results for any shape other than rectangular elements and solid three-dimensional based brick elements, respectively.

Deviation from brick elements for a considerable number of elements in case of a full 3-D model is unavoidable (especially towards the vertical centerline of the tank) and may lead to less accurate results. Fig. 1.1 highlights a considerable number of triangular and wedge shaped elements and quadrilateral based eight node elements near the central axis

of fluid filled tank. This shortcoming of a three dimensional model can be easily overcome by using two dimensional axisymmetric elements.

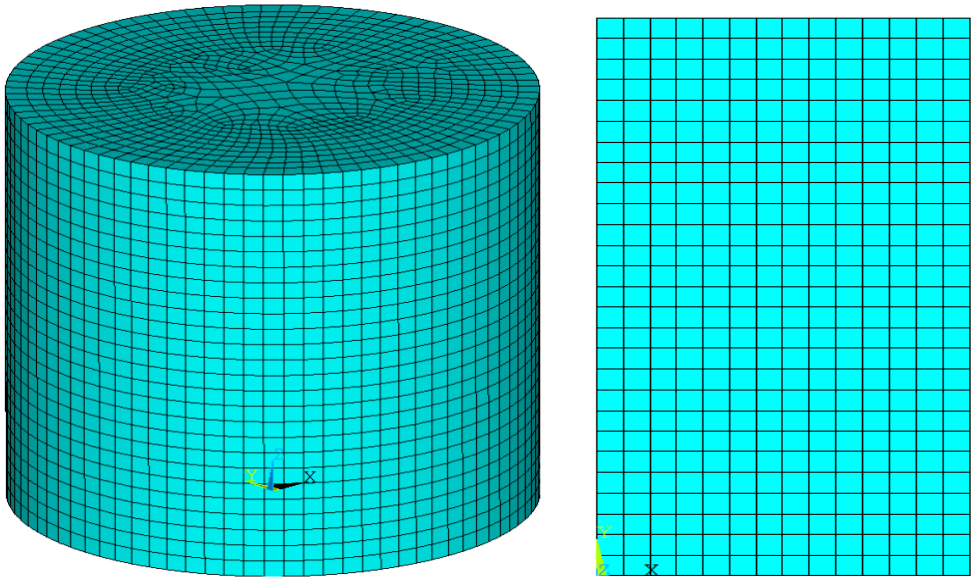

FIGURE 1.1: Comparison of Number of Elements in 3-D and 2-D Analysis

1.4 Axisymmetric Elements Subjected to Axisymmetric Accelerations

Axisymmetric elements are most closely associated with a cylindrical coordinate system. For both the axisymmetric elements and the axisymmetric harmonic elements, the global Cartesian Y-axis must be the axis of symmetry (central-axis); the global Cartesian X-axis represents the radial coordinate (r) axis; and the global Cartesian Z-axis represents the circumferential coordinate **θ** axis as shown below in Fig. 1.2.

Note that the reference measurement of **θ** is in the counterclockwise direction from the positive X-axis. These elements are modeled in X-Y plane and the model is developed in positive X-coordinates (radial coordinate) as negative X-coordinates cannot be used with axisymmetric elements. Axisymmetric elements are four node quadrilateral elements (rectangular in case of fluid elements) having only two translational degrees of

freedom one each in radial and axial directions. These elements allow only axisymmetric loads (only axial loads) to be applied to an axisymmetric geometry. The loads in case of axisymmetric elements are defined as a Fourier series given by Eq. (1.1). Each term of Fourier series given by Eq. (1.1) must be defined as a separate load step when applying the respective loads while using the finite element analysis code. For axisymmetric elements with axisymmetric loading, i.e., a uniformly applied axial loading, only the first term of Fourier series in Eq. (1.1) need be utilized, which is constant and independent of the circumferential coordinate **θ.** Vertical acceleration as shown in Fig. 1.3, is input in the longitudinal direction. The total acceleration in the axial direction due to an input acceleration is calculated using Eq. (1.3).

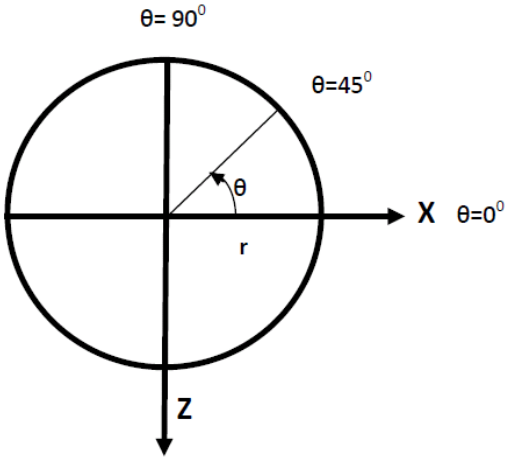

FIGURE 1.2: Cartesian and Cylindrical Coordinates for Axisymmetric Elements

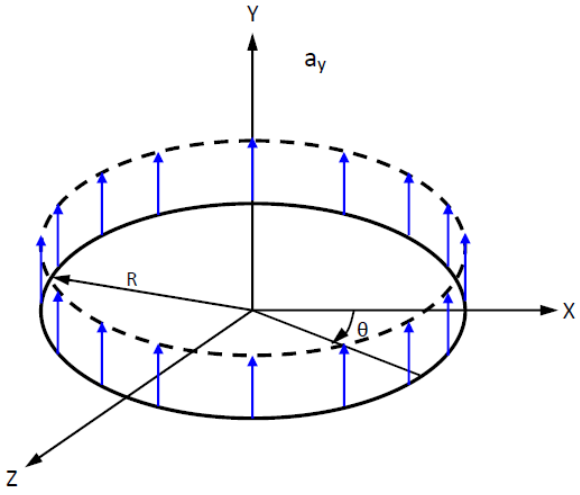

FIGURE 1.3: Axisymmetric Loading

$$F(\theta) = A_0 + A_1\cos(\theta) + B_1\sin(\theta) + A_2\cos(2\theta) + B_2\sin(2\theta) + \cdots \tag{1.1}$$

$$Acc = \int_0^{2\pi} (\text{Acc per unit length})(\text{Increment length}) \tag{1.2}$$

$$Acc = \int_0^{2\pi} \left(\frac{A_Y}{2\pi R} \right) (R d\theta) \tag{1.3}$$

$$Acc = A_Y \tag{1.4}$$

Fig. 1.4 shows an example of the conversion of an axial force from a 3-D model to be applied to an axisymmetric model. The total force all around the circumference of a 3-D model is added and applied at a single point in the case of an axisymmetric model.

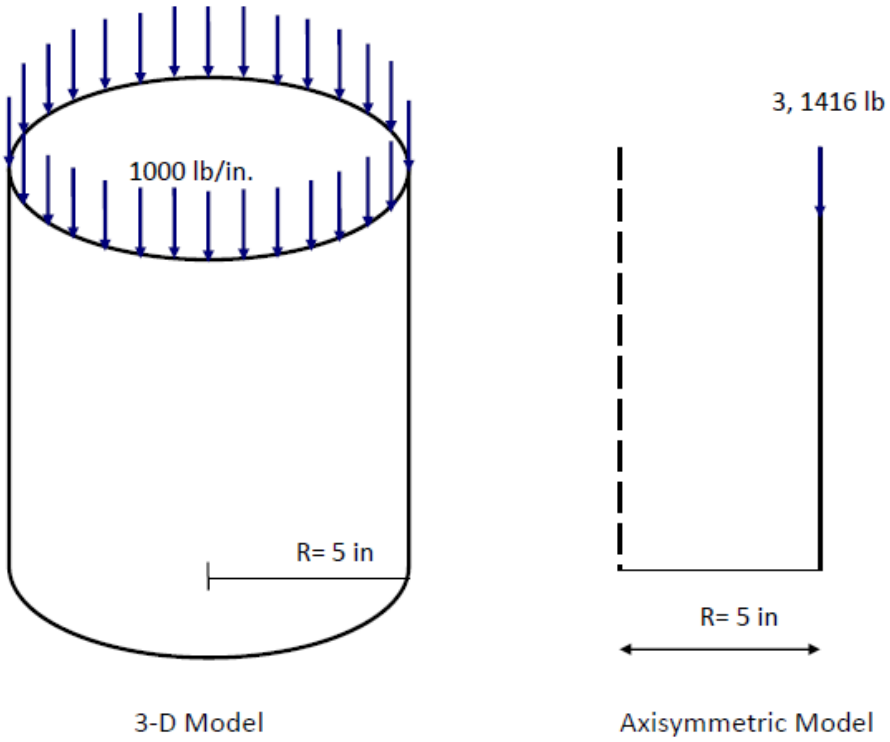

FIGURE 1.4: Conversion of Load from 3-D Model to Axisymmetric Model

1.5 Axisymmetric Harmonic Elements Subjected to Non-axisymmetric Response Spectrum Accelerations

Axisymmetric harmonic elements are a more generalized version of axisymmetric elements with the added benefit of allowing non-axisymmetric (asymmetric) loads to be applied to an axisymmetric geometry. Each axisymmetric harmonic element is defined

by four nodes and three translational degrees of freedom at each node in radial, axial and circumferential directions. These elements are quadrilateral in shape with the exception of the axisymmetric harmonic fluid element, which is rectangular in shape. The accuracy of the computed results for harmonic fluid elements decrease with shapes other than a rectangle [27]. It is highly recommended to avoid general quadrilateral and triangular shapes for harmonic fluid elements, if at all possible, in order to obtain sufficiently accurate results. For axisymmetric harmonic elements with lateral (horizontal) loading, the second term of the Fourier series in Eq. (1.1) is considered, which then becomes a function of the circumferential coordinate **θ**. Application of a uniform horizontal acceleration is the sum of two orthogonal (radial and circumferential) accelerations as shown in Fig. 1.5. Acceleration to an axisymmetric model is applied as a gravity load and the total acceleration in horizontal direction is the sum of the radial and tangential accelerations as calculated through the use of Eq. (1.7).

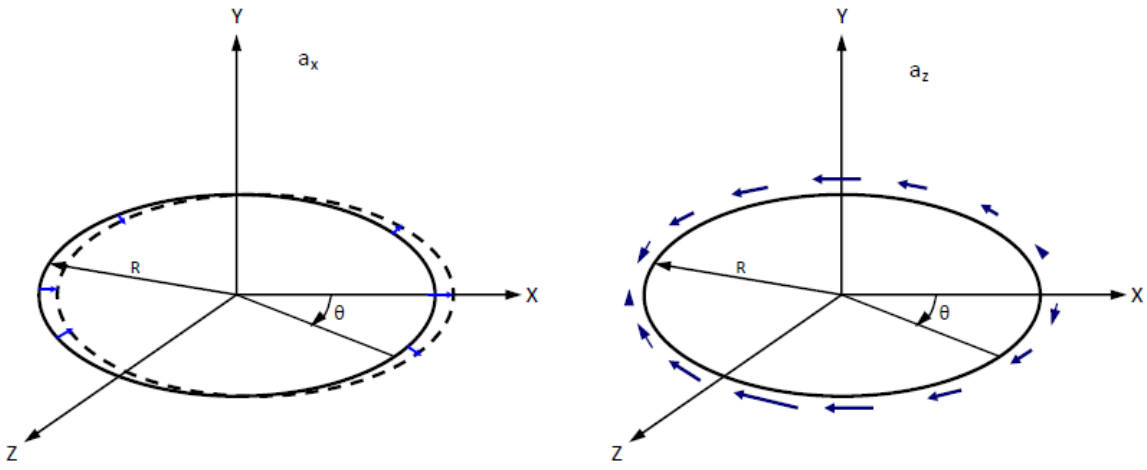

FIGURE 1.5: Non-axisymmetric Acceleration (Bending Loading)

$$Acc = \int_0^{2\pi} (\text{Acc per unit length})(\text{Directional cosines})(\text{Increment length}) \qquad (1.5)$$

$$Acc = \int_0^{2\pi} \left(\frac{A_X \cos(\theta)}{2\pi R} (\cos(\theta)) + \frac{A_Z \sin(\theta)}{2\pi R} (-\sin(\theta)) \right) (Rd\theta) \tag{1.6}$$

$$Acc = \frac{A_X - A_Z}{2} \tag{1.7}$$

The inertia load (acceleration) as shown in Fig. 1.5 is analogous to bending of a pipe. The first segment of the subject figure depicts the radial acceleration and the second part of figure depicts the circumferential acceleration. The addition of these two orthogonal accelerations, i.e., the radial and the circumferential contributors, results in the uniform linear acceleration in the horizontal direction (i.e., the global Cartesian X-direction). The peak values of translations, UX, UY and forces, FX and FY in the case of axisymmetric harmonic elements occur at θ = 0°, whereas the peak values of translations, UZ and forces, FZ appear at the circumferential location θ = 90°.

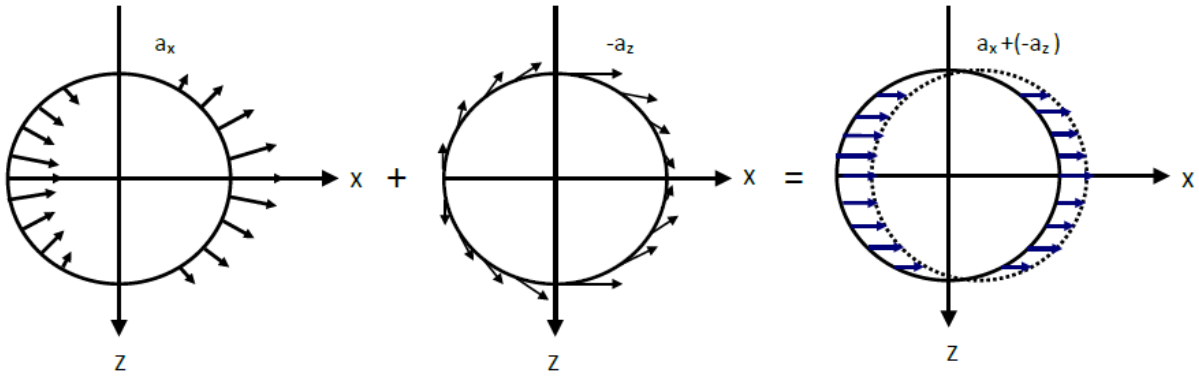

FIGURE 1.6: Asymmetric Acceleration (Uniform Loading)

The uniform lateral loading, as in the case of a cylindrical tank, is explained by Fig. 1.6. The total acceleration in the horizontal direction is the sum of equal magnitudes of radial and tangential accelerations. The concept can be more clearly explained by viewing Fig. 1.7 where the radial and tangential accelerations are resolved into X and Z

components, and then the respective X-components are summed, whereas the Z-components cancel out, creating the resultant horizontal acceleration purely in the global Cartesian X-direction. This summation and transformation from the desired uniform lateral acceleration (as seen in a Cartesian coordinate system) to the cylindrical coordinate system (as required in all axisymmetric analyses) forms the critical basis for the present work described in this dissertation.

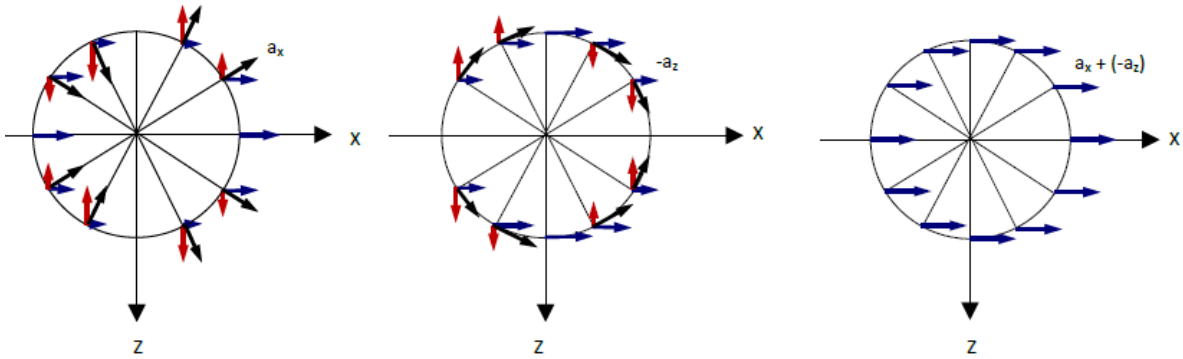

FIGURE 1.7: Detailed Descriptions of Asymmetric Acceleration

CHAPTER 2: FLUID SLOSHING AND ITS EFFECTS ON VESSEL DESIGN AND ANALYSIS

2.1 Background of Sloshing and Literature Review

Vertical ground supported cylindrical tanks and vessels subjected to a seismic event experience hydrodynamic forces due to sloshing of the fluid in addition to already existing hydrostatic loads. These hydrodynamic forces on elevated tanks and vessels are even higher due to the increased center of gravity of the mass of the fluid and hence require more robust support designs. Fluid-structure interaction is of tremendous interest in the design and analysis of these tanks because history has shown that earthquakes have resulted in significant damage to a large number of ground supported fluid tanks [1, 2]. A number of researchers have contributed towards quantifying the effects of earthquake-induced sloshing on storage tanks. The initial work of Housner [3] on non-deformable tanks resting on rigid foundations was based on dividing the liquid into two structural components (masses): the lower mass of the liquid moving with rigid walls, was termed the impulsive mass, and the upper mass of the liquid moving freely (relative to the walls of the tank) was termed the convective mass. Later, flexibility of the tank wall was taken into consideration by Haroun and Housner [4] and it was shown that the fluid experiences larger accelerations than the peak ground accelerations due to the flexibility of the tank wall. Malhotra [5] developed a simple procedure for seismic analysis of fluid filled cylindrical tanks with flexible walls and his results were in agreement with a more detailed modal analysis. Fisher [6] conducted a theoretical, quantitative study of a fluid-

filled tank that included the wall deformation (flexibility) of the tank due to both the convective and impulsive liquid masses. From the aforementioned research, it was concluded that during tank design, contributions from higher frequency sloshing modes should be considered along with the fundamental frequency sloshing modes. Shrimali and Jangid [7] conducted extensive study on elevated tanks of different aspect ratios and presented a simple two degrees of freedom solution to analyze fluid filled elevated tanks. Livaoglu et al. [8, 9] provided an insight into fluid-structure-soil interaction of elevated tanks. References [10] through [13], inclusive, provide an insight into numerical analyses of fluid sloshing problems while references [11] through [13], inclusive, provide details of various finite element analysis (FEA) results that exemplify the consistency amongst the two methods [10-13]. Barron et al. [14] conducted an experimental investigation of sloshing problems by exciting a fluid filled container using a vibration generator and the results compared favorably with the same experimental conditions simulated with various computer models.

In the last decade, finite element analysis (FEA) has emerged as a dominant tool to analyze seismically induced fluid-structure interaction (sloshing) problems employing a single point response spectrum (SPRS) analysis. Many analysts used a full 3-D or half-model of the geometry and loads to be analyzed [15-19]. Very few researchers have utilized geometrically axisymmetric harmonic elements for the seismic design and analysis of tanks [20-24] which permit the application of asymmetric loads through Fourier series implementations. Due to the complexity of a fluid-structure interaction problem, no exact closed form solution is available. The approximate solutions that have

been widely used are based on approximations from results of empirical studies of the sloshing simulations.

2.2 Impulsive and Convective Sloshing

Housner [3] was one of the first researchers to propose an analytical solution based on the assumption that the tank walls are rigid and the tank completely anchored to rigid foundation. A closed tank completely filled with fluid or completely empty is essentially a one mass structure, but a partially filled fluid tank was assumed to be a two mass structure as shown in Fig 2.1. The lower mass of fluid, called impulsive mass, was assumed to move with the tank walls and experienced the same seismic accelerations as the ground accelerations. The impulsive mass vibrates in higher frequency modes than the rest of the fluid mass. The impulsive mass of the fluid, resulting in impulsive sloshing, contributes mainly to seismic loads (overturning moment and base shear of the tank). Later, flexibility of the tanks was taken into consideration [4] and it was shown that the impulsive fluid experiences higher accelerations than the peak ground accelerations and therefore, the overturning moment and base shear calculated by assuming rigid tank walls can be non-conservative in some instances.

The upper mass of fluid moving in long period sloshing, called the convective mass, was assumed to move relative to tank walls and accounts for the convective sloshing. The convective mass experiences accelerations equal to the ground acceleration. The contribution of convective mass is much less than the impulsive mass but is important in determining the freeboard (height of the top tank head from the free liquid surface) requirements for the tank. Insufficient freeboard may result in impact loading on the roof of the tank and possible damage to the top part of tank.

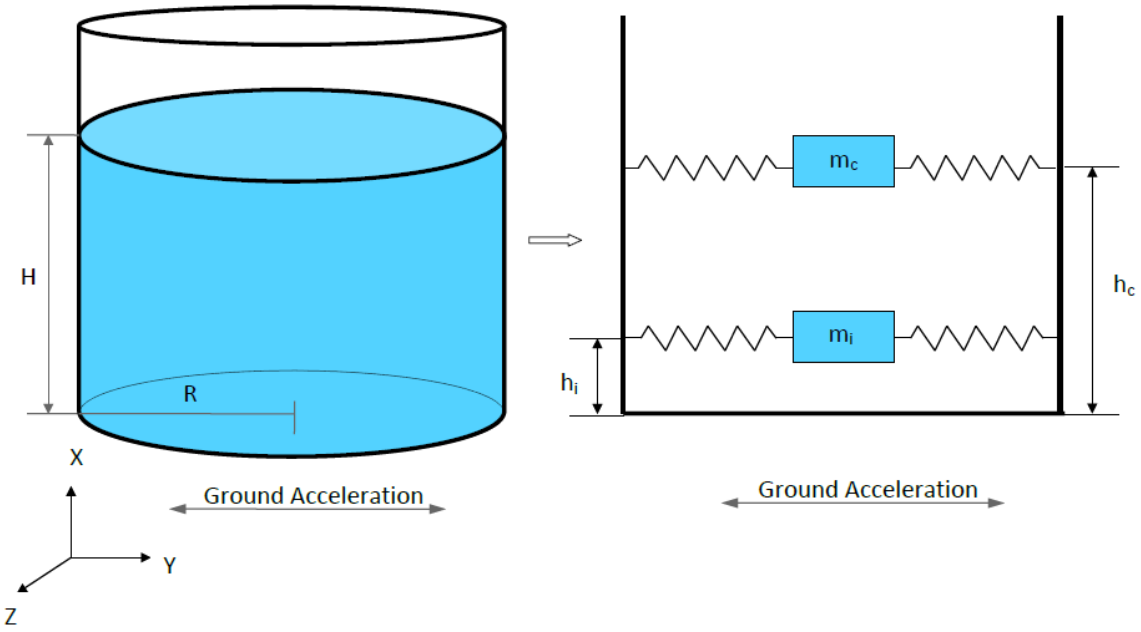

FIGURE 2.1: Liquid Filled Tank Modeled as Generalized Single Degree of Freedom System

Malhotra [5] proposed a simplified procedure for flexible tanks with a rigid (i.e., fully anchored) foundation. The dynamic analysis of the fluid filled tank was carried out using a generalized, single-degree of freedom system by dividing the fluid mass into two parts: impulsive and convective masses based on the work of Housner [3]. An expression to calculate the period of impulsive vibration, Eq. (2.1); period of convective vibration, Eq. (2.2); and the natural frequency, Eq. (2.3) due to a horizontally applied linear acceleration, was suggested by Malhotra [5]. Also the expression to calculate fundamental frequency of sloshing as suggested by Eurocode [25] is given by Eq. (2.4)

$$T_{imp} = C_i \frac{H\sqrt{\rho}}{\sqrt{t_h / R}\sqrt{E}} \tag{2.1}$$

$$T_{con} = C_c \sqrt{R} \tag{2.2}$$

$$f = \frac{1}{T_{con}} \tag{2.3}$$

$$f = \frac{1}{2\pi}\sqrt{\frac{1.84g\tanh(1.84(H/R))}{R}} \tag{2.4}$$

The impulsive coefficient, C_i and convective coefficient, C_c appearing in Eq. (2.1) and Eq. (2.2) may be obtained from Fig. 2.2 or Table 2.1 (as a function of H/R ratio) as defined by Malhotra [5]. The aforementioned analytical expressions for natural frequency are only useful in calculating the fundamental natural frequency (i.e., the first mode) and do not provide any higher modal frequencies. In addition, the expressions for the sloshing height given by references [5, 25], only yield information on the maximum sloshing height at a single location within a tank or vessel.

TABLE 2.1: Recommended Design Values for the First Impulsive and Convective Modes of Vibration as a Function of the Tank Height-to-Radius Ratio (H/R).

H/R	C_i	C_c	m_i/m_l	m_c/m_l	h_i/H	h_c/H	h_i'/H	h_c'/H
0.3	9.28	2.09	0.176	0.824	0.400	0.521	2.640	3.414
0.5	7.74	1.74	0.300	0.700	0.400	0.543	1.460	1.517
0.7	6.97	1.60	0.414	0.586	0.401	0.571	1.009	1.011
1.0	6.36	1.52	0.548	0.452	0.419	0.616	0.721	0.785
1.5	6.06	1.48	0.686	0.314	0.439	0.690	0.555	0.734
2.0	6.21	1.48	0.763	0.237	0.448	0.751	0.500	0.764
2.5	6.56	1.48	0.810	0.190	0.452	0.794	0.480	0.796
3.0	7.03	1.48	0.842	0.158	0.453	0.825	0.472	0.825

Hamdan [19] compared sloshing height predictions by API, Japanese guidelines, ASCE recommendations, New Zealand guidelines, Australian design recommendations, and Eurocode 8. The New Zealand guidelines, Australian design recommendations, and Eurocode 8 follow similar approaches to calculate natural frequency and sloshing height. Differences between predicted sloshing heights and natural frequencies, as calculated by

different codes, were also highlighted by Hamdan [19]. Finally, Hamdan [19] was able to show consistency among the results of the FEA and Eurocode 8 [25].

2.3 Effect of Sloshing on Vessel Design and Analysis

Earthquake induced sloshing is a major consideration while designing a tank or a vessel. The free wave sloshing height as given by [5] is shown in Eq. (2.5) and as given by reference [25] is shown in Eq. (2.6). The sloshing height given by [5, 25] is a function of tank radius and spectral acceleration applied to base of the tank. For tanks with large radius, it may not always be possible to provide sufficient freeboard. In such cases, a sufficiently strong top head may be designed for the tank to perform satisfactorily in case of an earthquake.

$$d = R\frac{S_{ai}}{g} \tag{2.5}$$

$$d = 0.84RS_{ai} \tag{2.6}$$

The tank wall thickness, foundation and skirt support, if any, should be designed for seismic load taking into account the base shear and the overturning moment. An expression to calculate the total base shear, Eq. (2.7); overturning moment immediately above the base plate, Eq. (2.8); and overturning moment immediately below the base plate, Eq. (2.9) is given below as suggested by Malhotra [5]. The impulsive mass, m_i and convective mass, m_c may be calculated from Table 2.1 or Fig 2.3. The corresponding heights of impulsive and convective masses; h_i, h'_i and h_c, h'_c, respectively, can be obtained from Table 2.1.

$$Q_b = (m_i + m_w + m_r)S_{ai}(T_{imp}) + m_c S_{ai}(T_{con}) \tag{2.7}$$

$$M_o = \left(m_i h_i + m_w h_w + m_r h_r\right) S_{ai}(T_{imp}) + m_c h_c S_{ai}(T_{con}) \tag{2.8}$$

$$M_o^{'} = \left(m_i h_i^{'} + m_w h_w + m_r h_r\right) S_{ai}(T_{imp}) + m_c h_c^{'} S_{ai}(T_{con}) \tag{2.9}$$

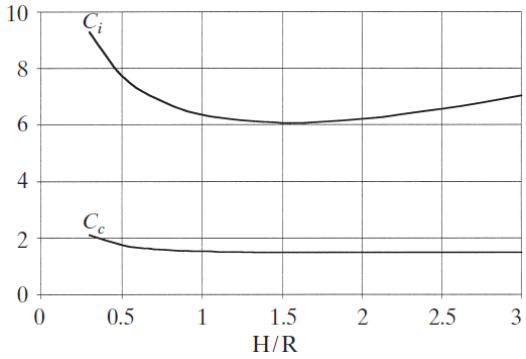

FIGURE 2.2: Impulsive and Convective Coefficients

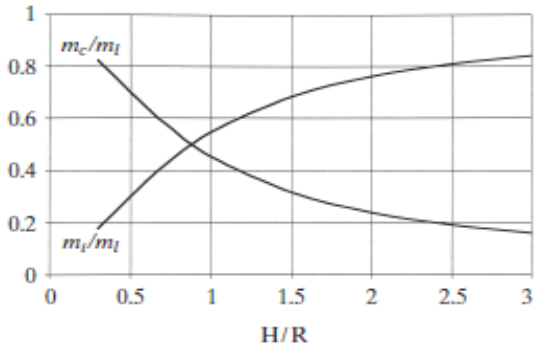

FIGURE 2.3: Impulsive and Convective Mass as Fraction of Total Fluid Mass

Tanks designed inadequately for seismic loading can suffer extensive damages during an earthquake, resulting in loss of contained fluid and loss of tank beyond repair. One of the common damages in fixed base tanks as shown in Fig. 2.4 is elephant-foot buckling. It is an outward bulge just above the tank base and usually occurs in tanks with low height-to-radius ratios. Elephant-foot buckling is mainly attributed to high compressive stresses (beam like bending) in the tank wall, high hoop tension and local bending stresses due to restraints at the tank base [19]. Other types of damage to tanks include the diamond shape buckling as shown in Fig. 2.5. High axial compressive stresses in unanchored tanks are mainly responsible for diamond shape buckling. The impulsive mass experiences accelerations higher than the peak ground accelerations. The magnitude of accelerations experienced by impulsive mass depends on the flexibility of tank. Larger flexibility of a tank may result in higher accelerations experienced by the impulsive mass, resulting in higher overturning moments and base shear forces, whereas

a stiffer tank will result in lower impulsive accelerations as compared to a more flexible tank. Higher accelerations experienced by the impulsive mass as compared to peak ground accelerations should be kept in mind while designing the tank for seismic loads.

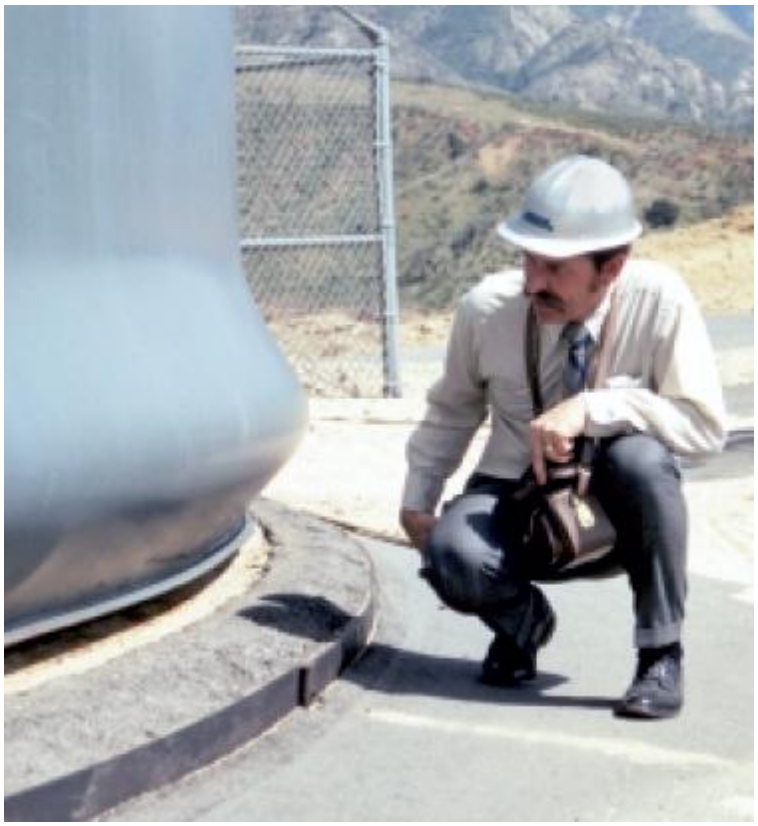

FIGURE 2.4: Elephant Foot Buckling of a Tank Wall

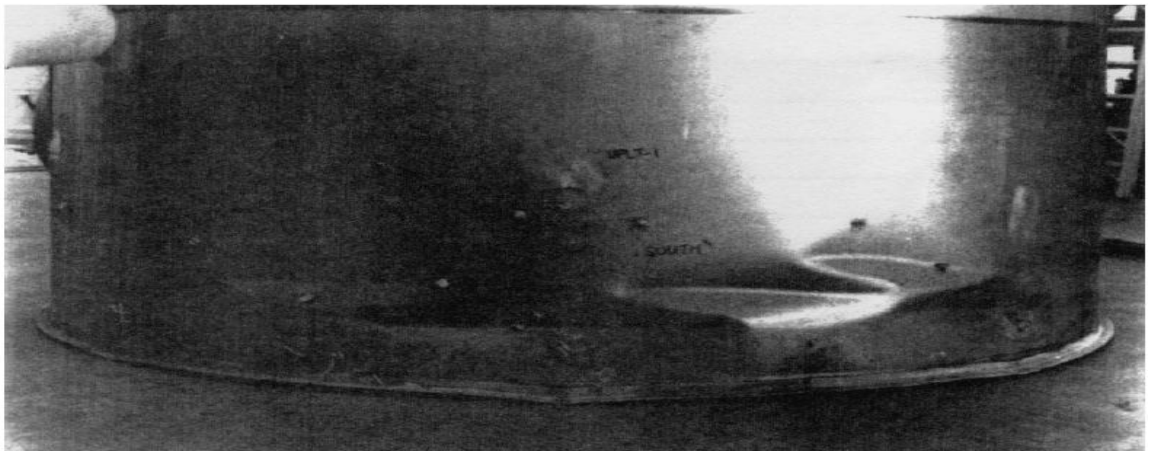

FIGURE 2.5: Diamond Shape Buckling of a Tank Wall

As a result of convective sloshing, the free wave of high amplitude can damage or rupture the tank roof and top wall of a tank as shown in Fig. 2.6 and Fig. 2.7. Furthermore, due to insufficient free board, the tank roof may restrict convective sloshing [1] i.e., the free fluid wave may strike the roof of tank and fall back in the tank. This will result in increased impulsive mass making the problem more severe and complicated. Due to the increased impulsive mass, a tank or vessel may experience even higher shear forces and overturning moments. For a majority of tanks having a height to radius ratio between 0.3 and 3 ($0.3 < H/R < 3$), the first impulsive and the first convective modes together account for more than 85 percent of the total liquid mass in the tank The remaining mass of the liquid vibrates primarily in higher impulsive modes for tall tanks ($H/R > 1$), and higher convective modes for broad tanks ($H/R \leq 1$). It is highly recommended that the higher modes of impulsive and convective sloshing should be considered [5, 6] and combined with the first fundamental mode of impulsive and convective sloshing, respectively, while designing the tank or vessel for seismic loads.

FIGURE 2.6: Damage to Roof and Wall Junction of Tank due to Convective Sloshing

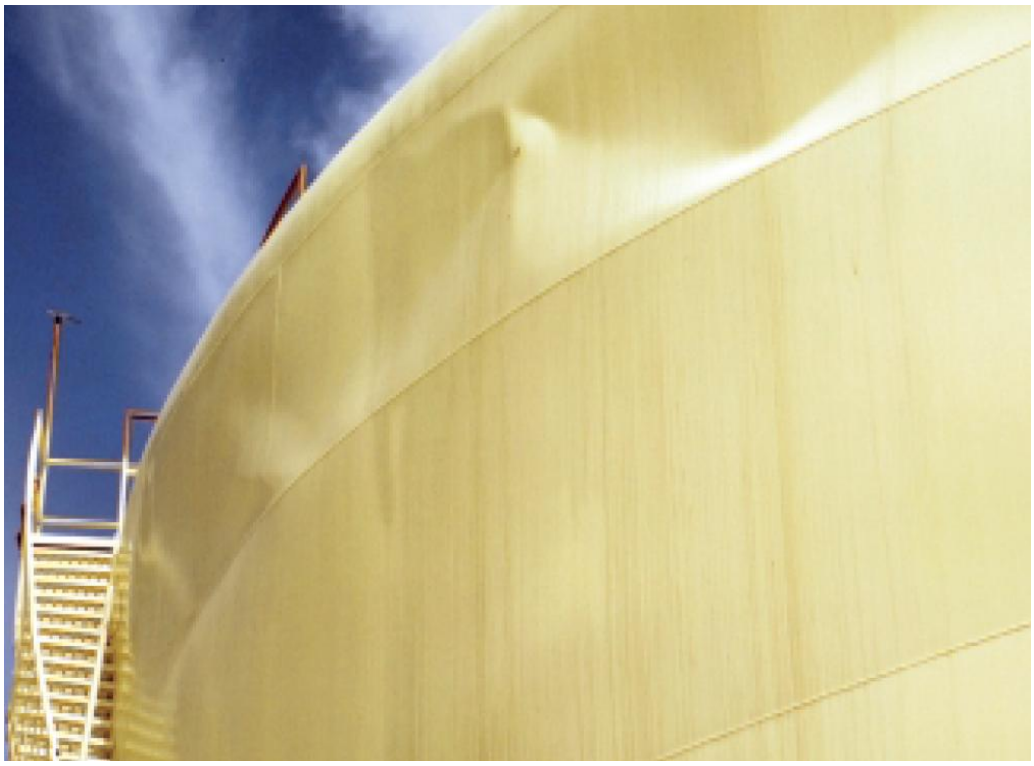

FIGURE 2.7: Damage to Upper Wall of Tank due to Convective Sloshing

CHAPTER 3: RESPONSE CALCULATIONS

3.1 Single Degree of Freedom System

A system having only one free displacement coordinate is termed as a single degree of freedom system. Simple structures like empty tanks or vessels (without any fluid) can be idealized as single degree of freedom systems for vibration analysis of the structure. These structures are termed as simple and can be idealized as a lumped (concentrated) mass, m and supported by a mass-less structure having stiffness, k. A single degree of freedom system as shown in Fig. 3.1 consist of a concentrated mass, m attached to a mass less spring of stiffness, k. The translation u(t) in X-direction is the only displacement coordinate sufficient to describe the motion of the mass, m at any particular instant of time, t. The stiffness of the spring, k, is defined as the force required to produce a unit change in the length of the spring.

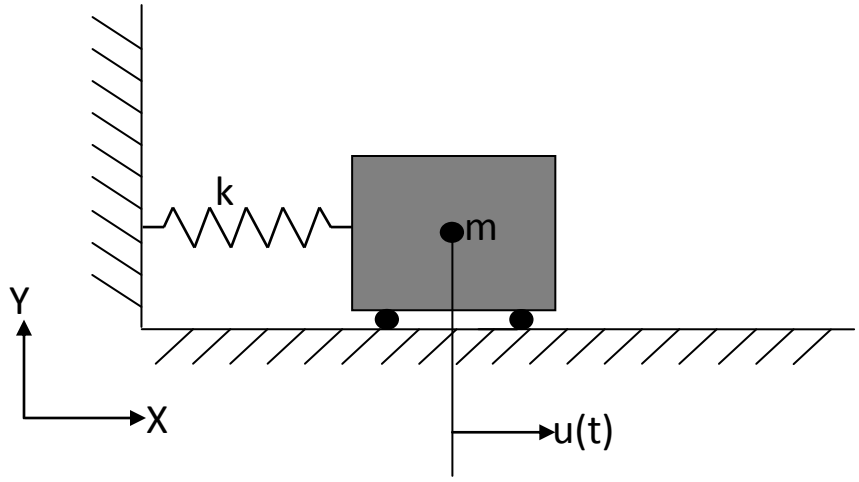

FIGURE 3.1: Single Degree of Freedom System

3.1.1 Equation of Motion

The equation of motion for a single degree of freedom (SDOF) system in its general form is given by Eq. (3.1) where c is the coefficient of damping and F(u, t) is the external force applied to mass, m. In order to calculate the natural frequency without damping, the external force is set to zero. The equation of motion for a SDOF system for free undamped vibrations is given by Eq. (3.2).

$$m\ddot{u} + c\dot{u} + ku = F(u,t) \tag{3.1}$$

$$m\ddot{u} + ku = F(u,t) \tag{3.2}$$

The differential equation of motion for free vibrations is independent of the gravitational forces. Dividing both sides of Eq. (3.2) by mass, m we obtain Eq. (3.3) After substituting $k/m = \omega^2$ in Eq. (3.3), the equation of motion is rewritten for free undamped vibrations as in Eq. (3.4), where ω, as given by Eq. (3.5) is known as the circular frequency of free vibration. The units of ω are radians per second. The natural frequency of vibration is given by Eq. (3.6). The units of natural frequency are cycles per second (or Hertz).

$$\ddot{u} + \frac{k}{m}u = 0 \tag{3.3}$$

$$\ddot{u} + \omega^2 u = 0 \tag{3.4}$$

$$\omega = \sqrt{\frac{k}{m}} \tag{3.5}$$

$$f = \frac{\omega}{2\pi} \tag{3.6}$$

The general solution of free undamped vibrations, Eq. (3.4) is given by Eq. (3.7), where A is the amplitude of vibration and α is known as phase angle. The displacement u

is measured from the static equilibrium position and is positive as the mass moves in the positive X-direction (to its right in Fig. 3.1) relative to its static equilibrium position.

$$u = A(\cos \omega t - \alpha) \tag{3.7}$$

3.1.2 Periodic Forcing Function

A SDOF system subjected to external time varying force is shown in Fig. 3.2. The equation of motion for SDOF system for forced vibrations, i.e., if an external force is applied to the mass, m is given by Eq. (3.8). Assuming that the force applied to the mass m is periodic and the magnitude of force is given by $F(u,t) = P\sin\Omega t$, Eq. (3.8) can be modified to be written as Eq. (3.9). Dividing both sides of Eq. (3.9) by m we obtain Eq. (3.11) where q(sin(ωt)) is the periodic force per unit mass applied to mass, m. The periodic forcing function and forced vibrations has same time period, $T = 2\pi/\Omega$.

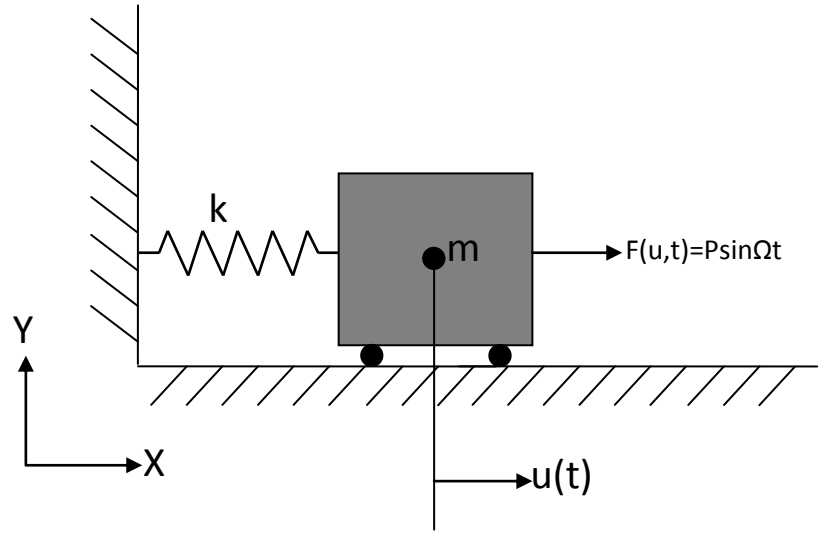

FIGURE 3.2: Single Degree of Freedom System Subjected to Periodic Force

$$m\ddot{u} + ku = F(u,t) \tag{3.8}$$

$$m\ddot{u} + ku = P\sin\Omega t \tag{3.9}$$

$$\ddot{u} + \frac{k}{m}u = \frac{P}{m}\sin\Omega t \tag{3.10}$$

$$\ddot{u} + \omega^2 u = q\sin\Omega t \tag{3.11}$$

$$u = \left(\frac{P}{k}\sin\Omega t\right)\left(\frac{1}{1-\Omega^2/\omega^2}\right) \tag{3.12}$$

The general solution of forced undamped vibrations is given by Eq. (3.12). The factor $P/k\sin\Omega t$ is the amplitude of deflection that the periodic force would produce if it was applied statically. The factor $1/(1-\Omega^2/\omega^2)$ is responsible for dynamic action of the periodic force applied to mass, m. The absolute value of the dynamic action factor is known as the magnification factor and its expression is given by Eq. (3.13). The value of the magnification factor depends only on the frequency ratio Ω/ω (ratio of frequency of applied force and natural frequency of the system).

$$\beta = \left|\frac{1}{1-\Omega^2/\omega^2}\right| \tag{3.13}$$

3.1.3 Periodic Support Acceleration

In case of a seismic event, the earthquake ground motion is generally measured in terms of ground accelerations. It becomes important to investigate the response to support motions. Fig. 3.3 depicts a SDOF system subjected to ground accelerations. The frame to which SDOF system is attached is subjected to a horizontal harmonic acceleration $\ddot{u}_g = a\sin\Omega t$ relative to ground. Under the influence of applied acceleration, assume the frame moves a distance of u_g relative to the ground. The equation of motion then becomes that given by Eq. (3.14) .

$$m\ddot{u} + k(u - u_g) = 0 \tag{3.14}$$

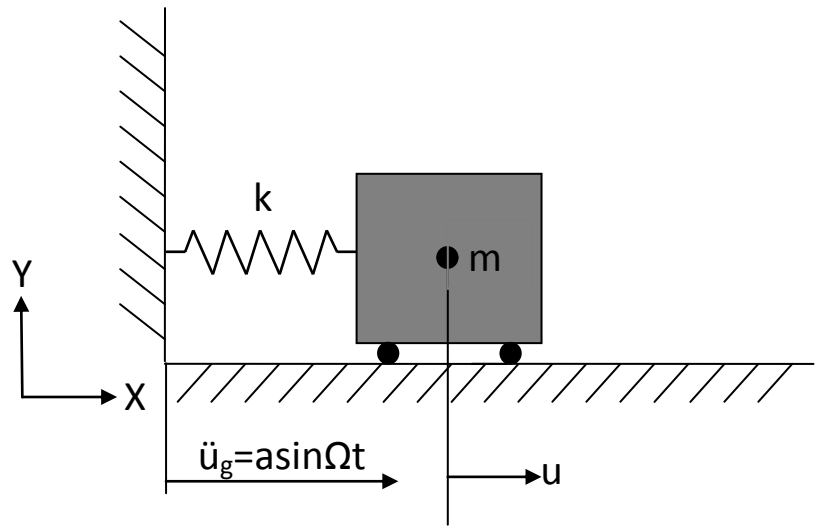

FIGURE 3.3: Single Degree of Freedom System Subjected to Periodic Acceleration

Defining a change of coordinates with $u^* = u - u_g$ and $\ddot{u}^* = \ddot{u} - \ddot{u}_g$, the relative displacement of mass with respect to ground is given by $u^* = u - u_g$. Substituting the expressions for changed coordinates in Eq. (3.14), we obtain Eq. (3.15). Using expression $q_g^* = -a$ to get rid of the negative sign, the equation of motion is then given by Eq. (3.16). Finally the response of SDOF system to harmonic ground accelerations is given by Eq. (3.17).

$$\ddot{u}^* + \omega^2 u^* = -a\sin\Omega t \tag{3.15}$$

$$\ddot{u}^* + \omega^2 u^* = q_g^* \sin\Omega t \tag{3.16}$$

$$u^* = \left(-\frac{ma}{g}\sin\Omega t\right)\left(\frac{1}{1-\Omega^2/\omega^2}\right) \tag{3.17}$$

The forcing functions as discussed above and used to calculate response for a SDOF system were simple harmonic forcing functions. In practice it is possible to come

across periodic functions which are more complicated. These complicated periodic functions can be represented in the form of a Fourier series as shown in Eq. (3.18). The expression to calculate Fourier coefficients a_o, a_i and b_i is given by Eq. (3.19), Eq. (3.20), and Eq. (3.21) respectively.

$$F(t) = a_o + \sum_{i=1}^{\infty} (a_i \cos i\Omega t + b_i \sin i\Omega t) \tag{3.18}$$

$$a_o = \frac{1}{T} \int_0^T F(t) dt \tag{3.19}$$

$$a_i = \frac{2}{T} \int_0^T F(t) \cos i\Omega dt \tag{3.20}$$

$$b_i = \frac{2}{T} \int_0^T F(t) \sin i\Omega dt \tag{3.21}$$

$$m\ddot{u} + ku = a_o + \sum_{i=1}^{\infty} (a_i \cos i\Omega t + b_i \sin i\Omega t) \tag{3.22}$$

The undamped equation of motion for a SDOF system subjected to a complicated periodic function is given by Eq. (3.22). The general solution of Eq. (3.22) is given by calculating the response from each term of the series. Each individual response is then plotted against time and the total response can be calculated by superimposing the ordinates of individual plotted responses by the principal of superposition.

3.1.4 Arbitrary Forcing Functions

In nature there exist forces which have no periodic character. These forces are called arbitrary forcing functions. The methodology described in previous sections fails to calculate response (displacements) for these types of forces. The response due to these

forces is calculated using Duhamel's integral. A damped SDOF system subjected to an arbitrary forcing function is shown in is shown in Fig. 3.4, which is expressed as a function of a dummy time variable.

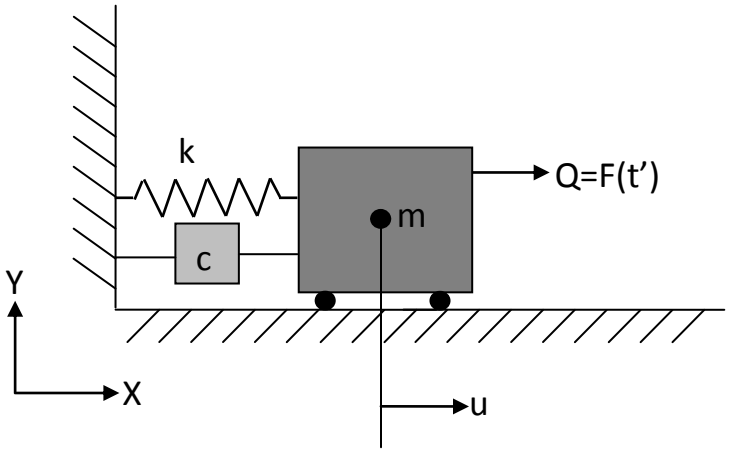

FIGURE 3.4: Single Degree of Freedom System Subjected to Arbitrary Force

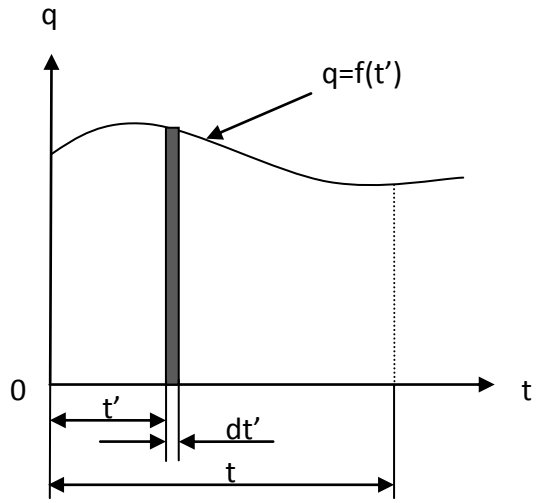

FIGURE 3.5: Arbitrary Force as a Function of Dummy Time Variable t'

Recalling equation of motion for SDOF system in the most general form including damping and subjected to an arbitrary forcing function F(t'). The differential equation of motion is given by Eq. (3.23) where c is called coefficient of damping.

Dividing Eq. (3.23) by m and using notations $2n = c/m$ and $q = Q/m$ where q is the arbitrary disturbing force per unit mass and is a function of dummy time variable t' we get Eq. (3.25). The arbitrary forcing function is shown in Fig. 3.5.

The shaded strip in Fig. 3.5 shows an increment impulse for a small increment in time dt'. This incremental impulse imparts an instantaneous incremental velocity to each unit of mass. The magnitude of instantaneous increase in velocity is given by area of shaded region and equals to as given by Eq. (3.26). The response of a damped SDOF system to initial conditions as given by Timoshenko [26] is given by Eq. (3.27), assuming that the initial displacement of the system is zero, Eq. (3.27) is reduced to Eq. (3.28).

$$m\ddot{u} + c\ddot{u} + ku = F(t') = Q \tag{3.23}$$

$$\ddot{u} + \frac{c}{m}\dot{u} + \frac{k}{m}u = \frac{F(t)'}{m} = \frac{Q}{m} \tag{3.24}$$

$$\ddot{u} + 2n\dot{u} + \omega^2 u = f(t') = q \tag{3.25}$$

$$d\dot{u} = qdt' \tag{3.26}$$

$$u = e^{-nt}\left(u_o \cos\omega_d t + \frac{u_o' + nu_o}{\omega_d}\sin(\omega_d t)\right). \tag{3.27}$$

$$u = e^{-nt}\left(\frac{u_o'}{\omega_d}\sin\left(\omega_d t\right)\right) \tag{3.28}$$

Treating the incremental velocity given by Eq. (3.26) as the initial velocity of the mass regardless of any already existing velocity, displacement, and forces on the mass at time t' and using Eq. (3.28), the incremental displacement of the system at any time t is given by Eq. (3.29). Each incremental impulse of magnitude qdt' will contribute to the total response as given by Eq. (3.29). The total response of the continuous disturbing

force as given by Eq. (3.30) can be calculated by integrating Eq. (3.29) form t'=0 to t'=t. For a undamped system the response of system can be calculated by putting n=0 and $\omega_d=\omega$ in Eq. (3.30), as given by Eq. (3.31) below:

$$du = e^{-n(t-t')}\left(\frac{q dt'}{\omega_d}\sin(\omega_d(t-t')\right) \tag{3.29}$$

$$u = \frac{e^{-n(t)}}{\omega_d}\int_0^t e^{-nt'} q\sin(\omega_d(t-t'))dt' \tag{3.30}$$

.

$$u = \frac{1}{\omega}\int_0^t q\sin\omega_d(t-t')dt' \tag{3.31}$$

The expression given by Eq. (3.30) is known as Duhamel's integral. It is useful in analyzing response of a system to any kind of disturbing force for both single degree of freedom systems and multiple degree of freedom systems.

3.1.5 Arbitrary Support Accelerations

In certain problems especially related to an earthquake, the response of system is due to arbitrary applied accelerations as a function of time on the supports instead of a directly applied arbitrary force. Fig. 3.6 shows a damped single degree of freedom system subjected to arbitrary support accelerations. Defining a change of coordinates with displacement $\ddot{u}^* = \ddot{u} - \ddot{u}_g$, velocity $\dot{u}^* = \dot{u} - \dot{u}_g$ and acceleration $\ddot{u}^* = \ddot{u} - \ddot{u}_g$, the relative displacement of mass with respect to ground is given by $u^* = u - u_g$ and relative velocity of mass with respect to ground is given by $\dot{u}^* = \dot{u} - \dot{u}_g$. The equation of motion for a damped SDOF system for arbitrary support acceleration is given by Eq. (3.32).

Using changed displacement, velocity and acceleration coordinates, the equation of motion is now given by Eq. (3.33)

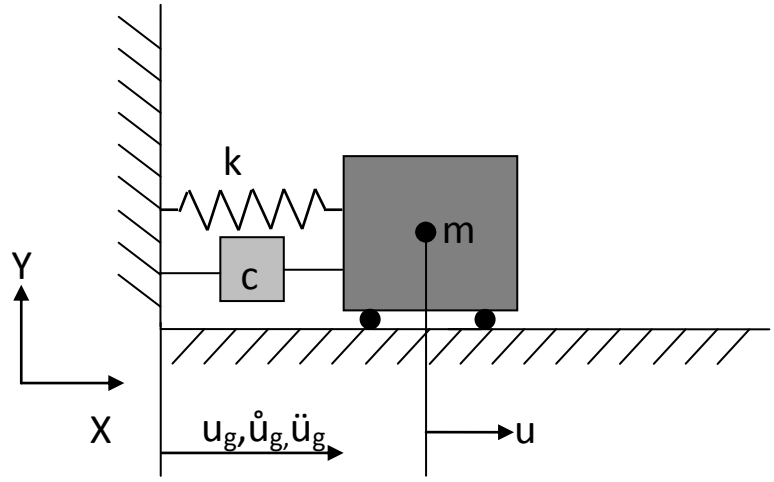

FIGURE 3.6: Single Degree of Freedom System Subjected to an Arbitrary Support Acceleration

$$m\ddot{u} = -c(\dot{u} - \dot{u}_g) - k(u - u_g) \tag{3.32}$$

$$m\ddot{u}^* + c\dot{u}^* + ku^* = -m\ddot{u}_g \tag{3.33}$$

The arbitrary ground acceleration as a function of dummy time variable is shown in Fig. 3.7. The expression $q_g^* = -\ddot{u}_g^* = -f(t')$ represents equivalent force per unit mass in the relative coordinates due to ground acceleration.

$$\ddot{u}^* + \frac{c}{m}\dot{u}^* + \frac{k}{m}u^* = -\ddot{u}_g \tag{3.34}$$

$$\ddot{u}^* + 2n\dot{u}^* + \omega^2 u^* = -\ddot{u}_g \tag{3.35}$$

Eq. (3.35) is mathematically the same as Eq. (3.25) and therefore the response due to arbitrary acceleration follows the same pattern as response due to an arbitrary forcing function. The expressions to calculate the response due to an arbitrary support

acceleration applied to a damped SDOF system and to an undamped SDOF system is given by Eq. (3.36) and Eq. (3.37), respectively.

$$u^* = \frac{e^{-nt}}{\omega_d}\int_0^t e^{nt'} q_g^* \sin\omega(t-t')dt' \tag{3.36}$$

$$u^* = \frac{1}{\omega}\int_0^t q_g^* \sin\omega(t-t')dt' \tag{3.37}$$

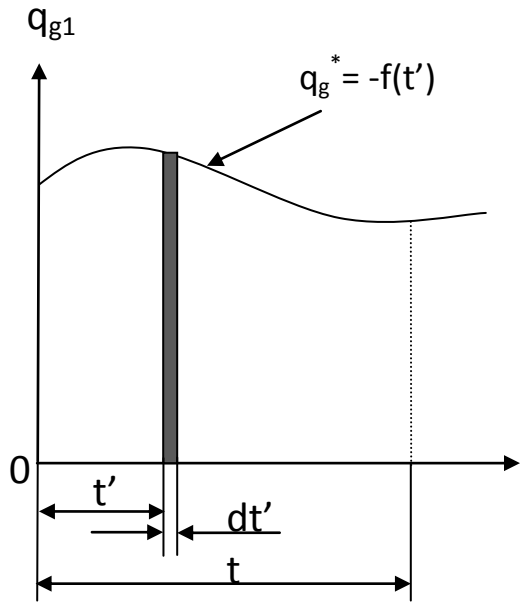

FIGURE 3.7: Arbitrary Support Acceleration as a Function of Dummy Time Variable t'

3.2 Multiple Degrees of Freedom System

A system having a minimum of two degrees of freedom (free displacement coordinates) but fewer than an infinite number of degrees of freedom is termed a multiple degree of freedom system (MDOF). A tank or vessel partially filled with fluid is an example of a multiple degree of freedom system. An MDOF problem is most often formulated in matrix form.

3.2.1 Equations of Motion

The equations of motion for a multiple degree of freedom (MDOF) system in its general form are given by Eq. (3.38) where [M] is the mass matrix, [K] is stiffness matrix, [C] is damping matrix and {F} is the forcing vector. Neglecting damping and any applied external force, the equations of motion for an MDOF system for free undamped vibrations are given by Eq. (3.39).

$$[M]\{\ddot{U}\}+[C]\{\dot{U}\}+[K]\{U\}=\{F(t)\} \tag{3.38}$$

$$[M]\{\ddot{U}\}+[K]\{U\}=0 \tag{3.39}$$

The differential equations of motion for free vibrations are independent of gravitational forces. Equations of motions represented by Eq. (3.39) represent ***n*** coupled differential equations. The solution to coupled equations of motion is obtained by solving simultaneous differential equations. The general solution (harmonic solution) of Eq. (3.39) is given by an assumed form of displacement as given in Eq. (3.40) or Eq. (3.41), in which the phase angle is neglected. Differentiating Eq. (3.41) twice and substituting Eq. (3.41) and Eq. (3.42) in Eq. (3.39), and simplifying, we obtain Eq. (3.44), which in turn represents a recognizable form of an Eigen value problem. The multiple solutions for Eq. (3.44) yield ***i*** number of modal (circular) frequencies from the Eigen values for ω_i^2. The desired natural frequency (in terms of Hertz or cycles per second) for the i^{th} mode is given by the following relation as shown below in Eq. (3.45). Solving for the non-trivial solutions for ***i*** number of Eigen values, Eigen vectors $\{\Phi\}_i$ are calculated using Eq. (3.46). In the present analysis, Eigen vectors are displacements at each degree of freedom for a particular frequency.

$$\{U\}_i = \{\Phi\}_i \left(\cos \omega_i t - \alpha\right) \tag{3.40}$$

$$\{U\}_i = \{\Phi\}_i \cos \omega_i t \tag{3.41}$$

$$\{\ddot{U}\} = -\omega_i^2 \{\Phi\}_i \cos \omega_i t \tag{3.42}$$

$$-\omega_i^2 [M]\{\Phi\}_i \cos \omega_i t + [K]\{\Phi\}_i \cos \omega_i t = 0 \tag{3.43}$$

$$[K] - \omega_i^2 [M] = 0 \tag{3.44}$$

$$f_i = \frac{\omega_i}{2\pi} \tag{3.45}$$

$$[K]\{\Phi\}_i = \omega_i^2 [M]\{\Phi\}_i \tag{3.46}$$

To solve an MDOF problem having n degrees of freedom, ***n*** numbers of differential equations are required to be solved simultaneously. As the number of degrees of freedom increase, the solution to problem becomes more complicated. Moreover, it is extremely difficult to calculate response of an MDOF system subjected to arbitrary forcing functions.

3.2.2 Principal and Normal Coordinates

The problems involving simultaneous solution of a large number of coupled differential equations and response calculations for arbitrary forcing functions can be overcome by changing the original coordinates to principal and normal coordinates. To understand conversion from the original coordinates to principal coordinates, consider the i^{th} and j^{th} modes of the Eigen value problem as given by Eq. (3.47) and Eq. (3.48), respectively. Pre-multiplying Eq. (3.47) by $\{\Phi\}_j^T$ and post multiplication of transpose of Eq. (3.48) by $\{\Phi\}_i^T$, yields Eq. (3.49) and Eq. (3.50), respectively.

$$[K]\{\Phi\}_i = \omega_i^2 [M]\{\Phi\}_i \tag{3.47}$$

$$[K]\{\Phi\}_j = \omega_j^2 [M]\{\Phi\}_j \tag{3.48}$$

$$\{\Phi\}_j^T [K]\{\Phi\}_i = \omega_i^2 \{\Phi\}_j^T [M]\{\Phi\}_i \tag{3.49}$$

$$\{\Phi\}_j^T [K]\{\Phi\}_i = \omega_j^2 \{\Phi\}_j^T [M]\{\Phi\}_i \tag{3.50}$$

Subtracting Eq. (3.50) from Eq. (3.49) results in the formulation shown in Eq. (3.51). On the other hand, dividing Eq. (3.49) by ω_i^2 and Eq. (3.50) by ω_j^2 and then subtracting the two equations we obtain Eq. (3.52). For the condition $i \neq j$ and the condition that Eigen values are not the same, i.e., $\omega_i^2 \neq \omega_j^2$, Eq. (3.53) and Eq. (3.54) must hold true.

$$\left(\omega_i^2 - \omega_j^2\right)\{\Phi\}_j^T [M]\{\Phi\}_i = 0 \tag{3.51}$$

$$\left(\frac{1}{\omega_i^2} - \frac{1}{\omega_j^2}\right)\{\Phi\}_j^T [K]\{\Phi\}_i = 0 \tag{3.52}$$

$$\{\Phi\}_j^T [M]\{\Phi\}_i = \{\Phi\}_i^T [M]\{\Phi\}_j = 0 \tag{3.53}$$

$$\{\Phi\}_j^T [K]\{\Phi\}_i = \{\Phi\}_i^T [K]\{\Phi\}_j = 0 \tag{3.54}$$

The expressions given by Eq. (3.53) and Eq. (3.54) demonstrate that the principal modes of vibration are orthogonal. For the condition that i=j, Eq. (3.51) and Eq. (3.52) become Eq. (3.55) and Eq. (3.56), respectively. The terms M_{pi} and K_{pi} are constants and depend upon the chosen normalization method of Eigen vector $\{\Phi\}_i$. For the ease of operation, the Eigen vectors corresponding to their respective natural frequencies are

assembled to form a square matrix of side ***n***. The Eigen vectors are placed column-wise as given by Eq. (3.57).

$$\{\Phi\}_i^T [M] \{\Phi\}_i = M_{Pi} \tag{3.55}$$

$$\{\Phi\}_i^T [K] \{\Phi\}_i = K_{Pi} \tag{3.56}$$

$$[\Phi] = \left[\{\Phi\}_1 \{\Phi\}_2 \{\Phi\}_3 ..... \{\Phi\}_n \right] \tag{3.57}$$

From Eq. (3.53), Eq. (3.55) and Eq. (3.57), we can write Eq. (3.58) and from Eq. (3.54), Eq. (3.56) and Eq. (3.57) we can write Eq. (3.59), where $[M_p]$ represents a diagonal matrix (array) known as the principal mass matrix and $[K_p]$ represent a diagonal matrix known as the principal stiffness matrix.

$$[\Phi]^T [M][\Phi] = [M_P] \tag{3.58}$$

$$[\Phi]^T [K][\Phi] = [K_P] \tag{3.59}$$

The identity matrix as a multiplier against the modal matrix and its inverse is given in Eq. (3.60). Recalling free, undamped equations of motion from Eq. (3.39), pre-multiplying by modal matrix [Φ] and inserting Eq. (3.60) in front of displacement and acceleration vectors produces Eq. (3.61). The expression given by Eq. (3.62) reduces to the generalized equation of motion having both generalized mass and generalized stiffness matrices. Both the generalized mass and generalized stiffness matrices are diagonal matrices. The generalized displacement vector (called principal coordinate) and generalized acceleration vectors in principal coordinates are given by Eq. (3.63) and Eq. (3.64), respectively.

$$I = [\Phi][\Phi]^{-1} \tag{3.60}$$

$$[\Phi]^T [M][\Phi][\Phi]^{-1}\{\ddot{U}\}+[\Phi]^T [K][\Phi][\Phi]^{-1}\{U\}=0 \tag{3.61}$$

$$[M_P]\{\ddot{U}\}_P+[K_P]\{U\}_P=0 \tag{3.62}$$

$$\{U\}_P=[\Phi]^{-1}\{U\} \tag{3.63}$$

$$\{\ddot{U}\}_P=[\Phi]^{-1}\{\ddot{U}\} \tag{3.64}$$

The principal mode response of an MDOF system is analyzed by calculating the generalized displacement vector as given by Eq. (3.63) and generalized acceleration vector as given in Eq. (3.64). The response results are then obtained in original coordinates by using expressions given by Eq. (3.65) and Eq. (3.66).

$$U=[\Phi]\{U\}_P \tag{3.65}$$

$$\ddot{U}=[\Phi]\{\ddot{U}\}_P \tag{3.66}$$

Formation of the generalized mass and generalized stiffness matrix results in decoupling of ***n*** number of coupled differential equations for both inertial and elastic coupling. The uncoupled equations represent ***n*** number of equations that can be solved as ***n*** number of single degree of freedom equations. As a result of uncoupling of equations, the need to solve simultaneous differential equations is eliminated and each uncoupled equation is solved independently from each other, which in turn decreases the complexity of the stated problem.

Further the principal coordinates are not unique as the Eigen vectors can be scaled or normalized arbitrarily. As a matter of fact there can be infinite number of sets of such generalized displacements. To overcome this small problem, the modal vectors are normalized with respect to mass matrix so that M_{pi} in Eq. (3.55) becomes unity as shown

in Eq. (3.67). The subscript N shows that the Eigen vectors are normalized with respect to the mass matrix. The procedure to normalize the Eigen vectors with respect to mass matrix is given in Eq. (3.68) to Eq. (3.70). It may be noted that Eq. (3.70) is used if the mass matrix is not a diagonal matrix and Eq. (3.71) is used if the mass matrix is a diagonal matrix.

$$\{\Phi\}_{Ni}^{T}[M]\{\Phi\}_{Ni}=1 \tag{3.67}$$

$$\{\Phi\}_{Ni}=\frac{\{\Phi\}_i}{C_i} \tag{3.68}$$

$$C_i=\pm\sqrt{\{\Phi\}_i^{T}[M]\{\Phi\}_i} \tag{3.69}$$

$$C_i=\pm\sqrt{\sum_{j=1}^{n}\Phi_{ji}\left(\sum_{k=1}^{n}M_{jk}\Phi_{ki}\right)} \tag{3.70}$$

$$C_i=\pm\sqrt{\sum_{j=1}^{n}M_j\Phi_{ji}^2} \tag{3.71}$$

If all the vectors in the modal matrix are mass normalized, the principal mass matrix as given by Eq. (3.58) can be rewritten in normal coordinates as an identity matrix in the form as described by Eq. (3.72). The principal stiffness matrix given by Eq. (3.59) can be rewritten in the form described by Eq. (3.73). The expression in Eq. (3.74) gives the stiffness for i^{th} mode, which along with Eq. (3.73), shows that the stiffness in principal coordinates is equal to Eigen values when the modes are normalized with respect to the mass matrix. This particular set of coordinates is termed as principal coordinates.

$$[\Phi_N]^T[M][\Phi_N]=[M_N]=I \tag{3.72}$$

$$[\Phi_N]^T[K][\Phi_N]=\left[\omega^2\right] \tag{3.73}$$

$$\{\Phi\}_{Ni}^{T}[K]\{\Phi\}_{Ni} = \omega_i^2 \tag{3.74}$$

3.2.3 Arbitrary Forcing Functions

The response of an MDOF system due to an arbitrary forcing function is calculated by transforming the equations of motions to normal coordinates in order to get ***n*** number of uncoupled equations. Duhamel's integral as previously discussed in the case of a single degree of freedom system, is used to calculate the response of each uncoupled equation in normal coordinates. The response results are then transformed back to the original coordinates. Consider an undamped MDOF system under the influence of an arbitrary forcing function as represented by Eq. (3.75), where $\{Q\}_i$ represents the time varying arbitrary forcing function. Eq. (3.75) is converted to principal coordinates using Eq. (3.60) to Eq. (3.64). The uncoupled equations of motion in principal coordinates are represented by Eq. (3.77), where $\{Q\}_p$ denotes vector of applied arbitrary forcing function in principal coordinates. Assuming that the modal matrix is normalized with respect to normal coordinates, the forcing function is computed in normal coordinates by the expression given in Eq. (3.78).

$$[M]\{\ddot{U}\} + [K]\{U\} = \{Q\}_i \tag{3.75}$$

$$[\Phi]^T[M][\Phi]\{\ddot{U}\}_P + [\Phi]^T[K][\Phi]\{U\}_P = [\Phi]^T\{Q\}_i \tag{3.76}$$

$$[M_P]\{\ddot{U}\}_P + [K_P]\{U\}_P = \{Q\}_P \tag{3.77}$$

$$\{Q\}_{Ni} = [\Phi_N]^T[Q]_i \tag{3.78}$$

As a result of normalization of modal matrix with respect to mass matrix, the i^{th} equation of motion in normal coordinates is represented by Eq. (3.79). Duhamel's

integral as given by Eq. (3.31) is used to calculate the response of ***n*** number of uncoupled equations one at a time. The expression to calculate response of ith normal coordinate to the applied arbitrary forcing function by the application of Duhamel's integral is given by Eq. (3.80). The response results calculated by Eq. (3.80) are then transformed to original coordinates by using Eq. (3.65) and Eq. (3.66).

$$\ddot{u}_{Ni} + \omega_i^2 u_{Ni} = q_{Ni} = \Phi_{N1i} Q_1 + \Phi_{N2i} Q_2 + \ldots\ldots\ldots \Phi_{Nni} Q_N \tag{3.79}$$

$$u_{Ni} = \frac{1}{\omega_i} \int_0^t q_{Ni} \sin \omega_i \left(t - t' \right) dt' \tag{3.80}$$

3.2.4 Arbitrary Support Accelerations

The change of coordinates with displacement and acceleration are given by Eq. (3.81) and Eq. (3.82), respectively. The relative displacement of a mass with respect to the ground is given by Eq. (3.81). The equation of motion for an undamped MDOF system for an arbitrary support acceleration, using changed displacement and acceleration coordinates of the equation of motion is given by Eq. (3.83), where vector {1} denotes a vector filled with values of unity and has the effect of reproducing ground displacement and ground acceleration ***n*** times. Substitution of Eq. (3.82) in Eq. (3.83) gives the equation of motion in relative coordinates as in Eq. (3.84).

$$\{U\}^* = \{U\} - \{1\} u_g \tag{3.81}$$

$$\{\ddot{U}\}^* = \{\ddot{U}\} - \{1\} \ddot{u}_g \tag{3.82}$$

$$[M]\{\ddot{U}\} = -[K](\{U\} - \{1\} u_g) \tag{3.83}$$

$$[M]\{\ddot{U}\}^* + [K]\{U\}^* = \{Q\}_g^* \tag{3.84}$$

$$\{Q\}_g^* = -[M]\{1\}\ddot{u}_g \tag{3.85}$$

$$\{Q\}_{Ng}^* = [\Phi_N]^T \{Q\}_g^* \tag{3.86}$$

$$\ddot{u}_{Ni}^* + \omega_i^2 u_{Ni}^* = q_{Ni}^* \tag{3.87}$$

$$u_{Ni}^* = \frac{1}{\omega_i}\int_0^t q_{Ni}^* \sin\omega_i\left(t - t'\right)dt' \tag{3.88}$$

Assuming that the modal matrix is normalized with respect to normal coordinates, the arbitrary acceleration computed in normal coordinates is given by the Eq. (3.86). Equation (3.88) gives the expression to calculate the response of i^{th} normal coordinate to the applied arbitrary acceleration by the application of Duhamel's integral. The response results calculated by Eq. (3.88) are then transformed to original coordinates by using Eq. (3.65) and Eq. (3.66).

CHAPTER 4: OUTLINE OF METHODOLOGY EMPLOYED IN SINGLE POINT RESPONSE SPECTRUM ANALYSIS

4.1 Coordinate System.

In general a coordinate system can be defined as a reference system consisting of a set of points, lines or surfaces, and a set of rules, which are used to define the position of points in space in either two or three dimensions. In other words, it is a system for describing absolute position in terms of distance and direction from a given reference point. While working with a finite element analysis code, the following coordinate systems must be clearly understood by the analyst.

- Global and local coordinate systems.
- Nodal coordinate system.
- Element coordinate system.
- Result coordinate system.

The global and local coordinate systems are used to define and track geometry items such as nodes and key points in space. The global Cartesian, global cylindrical and global spherical coordinate systems are the most commonly used coordinate systems. These coordinate systems share the same origin and are right handed coordinate systems. The global Cartesian system is a rectangular coordinate system and is defined by three orthogonal axes labeled as X, Y and Z-axes as shown in Fig. 4.1. The X, Y and Z-axes can be thought of representing the length, height and width respectively of a cube.

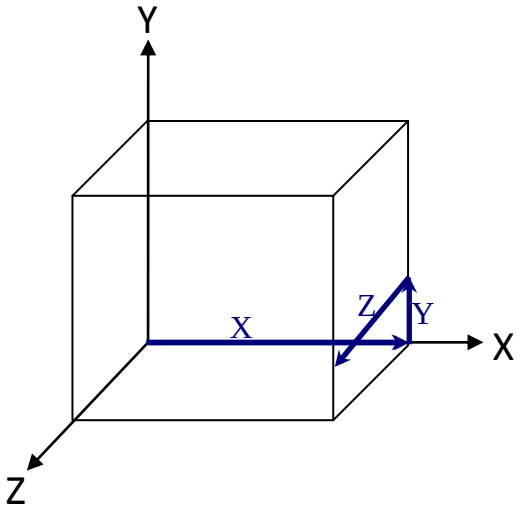

FIGURE 4.1: Global Cartesian Coordinates

The global cylindrical coordinate system is defined by three axes, namely, R, Θ, and Z-axes as shown in Fig. 4.2. The R, Θ, and Z-axes represent the radial, circumferential and vertical directions.

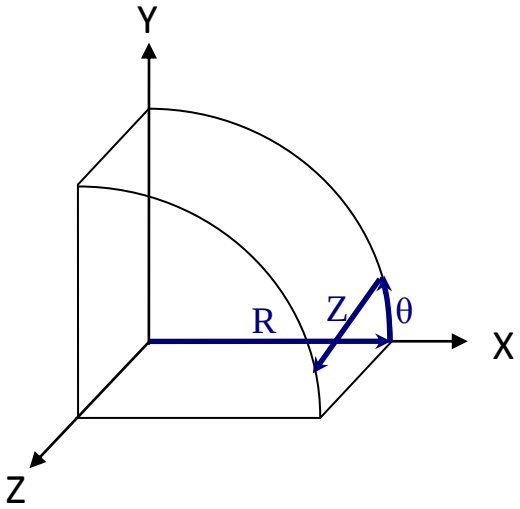

FIGURE 4.2: Global Cylindrical Coordinates

The global spherical coordinate system is also defined by three axes, which are represented by R, Θ, and Φ-symbols, where R, Θ, and Φ represent the radial, circumferential and azimuthal coordinates. In this dissertation, only global Cartesian and

global cylindrical coordinates have been used. The variables in one global coordinate system can be converted to other coordinate systems by using simple mathematical expressions. The conversion from global cylindrical system to global Cartesian system can be done by using Eq. (4.1), Eq. (4.2) and Eq. (4.3). The expression in Eq. (4.1) gives the conversion for an X-coordinate of a global Cartesian system as a function of radial and circumferential coordinates of a global cylindrical system. Likewise, the expression in Eq. (4.2) gives the conversion for a Y-coordinate of a global Cartesian system as a function of radial and circumferential coordinate of a global cylindrical system. Equation (4.3) demonstrates that the vertical coordinate remains unchanged while switching from cylindrical to Cartesian coordinates.

$$x = r\cos(\theta) \tag{4.1}$$

$$y = r\sin(\theta) \tag{4.2}$$

$$z = z \tag{4.3}$$

For the ease of defining geometry items (modeling of a problem in an FEA code), local coordinate systems are used. Local coordinate systems are similar to global coordinate systems but their origin and orientation are often different from a global coordinate system and are user specified. Local Cartesian, cylindrical, and spherical systems can be defined.

Each node used in the geometrical modeling of a problem has its own coordinate system called the nodal coordinate system. A node generally has more than one degree of freedom (translational and rotational) depending on the elements used to model the problem. A nodal coordinate system orients the degree of freedom direction at each node. A nodal coordinate system can be rotated to any desired orientation. Degree of

freedom constraints (boundary conditions), forces, master degree of freedom, coupling equations, constraint equations, degree of freedom solution (results) and reactions are some of the important parameters that are interpreted in the nodal coordinate system. Nodal coordinate systems for a number of nodes having only two translational degrees of freedom per node, lying on a semicircle, having the local coordinate system at the center of semicircle and oriented parallel to global coordinate system is shown in Fig. 4.3. A nodal coordinate system oriented parallel to the global Cartesian system and a nodal coordinate oriented parallel to local cylindrical system are shown in Fig. 4.3a and Fig. 4.3b, respectively.

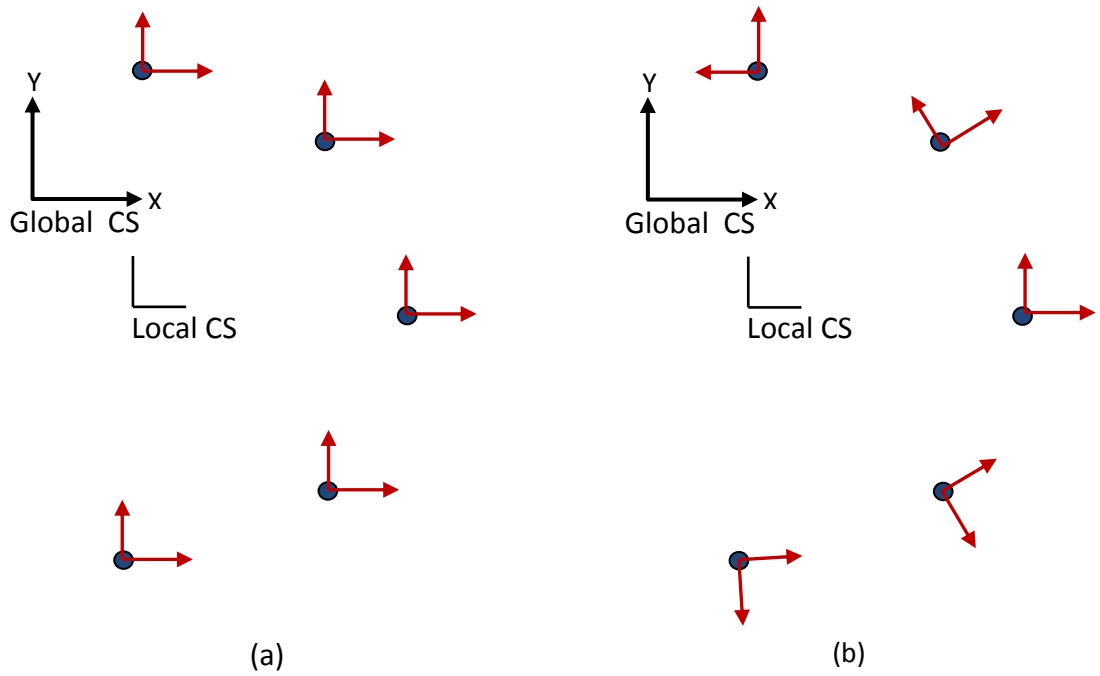

FIGURE 4.3: Nodal Coordinate System

The element coordinate system is used to determine the directions of orthotropic material properties (if any) for the material. In case of an isotropic material, any chosen element coordinate will produce the same results but utmost care should be taken in

choosing an element coordinate system while dealing with orthotropic materials. Further, the applied pressure direction is also dependent on the specific element coordinate system. Each element used to model the FEA problem has its own coordinate system, which is right-handed and an orthogonal system.

The finite element analysis results, calculated during the solution phase, are calculated in the nodal or element coordinate system, depending on the nodal or element solutions requested by the user. Generally more than one coordinate system is utilized while modeling the FEA problem. The calculated results from each coordinate system are then rotated into a single coordinate system, which is user defined, and called the result coordinate system.

4.2 Mathematical Modeling of the Physical Problem

Mathematical modeling of a physical problem using finite element analysis is referred to as mathematically recreating the behavior of an actual engineering system or problem to be solved at hand. In other words, FE analysis can be described as an accurate mathematical model of a physical prototype or system under load. The mathematical model comprises all the nodes, elements, material properties, real constants, boundary conditions, and other features that are used to represent the physical system.

A major commercial finite element code [27] was employed to make a mathematical model of a fluid structure interaction problem, i.e., a tank and a vessel partially filled with fluid. The partially fluid filled cylindrical containers were modeled using direct generation rather than solid modeling. By using the direct generation method, location of each and every node and the size, shape, and connectivity of each and every element is

determined manually instead of using an automatic mesh operation. The use of direct generation provides the analyst "the total control" over the mathematical model, or in other words, complete control over the geometry and numbering of every node and every element, which is extremely useful while verifying results.

Regardless of the sophistication of the hardware that may be utilized in such an analysis, inherent in a three-dimensional model of the cylindrical geometry is the eventual inclusion of triangular based (i.e., wedge shaped) fluid elements. Deviation from brick shaped fluid elements is not recommended and should be avoided if at all possible, especially at the fluid-solid structure interfaces. Given the choice between wedge shaped fluid elements being located along the axial centerline of the model or at the fluid-structure interface, obviously the former should be chosen. As previously identified, both the direct and indirect costs associated with three-dimensional models for sufficient grid convergence in the linear analysis become horrendous.

In an effort to avoid the previously identified undesirable features of a 3-D analysis, the advantages of the axisymmetric geometry of the cylindrical tank was maximized through the ingenious employment of the versatile axisymmetric harmonic four node contained fluid element "FLUID81" [27] and axisymmetric harmonic four node structural solid elements "PLANE25" [27]. The entire fluid-structure geometry was axisymmetric utilizing only rectangular elements to achieve quick grid convergence through a dense element mesh. This methodology to model and analyze the fluid structure interaction problem allowed highly accurate results to be obtained in reasonable times and man-hour expenditures, especially when compared to that required for any three-dimensional finite element model of fluid structure interaction problem. Axisymmetric harmonic elements

for the structure and the fluid finite elements are selected to model the subject problem. Both the structural and fluid elements have four nodes with three degrees of freedom (translations) at each node.

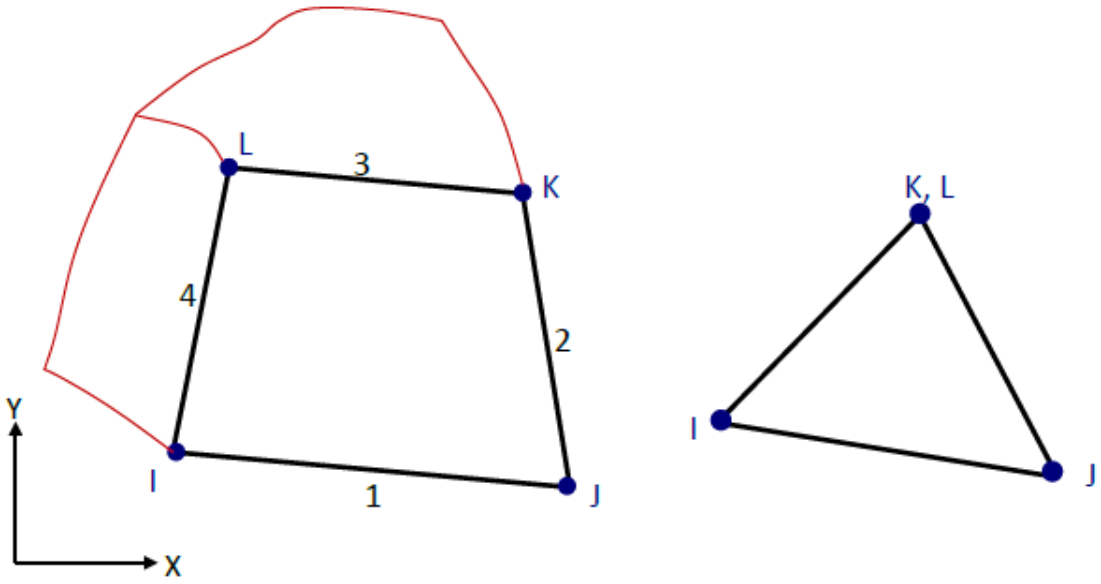

FIGURE 4.4: Axisymmetric Harmonic Structural Element

Fig. 4.4 shows the geometry of axisymmetric harmonic structural element. The structural element allows a triangular shape as shown in Fig. 4.4. The axisymmetric harmonic fluid element is shown in and Fig. 4.5.

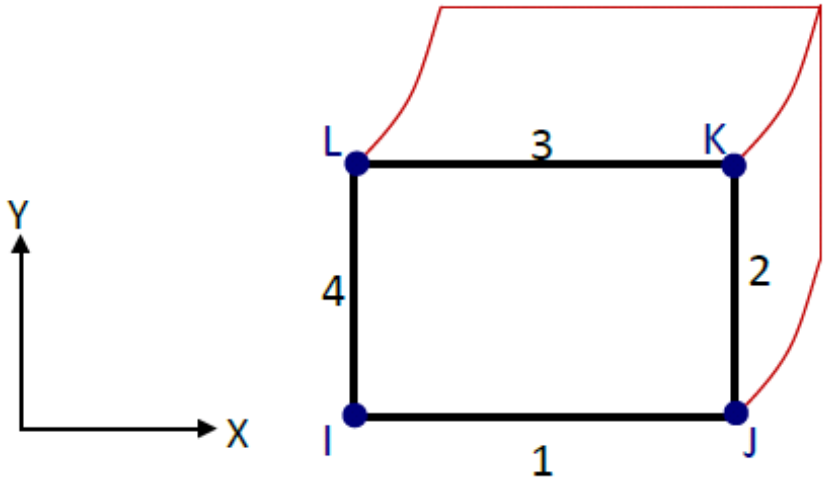

FIGURE 4.5: Axisymmetric Harmonic Fluid Element

For the structural portion of the model, at least two elements through the thickness are required to be included so that the shear effects may be determined. Only linear analysis should be used with selected axisymmetric elements. The axisymmetric geometry is modeled in the X-Y plane by taking the global Cartesian Y-axis as the axis of symmetry, i.e., it represents the axial direction (central-axis), the global Cartesian X-axis represents the radial coordinate (r) axis; and the global Cartesian Z-axis represents the circumferential coordinate **θ.** The model must be developed in positive global Cartesian X-coordinates as negative X-coordinates are not allowed. The free surface of the fluid is modeled at Y= 0.0 with the positive Y-direction vertically upward. At the fluid-structure interface, coincident nodes for the fluid and the tank were created. The axisymmetric geometric features of the math model for the container and its contents are shown in Fig. 4.6 below.

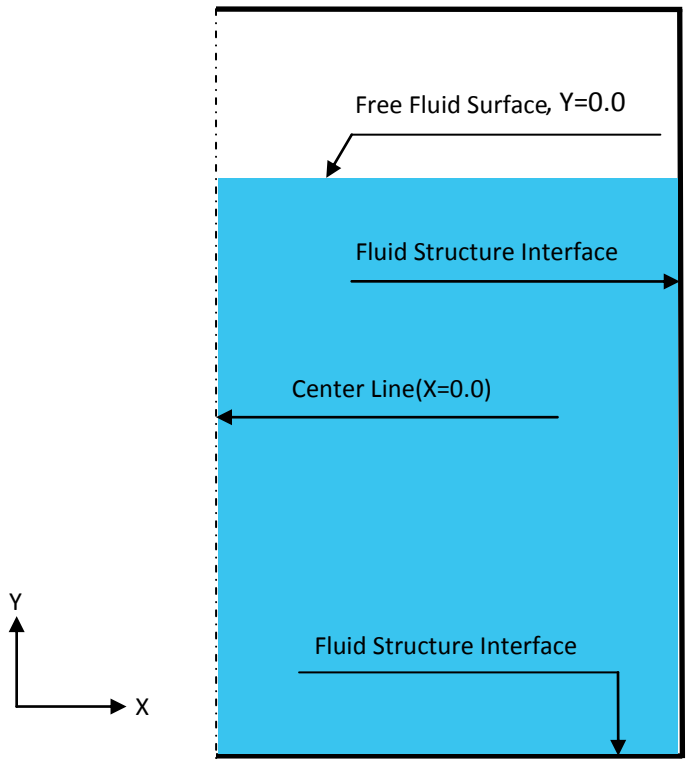

FIGURE 4.6: Axisymmetric Geometric Features of a Fluid Container Model

The material properties needed to model the problem include Young's modulus of elasticity and Poisson's ratio for structure elements, and the bulk modulus for fluid elements. The mass density for both structure and fluid material is also defined. The material properties and the geometrical properties (element size or dimensions of model) are used to form the stiffness matrix, whereas the inertial properties (mass) are used to form the mass matrix for the purpose of computation of results for static as well as dynamic analysis. The load applied to the model is used to form the load vector. There is no need to define real constants for axisymmetric harmonic elements.

All nodes on the bottom of structure were restrained against displacement in all three orthogonal directions thereby simulating the tank being rigidly fixed to the foundation and hence define the boundary conditions for the model. All nodes along the vertical centerline (both attached to structural and fluid elements) were restrained against displacement in vertical direction. Note that there was no vertical displacement along the vertical centerline for either structural or fluid nodes due to the horizontal motion of the tank. Further, fluid nodes along the vertical centerline at X=0.0 were forced to take the same displacements in the global Cartesian X and global Cartesian Z-directions (i.e., the two orthogonal horizontal directions) through the use of displacement constraint equations. The respective translations of coincident nodes were coupled in the direction normal to interface so that the fluid moved with the container walls only in the normal (i.e., orthogonal) direction while allowing fluid displacement in the other two shear directions. Different types of loads are applied to the mathematical model depending on the type of analysis (static analysis, modal analysis, and spectrum analysis) to be performed. These loads are discussed in the sections that follow.

4.3 Applied Mechanics (Static) Analysis

A static analysis is used to calculate the effects of steady loading conditions on the selected problem while ignoring inertia effects caused by time-varying loads. It is assumed that the loads and the selected problem's response vary slowly with respect to time. The steps to carry out a modal analysis are as given below:

- Constructing the mathematical model of the problem
- Appling loads to the model
- Obtaining the solution
- Reviewing the results

The mathematical model of the problem including boundary conditions and constraints is constructed as described in Section 4.2. The load (horizontal ground accelerations) is applied as sum of two orthogonal (radial and circumferential) accelerations. Generally loads in a static analysis are defined on nodes or elements, but the inertia loads are applied independent of model. Acceleration is applied as inertia load in terms of "g", the acceleration due to gravity. The total acceleration in the horizontal direction is the sum of radial and tangential accelerations as calculated by Eq. (1.5) through Eq. (1.7) and as shown in Fig. 1.6 in Chapter 1 of this dissertation. The expressions given by Eq. (1.5) through Eq. (1.7) are rewritten as Eq. (4.4), Eq. (4.5) and Eq. (4.6) in this section. For example a horizontal acceleration of 0.5g in the global Cartesian X-direction is input as the sum of 0.5g in the radial direction and -0.5g in the circumferential direction as calculated by Eq. (4.6.). Due to the use of fluid elements, acceleration due to gravity (in vertical direction) is applied as an inertia load, in addition to the already described horizontal inertia loads, to make the gravity springs on fluid

elements effective. The gravity springs are used to hold the free surface of the fluid in place, which is achieved by adding springs to each node, with the spring constants being positive on the top of the element, and negative on the bottom. For an interior node, the positive and negative effects cancel out. At the bottom (fluid-structure interface) where the fluid is contained, the negative spring has no effect as all degrees of freedom at the bottom of the container structure are fixed. An expression to calculate response (displacements), {U} for a static analysis is given in Eq. (4.7), where {F} is the applied static force vector. In the case of a horizontal acceleration, {Acc} is the applied inertia load and the response can be calculated by using Eq. (4.8).

$$Acc = \int_0^{2\pi} \left(\text{Acc per unit length}\right)\left(\text{Directional cosines}\right)\left(\text{Increment length}\right) \tag{4.4}$$

$$Acc = \int_0^{2\pi} \left(\frac{\mathrm{A_X}\cos(\theta)}{2\pi R}\left(\cos(\theta)\right) + \frac{\mathrm{A_Z}\sin(\theta)}{2\pi R}\left(\text{-}\sin(\theta)\right) \right)\left(\mathrm{Rd}\theta\right) \tag{4.5}$$

$$Acc = \frac{\mathrm{A_X} - \mathrm{A_Z}}{2} \tag{4.6}$$

$$[K]\{U\} = \{F\} \tag{4.7}$$

$$[K]\{U\} = -[M]\{Acc\} \tag{4.8}$$

The solution to the problem is obtained by running the analysis and results (displacements, strains and stresses) are available for viewing in the post-processing phase. It may be noted that the results for the static problem are available all around the circumference as in the case of a full 3-D analysis by the use of a Fourier series as given by Eq. (4.8). It is worth mentioning that the results in post-processing can be scaled by a multiplier as the analysis carried out is linear.

$$F(\theta) = A_0 + A_1 \cos(\theta) + B_1 \sin(\theta) + A_2 \cos(2\theta) + B_2 \sin(2\theta) + \cdots \quad (4.9)$$

4.4 Modal Analysis

A mode-frequency (modal) analysis is used to determine natural frequencies and mode-shapes of the subject water-filled cylindrical container. The natural frequencies and mode shapes are important parameters in the design of a structure for dynamic loading conditions. Modal analysis is the basis of any dynamic analysis. It is the first step in the direction of a dynamic analysis. Modal analysis results (frequencies and mode shapes) are also required for the subsequent single point response spectrum analysis. The only modal analysis valid while using fluid elements is a "reduced" modal analysis based upon the Householder-bisection-inverse algorithm, which condenses the mass and stiffness matrices using the familiar Guyan reduction method [28]. The steps to carry out a modal analysis are as given below:

- Constructing the mathematical model of the problem
- Appling loads to the model
- Obtaining the solution and expanding the modes
- Reviewing the results

The mathematical model of the problem including boundary conditions and constraints is constructed as described in Section 4.2. In addition to applied constraints appropriate master degrees of freedom (MDOF) were selected to perform the reduced modal analysis by reducing the size of the matrix. Matrix reduction allows the analyst to use only a portion of the problem at hand for a dynamic analysis. The dynamic portion is chosen by identifying master degrees of freedom that characterize the dynamic behavior of the model. All fluid nodes at the free surface were selected MDOF in vertical

direction as recommended by the selected FE code [27]. An additional number of structural nodes were selected as MDOF in all three directions based on the dynamic characteristics of the container structure. Assumptions were made that the inertia forces of slave degrees of freedom (DOF) are negligible as compared to the chosen MDOFs. Matrix reduction is a way to reduce the size of the matrices of a model and perform a quicker and cheaper analysis. Usually there are no external loads applied in the case of a modal analysis and it is independent of the gravitational field, but in the case of fluid elements, acceleration due to gravity (in vertical direction) is applied as an inertia load to make the gravity springs on fluid elements effective. The use of gravity springs is discussed in the previous section. The results were calculated for MDOF while ignoring slave DOFs, which were reduced out of the initial solution. The final solution was then expanded to the full DOF set for the subject model. The equations of motion for a free, undamped multiple DOF vibration problems, as discussed previously in Eq. (3.39), are given by Eq. (4.10). The **n** number of circular frequencies, natural frequencies and Eigen vectors can be calculated by method described in Section 3.2.1, by using expressions given by Eq. (3.39) through Eq. (3.46).

$$[M]\{\ddot{U}\}+[K]\{U\}=0 \tag{4.10}$$

The physical interpretation of the Eigen vector (mode shape) for this type of problem is a set of displacements at each node for the mode's respective natural frequency. The calculated Eigen vectors are normalized with respect to mass matrix for ease of future calculations are described in Section 3.2.2, by using Eq. (3.61) through Eq. (3.71). The mass participation factor for each mode is then defined as shown below in Eq. (4.11),

where the vector $\{D\}$ is the vector describing the direction for the base excitation (i.e., the acceleration in the case).

$$\gamma_i = \{\Phi\}_{iN}^T [M]\{D\} \tag{4.11}$$

In addition, the effective mass for each mode is defined as shown in Eq. (4.12). Substituting Eq. (3.67) into Eq. (4.12) results in the expression shown in Eq. (4.13). Ultimately, the mass normalized Eigen vector allows the mass participation factor to be represented by the square root of the effective mass and Eq. (4.13) gives a quantitative estimate of the fraction of mass that is involved in each mode of vibration.

$$M_{eff\_i} = \frac{\gamma_i^2}{\{\Phi\}_{iN}^T [M]\{\Phi\}_{iN}} \tag{4.12}$$

$$M_{eff\_i} = \gamma_i^2 \tag{4.13}$$

4.5 Single Point Response Spectrum Analysis

In the single point response spectrum (SPRS) analysis, the spectral accelerations from a requisite seismic response spectrum curve corresponding to the natural frequencies resulting from the modal analysis are applied to the fluid-filled container in the form of a base excitation, to calculate displacements and stresses in the model. SPRS analysis is used to determine the response of structures to random or time-dependent loading conditions such as earthquakes. The steps to carry out a modal analysis are as given below.

- Constructing the mathematical model of the problem
- Perform a modal analysis
- Appling the response spectrum curve

- Obtaining the solution, and combining the modes
- Reviewing the results

The first two steps of the procedure are explained in detail in the previous section of this dissertation. The IEEE-693-2005 response spectrum curve [29] shown in Fig. 4.7 was used in the analysis described herein. The individual response from each mode is calculated as given by Eq. (4.14), where Ψ_i is the generalized modal response corresponding to $\{\Phi\}_{iN}$ and A_i is termed the mode coefficient. In the current case of a base excitation (acceleration), A_i is defined by Eq. (4.15). The total response is then calculated by combining responses from the individual modes as given by Eq. (4.16).

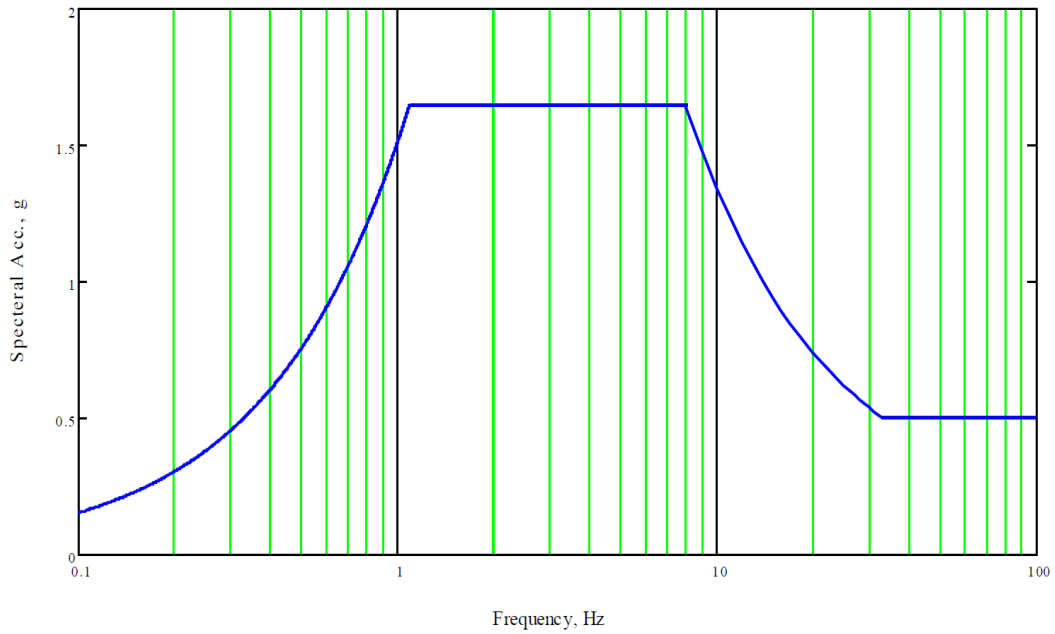

FIGURE 4.7: IEEE-693-2005 Response Spectrum Curve

For the current study, the participating modes are combined by the square root of the sum of the squares (SRSS) of the individual modal responses. Note that in practice, the combination method "chosen" by an analyst is most often specified by project design requirements and by the authority having design jurisdiction.

$$R_i = A_i \Psi_i \tag{4.14}$$

$$A_i = \frac{Sa_i \gamma_i}{\omega_i^2} \tag{4.15}$$

$$R_{total} = \sum_{i=1}^{N} \sqrt{R_i^2} \tag{4.16}$$

It is to be noted that all the computed modes do not contribute to the total response of the structural system. In fact, only a few modes (in general) are significant in the total response. The numbers of modes to be combined are ultimately user specified and depend on the design basis and Code for which the tank must be designed or analyzed. The mode coefficient ratio as defined by Eq. (4.17) is very useful in finding the first, second, third, and higher principal modes for the purpose of combining the significant modes. The maximum mode coefficient is identified and all other mode coefficients are normalized to the former mode coefficient (i.e., divided by the maximum mode coefficient). Again, in the present study, the first six significant modes were combined using SPRS analysis in this case.

$$A_{ratio\_i} = \frac{A_i}{A_{\max\_i}} \tag{4.17}$$

The SPRS analysis as discussed in the preceding paragraphs, does have a single disadvantage when compared to a full three dimensional model. When utilizing only the available axisymmetric harmonic elements, response results are typically only available at $\boldsymbol{\theta}$=0°, where the cos($\boldsymbol{\theta}$) is a maximum. For response values located around various circumferential locations on arbitrary planes, the use of the SPRS analysis in combination with the utilization of axisymmetric harmonic elements limits the full understanding of the effects of the applied linear horizontal acceleration on the fluid-filled tank.

4.6 Post-processing of Results

While designing a new tank or analyzing an existing tank, response results at several locations around the circumference should be checked. During careful examination of the mathematics involved in the axisymmetric SPRS analysis, one may observe that the analysis fails to give results all around the circumference or in the true three-dimensional form familiar to the experienced analyst. Through the implementation of a Fourier series in the applied base acceleration, a method was developed to obtain the desired results (both displacements and stresses) around the circumference while using axisymmetric harmonic elements.

For axisymmetric harmonic elements, loads are defined in terms of a series of a harmonic function (Fourier series) as shown in Eq. (4.18). A_0 is the constant term in the series that represents the axisymmetric portion of the loading and can be seen to be independent of the circumferential location (i.e., independent of **θ**). A_1 is the Fourier coefficient that is the multiplier against cos(**θ**) and represents the non-axisymmetric (or asymmetric) loading condition, which obviously is a function of circumferential coordinate **θ**. Then Eq. (4.14) can be rewritten to implement the Fourier series representation on the applied acceleration as given in the requisite seismic response spectrum as given by Eq. (4.19).

$$F(\theta) = A_0 + A_1 \cos(\theta) \tag{4.18}$$

$$R_i = A_i \Psi_i \cos(\theta) \tag{4.19}$$

Substituting θ=0° into Eq. (4.19) returns the previous definition as shown in Eq. (4.14). The aforementioned result, as previously discussed, gives the response due to n^{th} mode for the circumferential plane located at 0° of the cylinder. In practice, either a

built-in command for specifying the exact desired circumferential location that incorporates the cos(**θ**) multiplier in the commercial software or a user written mathematical operator can be utilized to achieve the form given by Eq. (4.19). The individual responses of participating modes were combined "manually" during post-processing. Each individual response to be combined in accordance with Eq. (4.16) was written as a separate load case to a results file and then the load cases were combined using an SRSS load case operator. It may be noted that there was no need to calculate mode coefficients and mode coefficient ratios manually as they were easily obtained from the FEA output file of SPRS analysis discussed in the previous section.

CHAPTER 5: VERIFICATION OF NON-AXISYMMERTIC LOADS APPLIED TO AN AXISYMMETRIC GEOMETRY

5.1 Tank Geometry

The ultimate goal of this dissertation was to develop a robust method to analyze fluid-structure interactions in partially fluid filled cylindrical vessels due to seismic loading, by taking advantage of the axisymmetric geometry of the cylindrical vessel and using axisymmetric harmonic elements. Some cylindrical vessels have a complex geometry (cylindrical vessel with torospherical heads) and are elevated from the ground by skirt supports. The method to analyze tanks or vessels using axisymmetric harmonic elements for response results all around the circumference was first developed for a simpler geometry, i.e., a fluid filled cylindrical tank with flat top and bottom heads and supported by a fully anchored base attached to a rigid foundation on the ground. The finite element analysis method developed for the simple geometry was then applied to the complex vessel geometry. The liquid filled vertical cylindrical tank geometry utilized for the development of the analysis method is shown in Fig. 5.1. The tank has an outside diameter of 20 ft. and has an overall height of 20 ft. The tank has a uniform wall thickness of 0.5 in and has flat top and bottom heads 0.500 in. thick. The tank is simulated to be rigidly fixed to its foundation on the ground. The material properties of tank material include a Young's modulus of elasticity of 30,000,000 psi and a Poisson's ratio of 0.3. The mass density of the tank material is 7.32×10^{-4} $lb_m/in.^3$. The tank is filled with fluid to a height of 18 ft. from the tank base. The contained fluid utilized in

the analysis was water having a mass density of 9.29 $x10^{-5}$ $lb_m/in.^3$. The tank was first analyzed without any fluid in it and then the analysis was carried out for a fluid filled tank. The methodology developed in the previous chapter was employed in analysis of the tank.

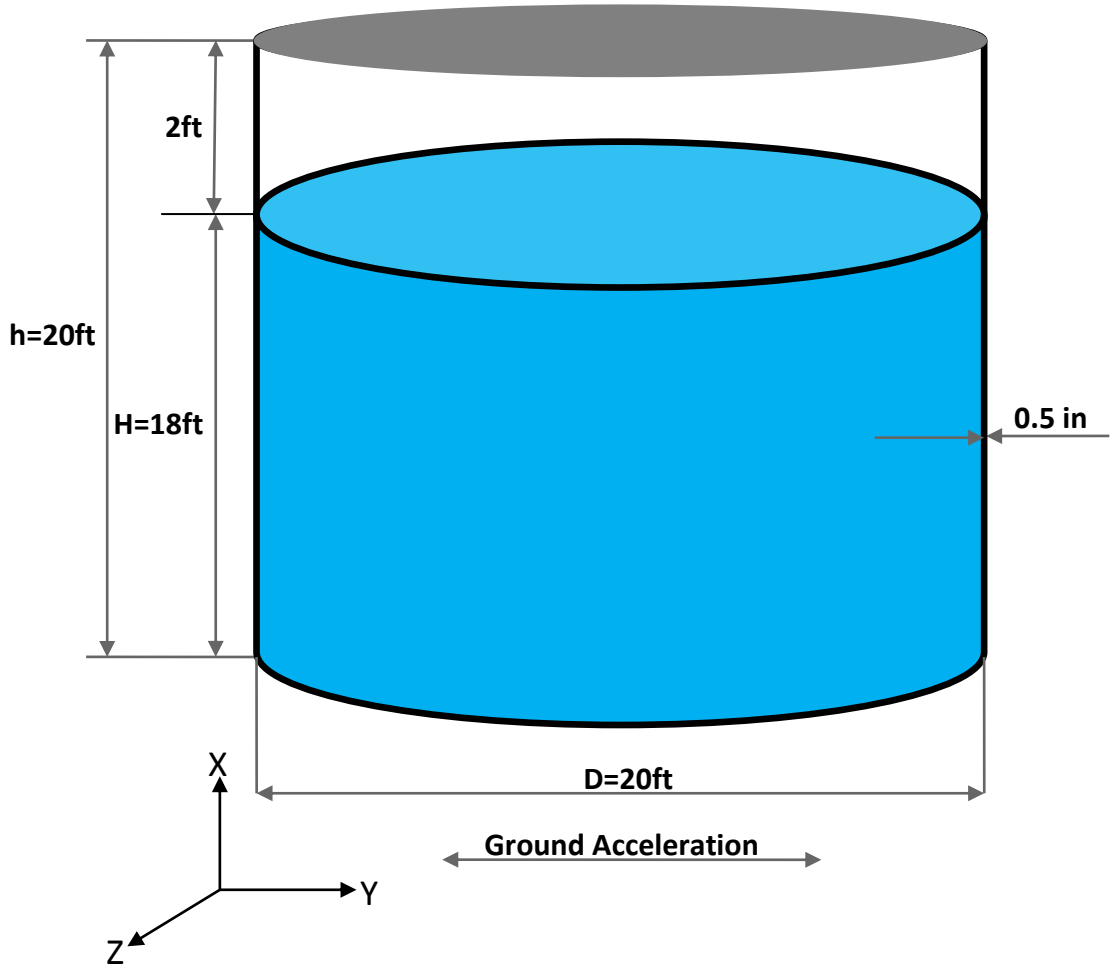

FIGURE 5.1: Vertical Cylindrical Tank Dimensions

5.2 Analysis of Empty Tank

The empty tank was analyzed for static and dynamic loads (ground acceleration). The axisymmetric geometric features of the ground supported empty tank with flat heads are shown in Fig.5.2. The empty tank was modeled with two elements through the

thickness of the top head, bottom heads and shell wall to include the shear effects due to both the applied loads. Three test cases having two, four and six elements through the thickness of tank structure were run to check for convergence of the FEA results. The results of three analyses were compared and based on these results it was decided that two elements through the thickness of structure are sufficient for grid convergence. The element and nodal coordinate systems were chosen parallel to global Cartesian coordinate system. The structural elements utilized a geometric aspect ratio of approximately 2:1 throughout with element dimensions of approximately 0.250 in. x 0.500 in.

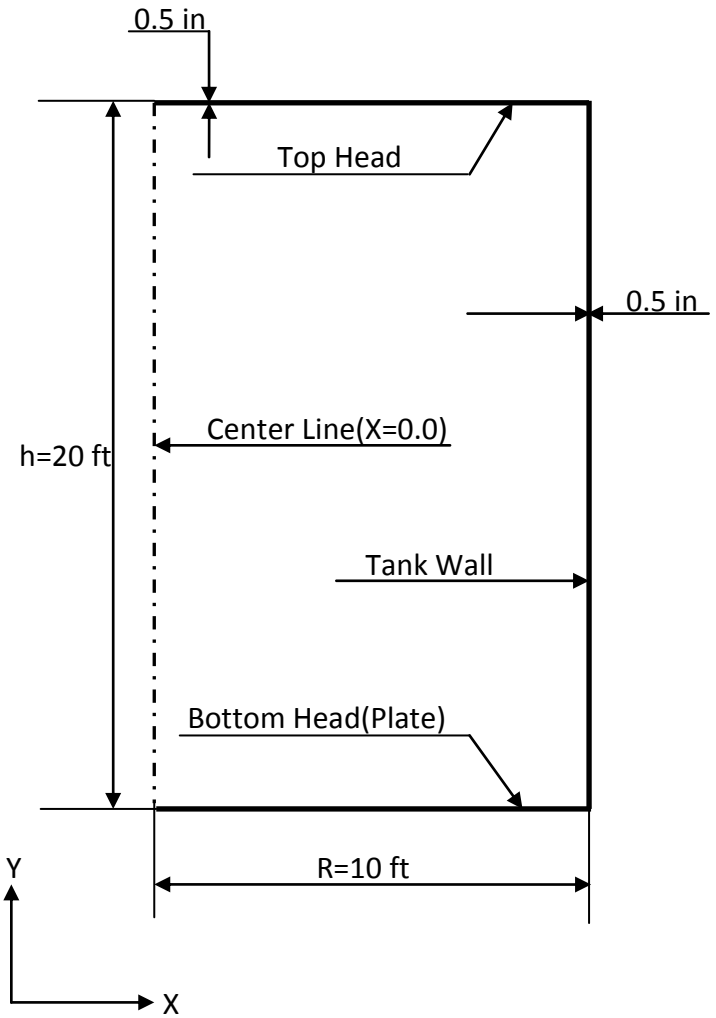

FIGURE 5.2: Axisymmetric Model Features of Empty Tank

The analysis of the empty tank was carried out in three phases. First a static analysis of tank was performed, followed by a detailed modal analysis, and concluded with a spectrum analysis of the axisymmetric model. Finally the participating modes were combined in post-processing of the results to obtain the required responses.

5.2.1 Static Analysis of Empty Tank

The tank was analyzed for static loading by applying a ground acceleration of 0.5g in the horizontal direction. The acceleration in static analysis is applied as an inertia (gravity) load. Acceleration of 0.5g in the horizontal direction was applied by applying a combination of 0.5g acceleration in the radial and -0.5g in the circumferential directions as per Eq. (4.6). The displacements as well as stresses in the structure are then calculated by the FEA code, which can be viewed at any desired location around the circumference.

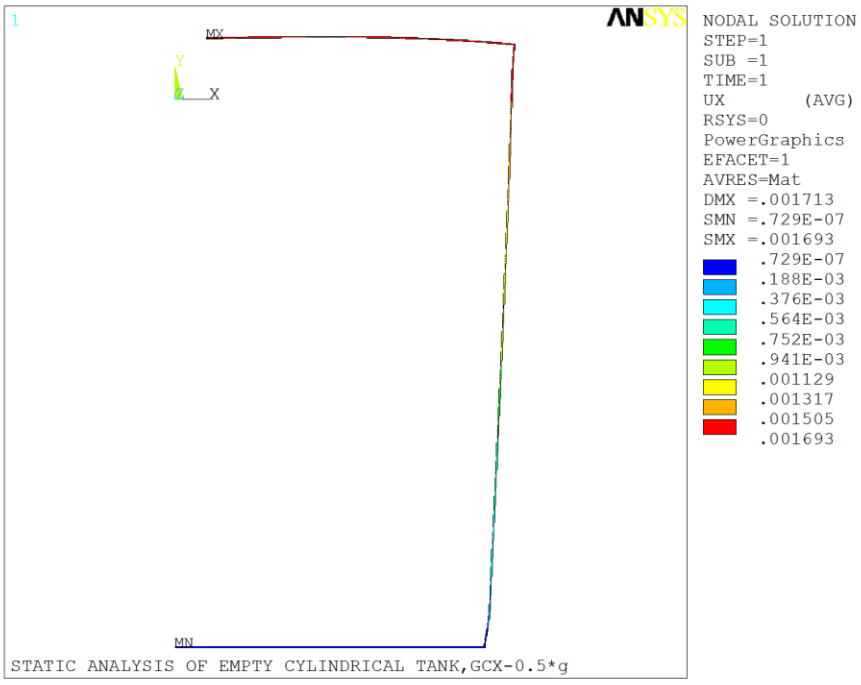

FIGURE 5.3: Horizontal Translations in Tank Structure at **θ=0°**

Displacements (translations) of the tank structure in the horizontal direction at zero degrees and forty five degrees around the circumference (i.e., at the chosen locations for response results) are shown in Fig. 5.3 and Fig. 5.4, respectively.

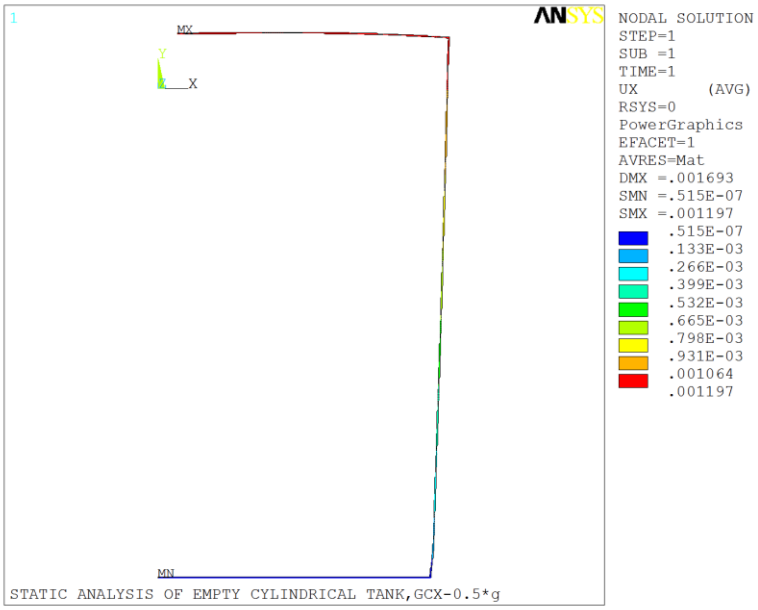

FIGURE 5.4: Horizontal Translations in Tank Structure at **θ=45°**

The maximum horizontal displacement of 0.169×10^{-2} in. was observed at the top plate of tank as shown in Fig.5.3 at a location of zero degrees around the circumference and a maximum horizontal displacement of 0.120×10^{-2} in. is observed at the same node as shown in Fig.5.4 but at a location of forty five degrees around the circumference of the tank. It may be observed that the displacement at forty five degrees around the circumference can be calculated by multiplying the displacement at zero degrees by the cosine of forty five degrees. This observation holds true not only at forty five degrees but also for any angle around the circumference, and hence confirming the use of Fourier series as given by Eq. (4.18). The results for vertical displacements, strains, stresses and reaction forces can also be observed by plotting the respective contours or by listing the respective solution at all the nodes in the post-processing phase.

5.2.2 Modal Analysis of Empty Tank

A mode-frequency (modal) analysis was carried out to determine natural frequencies and mode-shapes of the empty tank. A "reduced" modal analysis was employed based upon the Householder-bisection-inverse algorithm by condensing mass and stiffness matrices using the familiar Guyan reduction method [28]. A number of nodes, approximately one sixth of the nodes equally spaced on the tank wall, were selected as master degrees of freedom (MDOF) in two horizontal directions as the tank wall is expected to vibrate in the horizontal direction. Very few nodes were selected MDOF in the vertical direction as the tank wall is not expected to vibrate in the vertical direction. A number of nodes on the top head, approximately one fifth of nodes and equally spaced from each other, on the top head of the tank were selected as MDOF in vertical direction as the top head is expected to vibrate in the vertical direction and some nodes were selected as MDOF in the horizontal direction as the tank head may also vibrate in the horizontal direction with the tank wall. No node on the bottom head was a selected MDOF as it is not expected to vibrate at all, because it is rigidly fixed to the foundation. Natural frequencies and Eigen vectors for fifty modes were determined by using the FEA code. The calculated natural frequencies, participation factors, participation factor ratios and effective masses for the first ten modes are shown in Table 5.1. It may be noted that the participation factors and effective masses as shown in Table 5.1 are for the horizontal direction, which is the direction of the applied ground acceleration to the subject tank. Participation factors and effective masses for the vertical direction and the other horizontal (Z-direction) are also calculated during the modal analysis. These can be used to apply the ground acceleration in the respective vertical

and Z-directions and are not used in the analysis carried out herein. The participation factor ratio helps to determine the principal modes for a particular direction. The first principal mode shape in the horizontal direction is the fourth mode corresponding to the frequency of 60.400 Hertz and corresponding to the largest participation factor. The second principal mode shape in the horizontal direction is the eighth mode corresponding to the frequency of 172.185 Hertz and corresponding to the second highest participation factor as shown by the data in Table 5.1.

TABLE 5.1: Participation Factors in Horizontal Direction

Mode	Frequency (Hz)	Participation Factor ($lb_m^{1/2}$)	Participation Factor Ratio	Effective Mass (lb_m)
1	6.912	-0.366E-03	0.333E-4	0.134E-06
2	19.832	0.137E-01	0.179E-3	0.188E-03
3	39.233	-0.729E-01	0.123E-1	0.532E-02
4	**60.400**	**-5.816**	**1.000**	**33.822**
5	65.192	**-0.5782**	0.995E-1	**0.334**
6	97.558	0.109	0.189E-1	0.120E-01
7	136.348	-0.776E-01	0.135E-1	0.602E-02
8	**172.185**	**2.486**	**0.427**	**6.183**
9	181.132	-0.301E-01	0.503E-2	0.908E-03
10	226.087	-0.509	0.876E-1	0.259

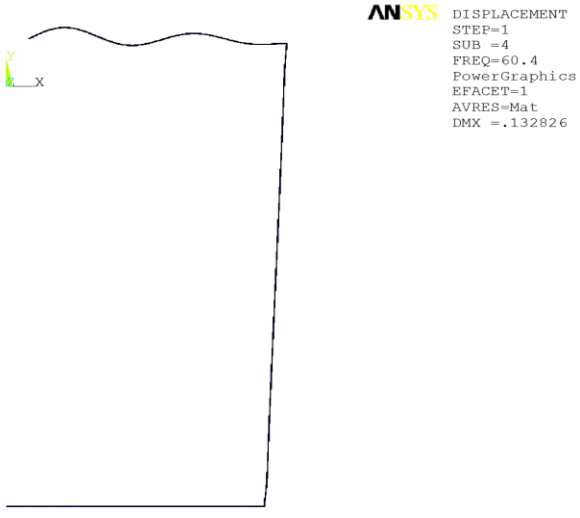

FIGURE 5.5: First Mode Shape for Empty Tank

The mode shapes for the first two principal modes, i.e., the fourth and eighth modes in the horizontal direction are shown in Fig. 5.5 and Fig. 5.6, respectively.

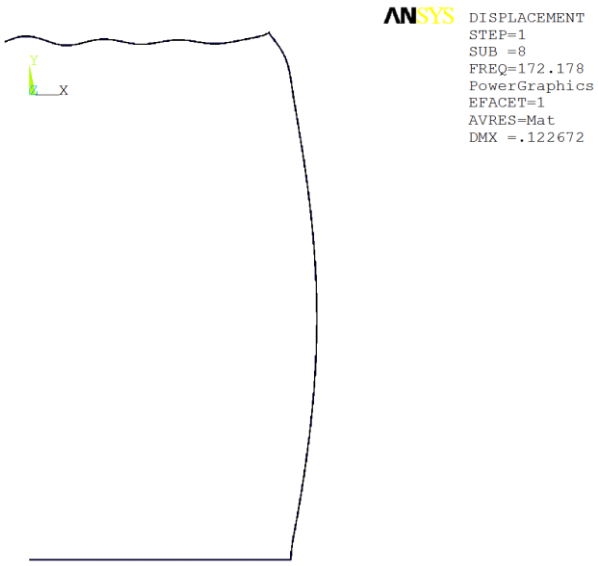

FIGURE 5.6: Second Mode Shape for Empty Tank

5.2.3 Single Point Response Spectrum Analysis of Empty Tank

A single point response spectrum (SPRS) analysis of the empty tank was initiated to determine the mode coefficients and mode coefficient ratios, which in turn are used to determine the modes to be combined and also the number of modes to be combined to obtain the final response. The required mode coefficients and mode coefficient ratios can be obtained from the output file of the FEA code [27]. The IEEE-693-2005 response spectrum curve [29] shown in Fig. 4.7 was used to carry out the SPRS analysis. The calculated spectral acceleration values (in base units, and not multiples of g), mode coefficients, mode coefficient ratios along with natural frequencies, participation factors and effective mass are shown in Table 5.2. It can be observed for the data given in Table 5.2 that the fourth mode, i.e., the first principal mode in the horizontal direction, having a

mode coefficient ratio of one is the most dominant mode contributing to the total response followed by the fifth and eighth modes. The contribution to the total response for a particular mode is proportional to its mode coefficient ratio. The higher the mode coefficient ratio, the higher its contribution to the total response. The contribution decreases as the mode coefficient decreases.

TABLE 5.2: Mode Coefficients in Horizontal Direction

Mode	Frequency (Hz)	S.V. (in/s^2)	Participation Factor ($lb_m^{1/2}$)	Mode Coefficient ($in\text{-}lb_m^{1/2}$)	M.C. Ratio	Effective Mass (lb_m)
1	6.912	645.291	-0.366E-03	-0.125E-03	0.160E-1	0.134E-06
2	19.832	287.582	0.137E-01	0.254E-03	0.325E-1	0.188E-03
3	39.233	193.202	-0.729E-01	-0.232E-03	0.297E-1	0.532E-02
4	**60.400**	**193.200**	**-5.816**	**-0.780E-02**	**1.000**	**33.822**
5	65.192	**193.200**	**-0.5782**	**-0.666E-03**	**0.853E-1**	**0.334**
6	97.558	193.200	0.109	0.564E-04	0.723E-2	0.120E-01
7	136.348	193.200	-0.776E-01	-0.204E-04	0.262E-2	0.602E-02
8	**172.185**	**193.200**	**2.486**	**0.410E-03**	0.526E-1	**6.183**
9	181.132	193.200	-0.301E-01	-0.449E-05	0. 576E-3	0.908E-03
10	226.087	193.200	-0.509	-0.488E-04	0.625E-2	0.259

5.2.4 Combination of Modes for Empty Tank

The participating modes were identified by their respective mode coefficient ratios and the individual participating modes were combined “manually” in the post-processing phase using the square root of the sum of the squares (SRSS) load case operator. Two locations around the circumference, zero degrees and forty five degrees were chosen as the desired location for response results. As discussed earlier in this dissertation, all the computed modes do not contribute to the total response of the structural system and only a few modes, in general, are significant in the total response. It was decided to combine modes having mode coefficient more than 0.05, i.e., for this case, modes numbered four, five and eight were combined. Displacements in the

structure in the horizontal direction at zero and forty five degrees around the circumference (the chosen location for response results) were calculated and are shown below in Fig. 5.7 and Fig. 5.8, respectively.

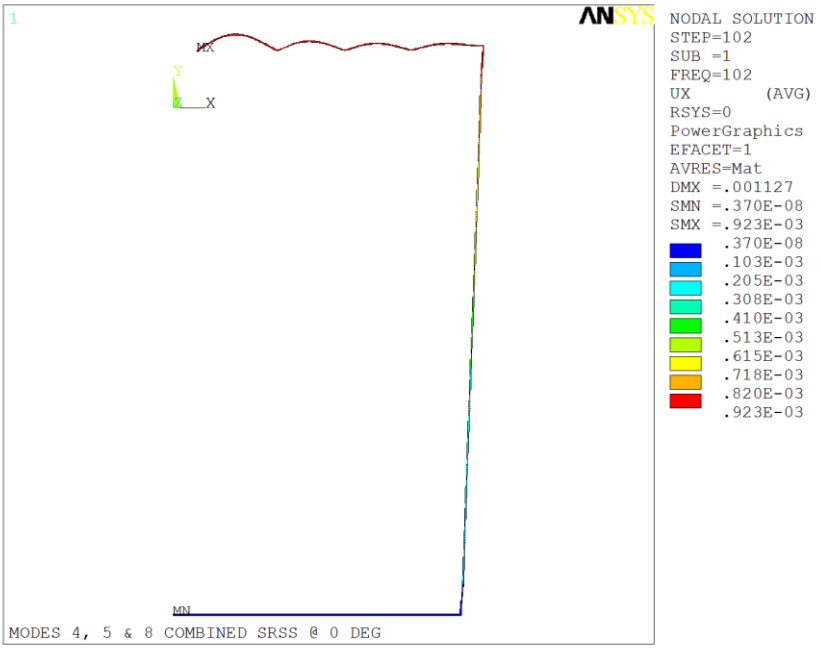

FIGURE 5.7: Horizontal Translations in Tank Structure at **θ=0°**

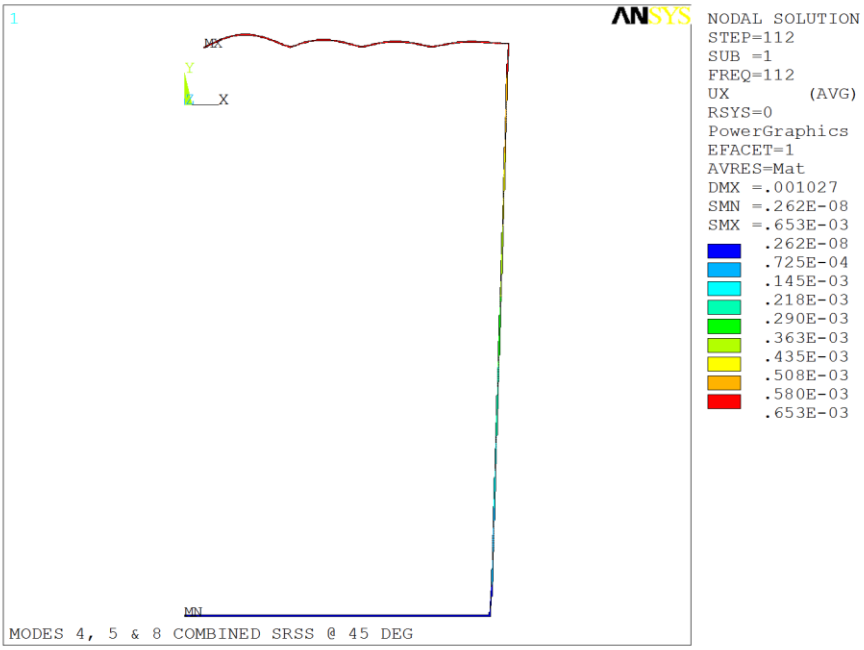

FIGURE 5.8: Horizontal Translations in Tank Structure at **θ=45°**

It can be clearly concluded by comparing plots for displacement (response) in Fig. 5.7 and Fig. 5.8 and plots for mode shapes in Fig. 5.5 and Fig. 5.6 that the first significant mode dominates the response results and is the major contributor towards the total response. The higher modes do not provide a significant contribution to the total response of the structure.

5.3 Analysis Water Filled Tank

The empty tank analyzed in the previous section was filled with water and was analyzed for both static as well as dynamic loads (ground acceleration). The geometric features of the axisymmetric model of the ground supported water filled tank with flat heads are shown in Fig. 5.9. In addition to nodes and elements for the empty tank, nodes and elements for the fluid were created. The free surface of the liquid was modeled at Y= 0.0 with the positive Y-direction vertically upwards. Coincident nodes were created at the fluid structure interface for the fluid and the tank wall. The coincident nodes were coupled in the direction normal to the interface, i.e., at the base plate coincident fluid and structure nodes were coupled in the vertical direction. At the tank wall, the coincident fluid and structure nodes were coupled in the horizontal direction so that the fluid moved with the tank walls only in the normal direction, while allowing fluid displacement in the other two shear directions. In addition to already existing boundary conditions for structure elements, all fluid nodes along the vertical centerline were restrained against displacement in the vertical direction. All the fluid nodes along the vertical centerline at X=0.0 were forced to take the same displacements in the two orthogonal horizontal directions by using displacement constraint equations. The four node axisymmetric fluid element shown in Fig. 4.5 was employed to model the contained fluid. The element and

nodal coordinate system were chosen parallel to the global Cartesian coordinate system. The geometric aspect ratio of fluid elements was chosen as 1:1 throughout the model with dimensions of approximately 0.500 in. on side. Acceleration due to gravity was applied to make the fluid springs effective, which are used to hold the free surface of fluid in place. The application of gravity springs is discussed in detail in the previous chapter of this dissertation. The acceleration due to gravity was applied irrespective of the type of analysis to be performed, i.e., for structural, modal, and spectrum analyses.

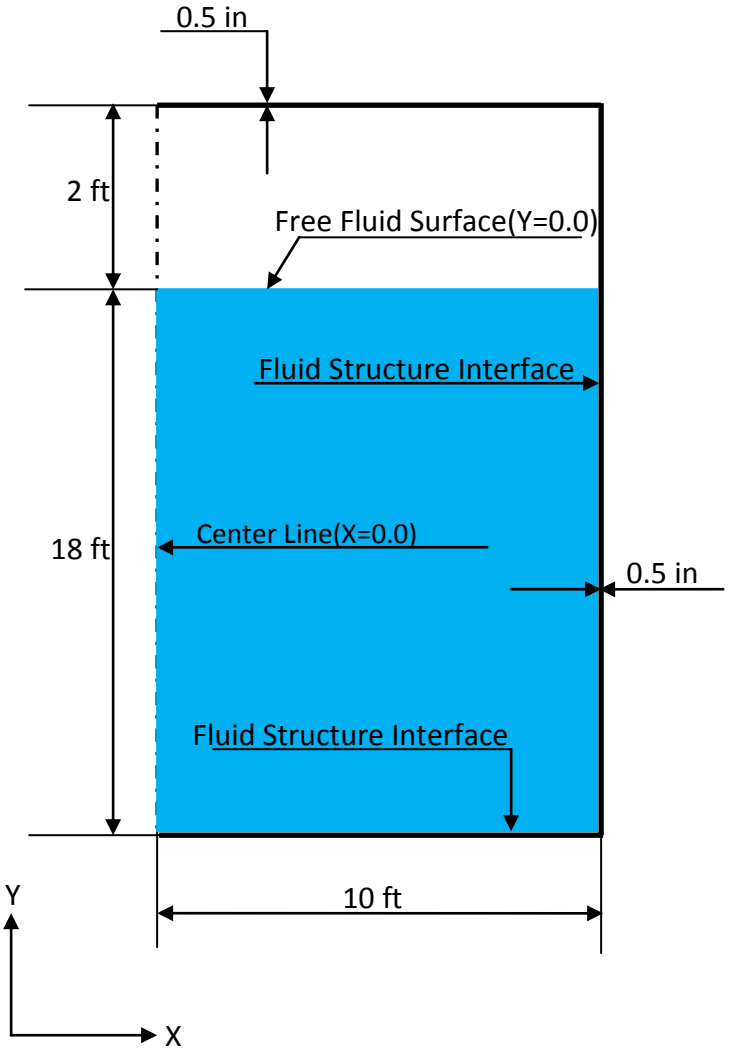

FIGURE 5.9: Axisymmetric Model Features of Fluid Filled Tank

The fluid filled tank was analyzed for static loads as well as dynamic analysis. The dynamic analysis is carried out in two phases, the modal analysis in the first phase to get the frequencies, mode shape and participation factors followed by the spectrum analysis to obtain the required mode coefficients, and finally, combining the participating modes to calculate the total response.

5.3.1 Static Analysis of Water Filled Tank

The tank was first subjected to a uniform ground acceleration of 0.5g in the horizontal direction as an inertia load. The ground acceleration was applied as per Eq. (4.6). The displacements and resulting stresses in the structure are then calculated by the FEA code, which can be viewed at a desired location around the circumference.

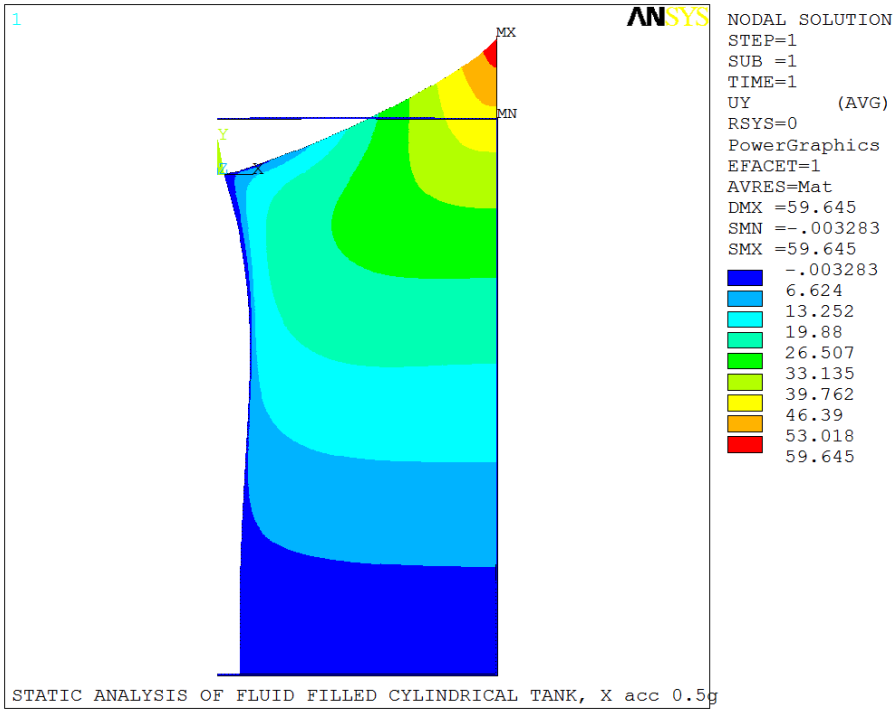

FIGURE 5.10: Vertical Translations in Fluid at **θ=0°**

Displacements of the fluid in the vertical direction at the chosen locations, zero degrees and forty five degrees around the circumference, are shown in Fig. 5.10 and Fig.

5.11, respectively. A maximum displacement of the fluid in the vertical direction at zero degrees around the circumference is observed to be 59.645 in. as shown in Fig.5.10 and at forty five degrees around the circumference is 42.176 in. as shown in Fig. 5.11. It may be observed that the displacement at forty five degrees around the circumference is the displacement at the zero degrees location, multiplied by the cosine of forty five degrees. This observation holds true for any angle around the circumference, and hence once again confirming the use of Fourier series as given by Eq. (4.18). The results for the horizontal displacements, strains, stresses and reaction forces can also be observed by plotting the respective contours or by listing the respective solution at all the nodes in the post-processing phase.

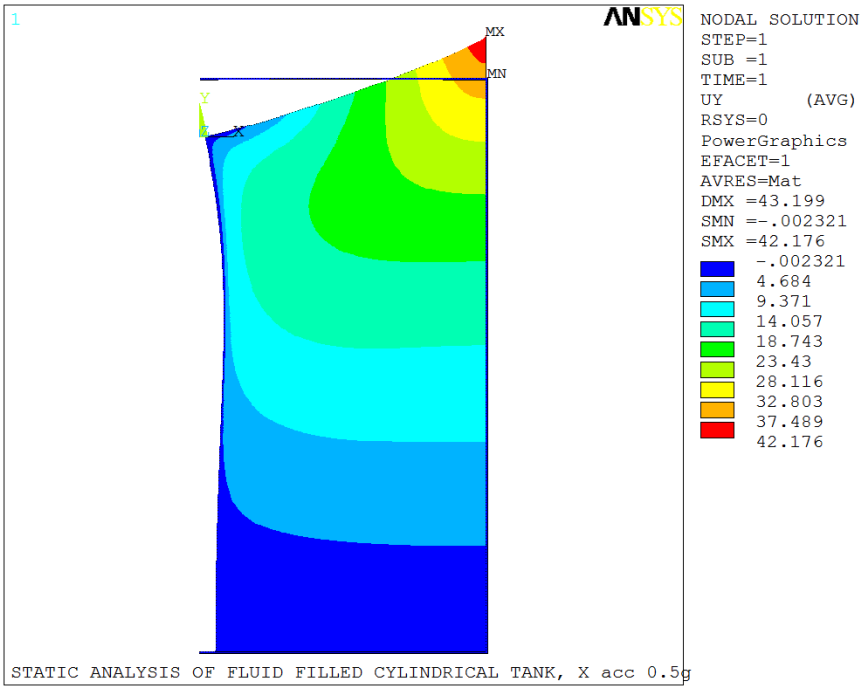

FIGURE 5.11: Vertical Translations in Fluid at **θ=45°**

The stress plot for the bottom head and vertical wall intersection is shown in Fig. 5.12. The maximum stress of 1903 psi is observed at the outside tank wall along the base plate tank wall intersection.

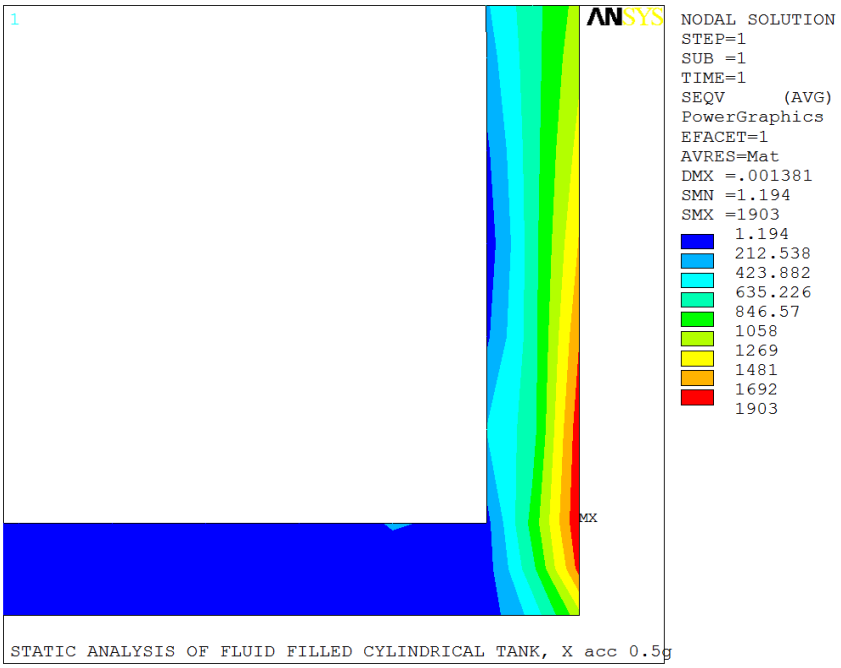

FIGURE 5.12: Stresses at Bottom Head and Vertical Wall Intersection

5.3.2 Modal Analysis of Water Filled Tank

The natural frequencies and mode-shapes of the fluid filled tank were determined by initiating a modal analysis. A "reduced" modal analysis was used based upon the Householder-bisection-inverse algorithm, which condenses the mass and stiffness matrices using Guyan reduction method [28]. In addition to selected master degrees of freedom (MDOF) for the empty tank, additional MDOF were selected for the fluid nodes. All the fluid nodes at the free surface (Y=0.0) were selected as MDOF in the vertical direction as required by the FEA code [27]. The upper part of the fluid in the tank near the free surface, vibrated in low frequencies and independent of the tank walls. This fluid as discussed earlier is termed the convective fluid. The remainder of the fluid, i.e., the part that moves with the tank walls, and that vibrates in higher frequencies, is the impulsive fluid. The calculated natural frequencies, participation factors, participation factor ratios, and effective masses for the convective and impulsive fluid masses are

shown in Table 5.3 and Table 5.4, respectively. The participation factor and effective masses as shown in Table 5.3 are for the horizontal direction, which is the direction of the applied ground acceleration. The first principal convective mode in the horizontal direction is the first mode corresponding to the frequency of 0.339 Hertz and the second convective mode in the horizontal direction is the second mode corresponding to the frequency of 0.604 Hertz as shown in Table 5.3.

TABLE 5.3: Convective Participation Factors in Horizontal Direction

Mode	Frequency (Hz)	Participation Factor ($lb_m^{1/2}$)	Participation Factor Ratio	Effective Mass (lb_m)
1	**0.339**	**18.546**	**0.522**	**343.956**
2	**0.604**	**-4.544**	**0.127**	**20.649**
3	**0.778**	**1.779**	**0.500E-1**	**3.166**
4	0.922	-1.329	0.374E-1	1.766
5	1.046	0.715	0.201E-1	0.511
6	1.156	-0.686	0.193E-1	0.470
7	1.258	0.404	0.113E-1	0.163
8	1.352	-0.436	0.122E-1	0.190
9	1.440	0.267	0.751E-2	0.712E-1
10	1.523	-0.308	0.869E-2	0.953E-1

TABLE 5.4: Impulsive Participation Factors in Horizontal Direction

Mode	Frequency (Hz)	Participation Factor ($lb_m^{1/2}$)	Participation Factor Ratio	Effective Mass (lb_m)
240	19.831	0.513	0.144E-1	0.263
241	**25.421**	**-35.519**	**1.000**	**1261.600**
242	39.237	0.509	0.143E-1	0.259
243	**52.595**	**13.241**	**0.372**	**175.322**
244	65.146	-0.796E-01	0.224E-2	0.635E-2
245	78.873	-0.913	0.257E-1	0.834
246	97.543	0.360	0.101E-1	0.130
247	**99.344**	**3.097**	**0.871E-1**	**9.591**
248	112.356	1.174	0.330E-1	1.380

The first principal impulsive mode in the horizontal direction is mode number two hundred forty one, corresponding to the frequency of 25.421 Hertz and the second

impulsive mode shape in X-direction is the two hundred forty third mode, corresponding to the frequency of 52.595 Hertz as given in Table 5.4. The mode shapes for first three convective modes are shown in Fig. 5.13, Fig. 5.14, and Fig. 5.15.

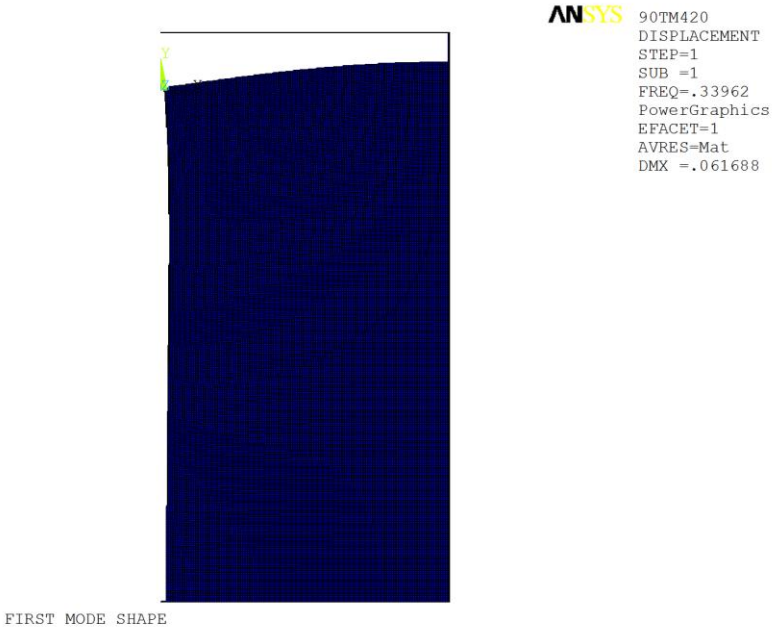

FIGURE 5.13: First Convective Mode Shape

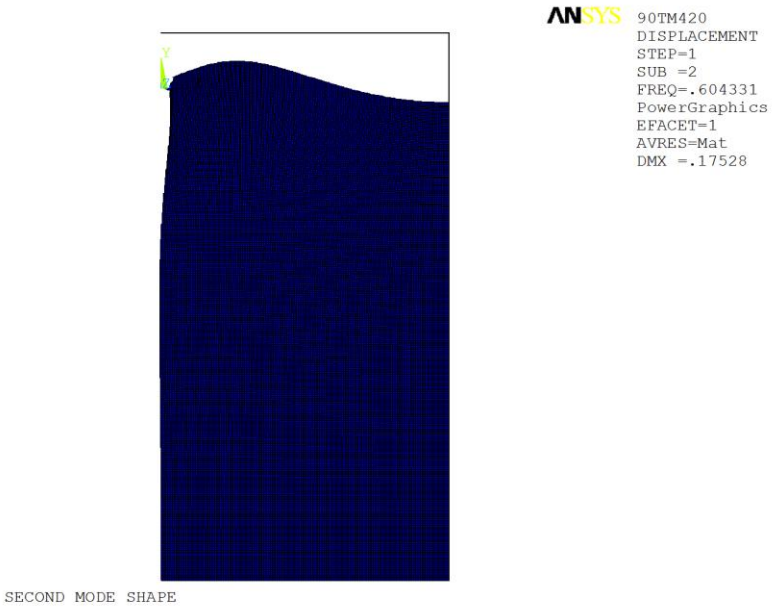

FIGURE 5.14: Second Convective Mode Shape

FIGURE 5.15: Third Convective Mode Shape

5.3.3 Single Point Response Spectrum Analysis of Water Filled Tank

A single point response spectrum (SPRS) analysis of the fluid tank was performed to determine the mode coefficients and mode coefficient ratios. The IEEE-693-2005 response spectrum curve [29] was used to carry out the SPRS analysis. Alternatively the mode coefficients and mode coefficient ratios can be calculated using the formulation given by Eq. (4.15) and Eq. (4.17) in Chapter 4 of this dissertation. The calculated spectral acceleration values are in base units, not multiples of acceleration due to gravity. The mode coefficients, mode coefficient ratios along with natural frequencies, participation factors, and effective masses for convective and impulsive modes are shown in Table 5.5 and Table 5.6, respectively. It can be observed for the data given in Table 5.5 that the first mode, i.e., the first principal convective mode in the horizontal direction, having a mode coefficient ratio of 1.000, is the most dominant mode that contributes to the fluid sloshing height. The first principal impulsive mode having a mode coefficient

of 1.000 is most dominant towards stresses in the structure and overturning moments as listed in Table 5.6.

TABLE 5.5: Convective Mode Coefficients in Horizontal Direction

Mode	Frequency (Hz)	S.V. (in/s^2)	Participation Factor ($lb_m^{1/2}$)	Mode Coefficient ($in\text{-}lb_m^{1/2}$)	M.C. Ratio	Effective Mass (lb_m)
1	**0.339**	**197.761**	**18.546**	**805.500**	**1.000**	**343.956**
2	**0.604**	**352.032**	**-4.544**	**-110.901**	**0.138**	**20.649**
3	**0.778**	**453.492**	**1.779**	**33.701**	**0.418E-1**	**3.166**
4	0.922	536.832	-1.329	-21.253	0.264E-1	1.766
5	1.046	609.033	0.715	10.0822	0.125E-1	0.511
6	1.156	636.904	-0.686	-8.270	0.103E-1	0.470

TABLE 5.6: Impulsive Mode Coefficients in Horizontal Direction

Mode	Frequency (Hz)	S.V. (in/s^2)	Participation Factor ($lb_m^{1/2}$)	Mode Coefficient ($in\text{-}lb_m^{1/2}$)	M.C. Ratio	Effective Mass (lb_m)
240	19.831	**285.012**	0.513	**0.942E-2**	**0.289E-1**	0.263
241	**25.421**	**235.472**	**-35.519**	**-0.326**	**1.000**	**1261.600**
242	39.237	193.200	0.509	0.162E-2	0.497E-2	0.259
243	**52.595**	**193.200**	**13.241**	**0.234**E-1	**0. 718E-2**	**175.322**
244	65.146	193.200	-0.796E-01	-0.900E-4	0. 276E-3	0. 635E-2
245	78.873	193.200	-0.913	-0.721E-3	0. 221E-2	0.834

5.3.4 Combination of Modes for Water Filled Tank

A mixture of the square root of the sum of the squares (SRSS) and algebraic sum rules was used to combine the participating modes in the post-processing phase. The first convective mode was combined with higher convective modes using SRSS. Similarly, the first impulsive mode was combined with higher impulsive modes using SRSS. Finally, the two resultant convective and resultant impulsive modes were combined using the algebraic sum method. Response results for two chosen locations, zero degrees and forty five degrees around the circumference were calculated. The first three convective

and first three impulsive modes were combined to obtain the total response. Displacements of the fluid in the vertical and horizontal directions at zero degrees are shown below in Fig. 5.16 and Fig. 5.17, respectively The calculated maximum sloshing height is 50.90 inches at **θ=0°.**

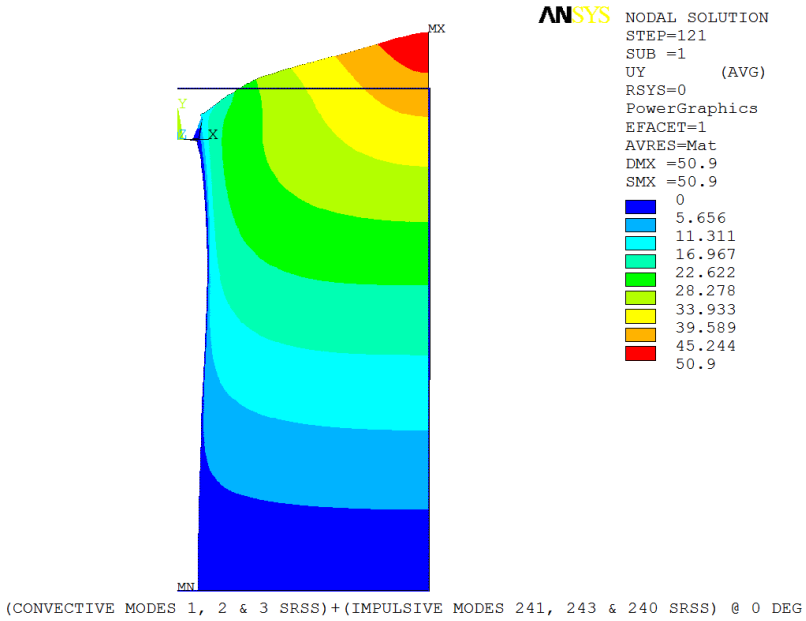

FIGURE 5.16: Vertical Translations in Fluid at **θ=0°**

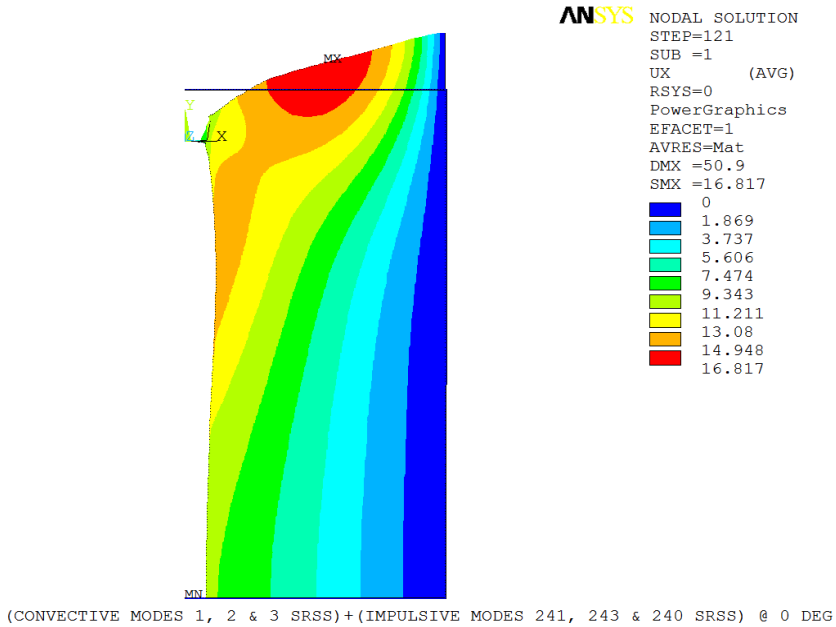

FIGURE 5.17: Horizontal Translations in Fluid UX at **θ=0°**

Displacements of the fluid in the vertical and horizontal directions at forty five degrees are shown in Fig. 5.18, Fig. 5.19, and Fig. 5.20 respectively.

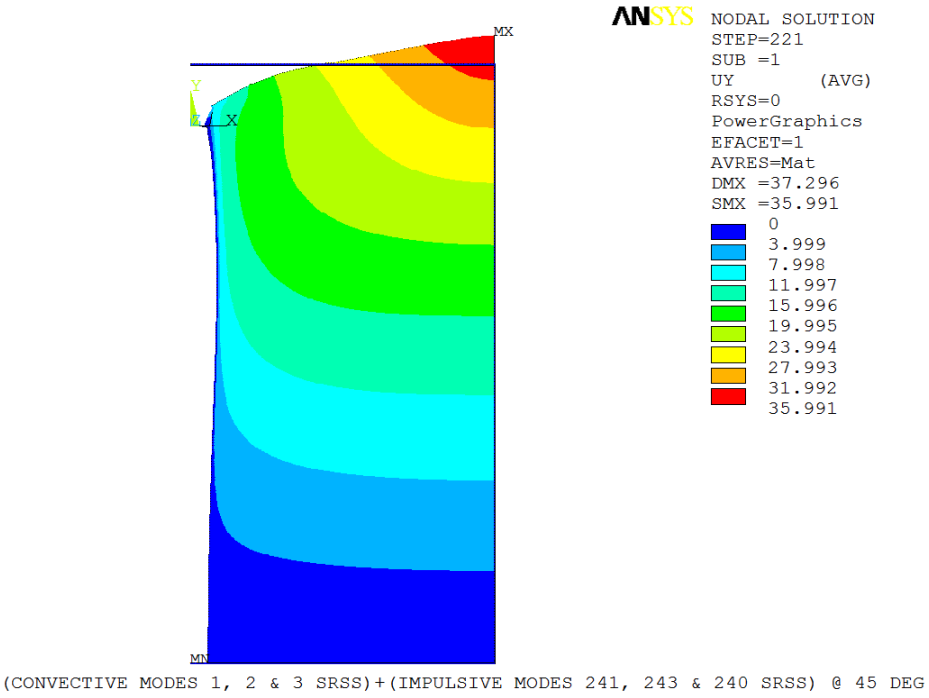

FIGURE 5.18: Vertical Translations in Fluid at **θ=45°**

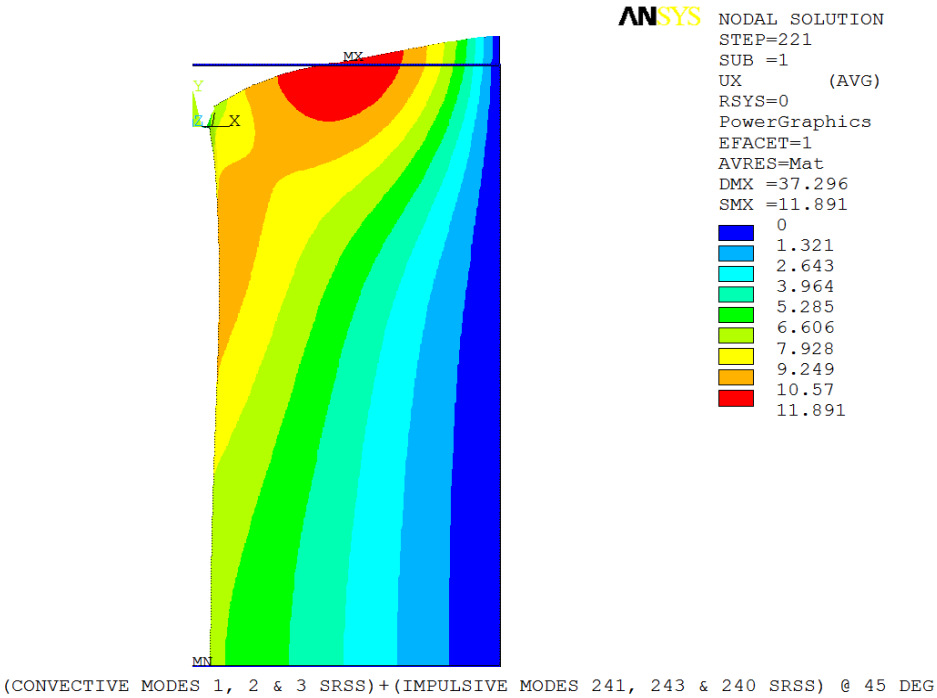

FIGURE 5.19: Horizontal Translations in Fluid UX at **θ=45°**

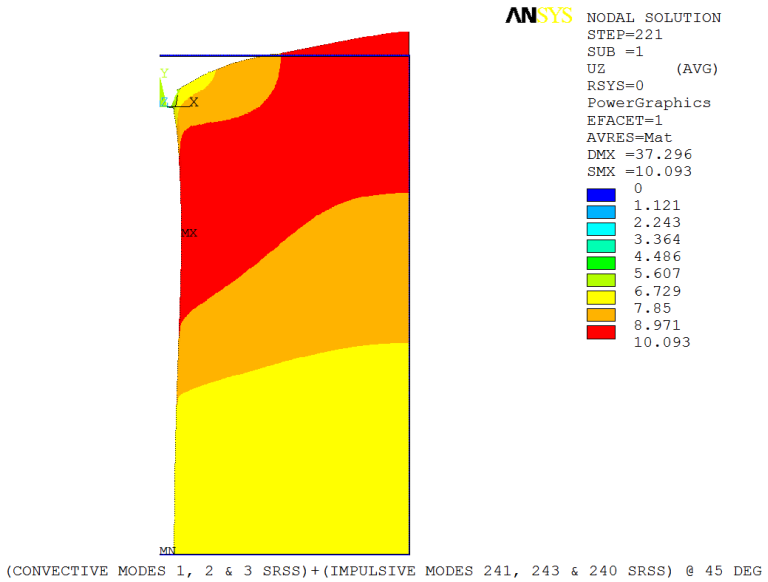

FIGURE 5.20: Horizontal Translations in Fluid UZ at **θ=45°**

The von Misses stresses at the plate and wall intersection are shown in Fig. 5.21 and Fig. 5.22 for **θ=0°** and **θ=45°** around the circumference, respectively. The maximum von Mises stresses of 1827 psi and 1736 psi were observed at the bottom head and tank wall juncture at **θ=0°** and **θ=45°**, respectively. It may be noted that all the stress plots are shown by removing the fluid elements for clarity.

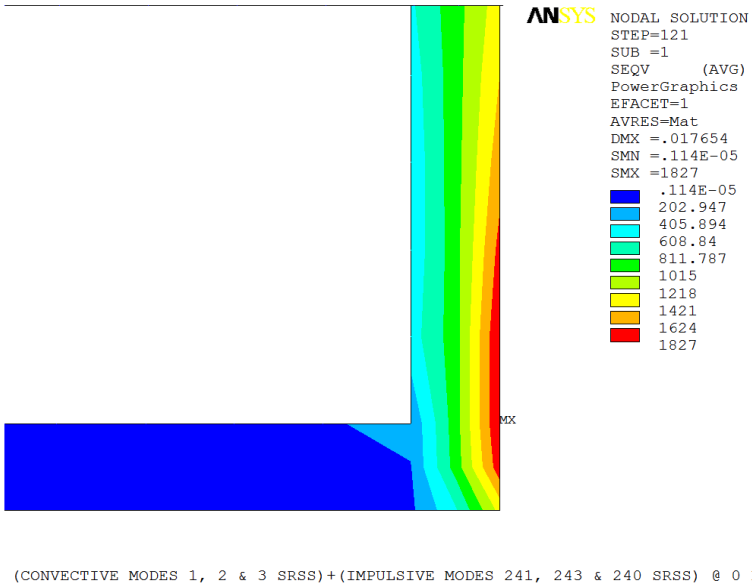

FIGURE 5.21: von Mises stresses at Tank Wall and Bottom Plate at **θ=0°**

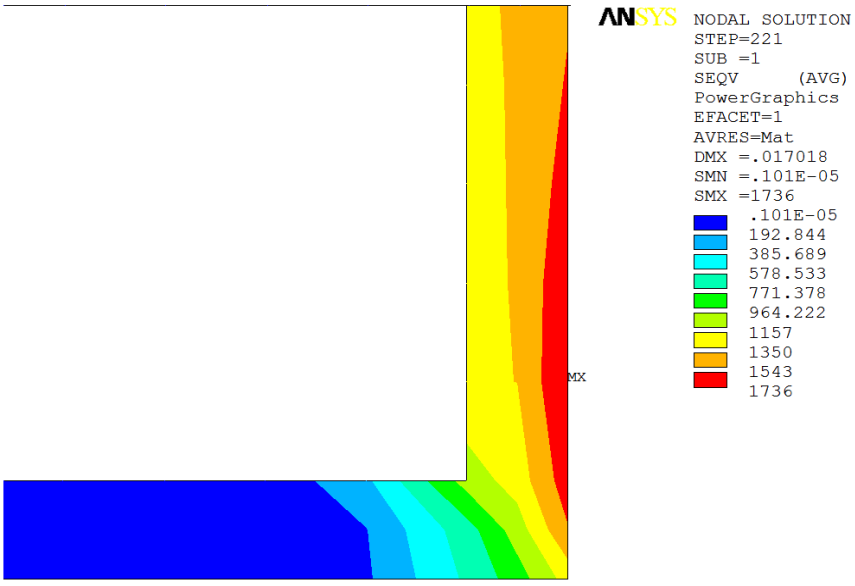

FIGURE 5.22: von Mises stresses at Tank Wall and Bottom Plate at **θ=45°**

CHAPTER 6: ANALYSIS OF CYLINDERICAL VESSEL WITH TOROSPHERICAL HEADS AND SKIRT SUPPORT

6.1 Vessel Geometry

The liquid filled vertical cylindrical vessel geometry utilized for the subject analysis is shown in Fig. 6.1. The vessel is elevated and supported by a cylindrical skirt.

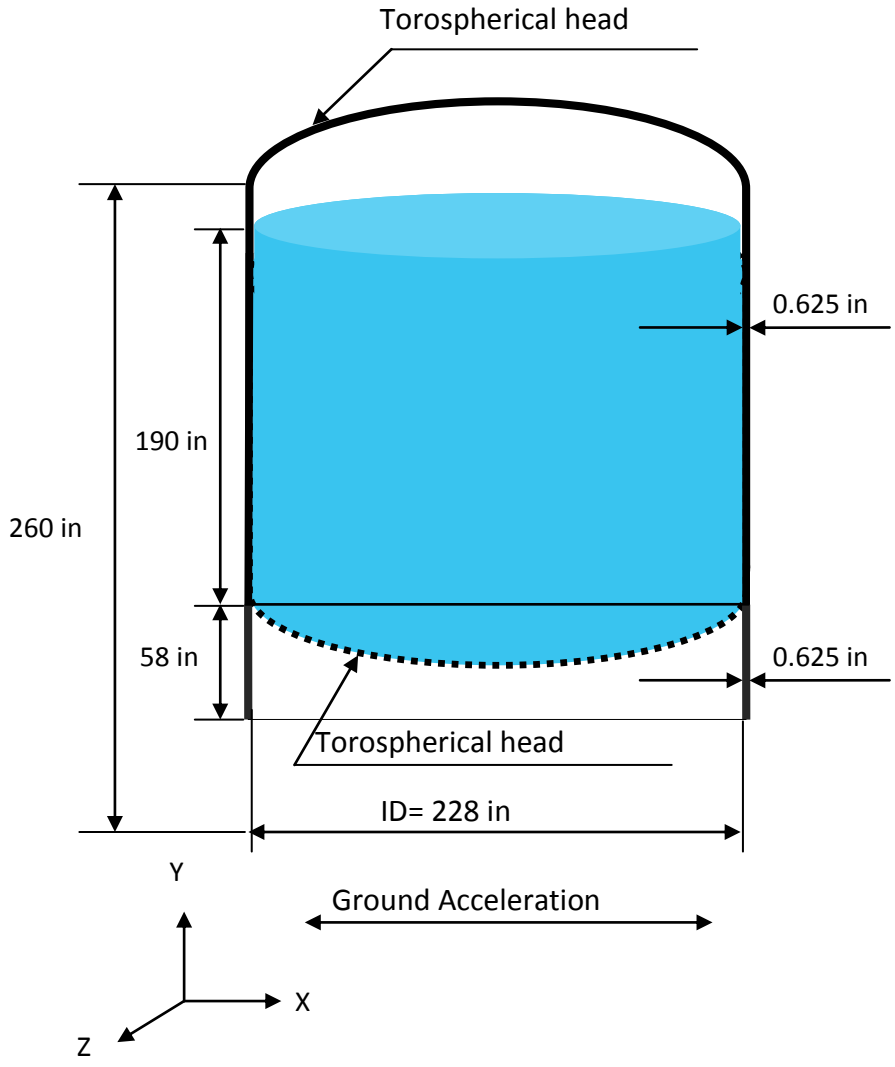

FIGURE 6.1: Vertical Cylindrical Vessel Dimensions

The vessel has 0.625 in. thick torospherical top and bottom heads formed with a 222 in. crown radius, complemented with a 13.755 in. knuckle radius. The vessel has an approximate overall height of 25 ft., measured from the base of the skirt to the top of torospherical head. The vessel has an inside diameter of 19 ft and the wall thickness of the vessel and skirt is 0.625 in. The material properties of the vessel and skirt include a Young's modulus of elasticity of 27,800,000 psi, a Poisson's ratio of 0.3. The mass density of vessel material is 7.50 $x10^{-4}$ $lb_m/in.^3$. The vessel is filled with a fluid to a height of approximately 248 in. from the skirt base. The mass density of the contained liquid utilized in the analysis is 9.29 $x10^{-5}$ $lb_m/in.^3$.

6.2 Analysis of Empty Vessel

The subject empty vessel was first analyzed for static loads i.e. ground acceleration as in case of a seismic event. The axisymmetric geometric features of skirt supported empty vessel with torospherical heads are shown in Fig.6.2. The empty vessel was modeled with four elements through the thickness of top and bottom heads and through the vessel wall to include the shear effects due to both the loads and the stresses. Three test cases were run, with the vessel structure having two, four and six elements though its thickness. All the three test cases produced similar results in term of deflections and stresses in the structure. Finally for grid convergence, it was decided to model the structure with four elements through the thickness instead of two elements due to a large discontinuity at the skirt, vessel wall and bottom head junction. The element coordinate system for the structure elements was chosen parallel to global Cartesian coordinate system. The structural elements utilized a geometric aspect ratio of

approximately 2:1 throughout with element dimensions of approximately 0.3125 in. x 0.15625in.

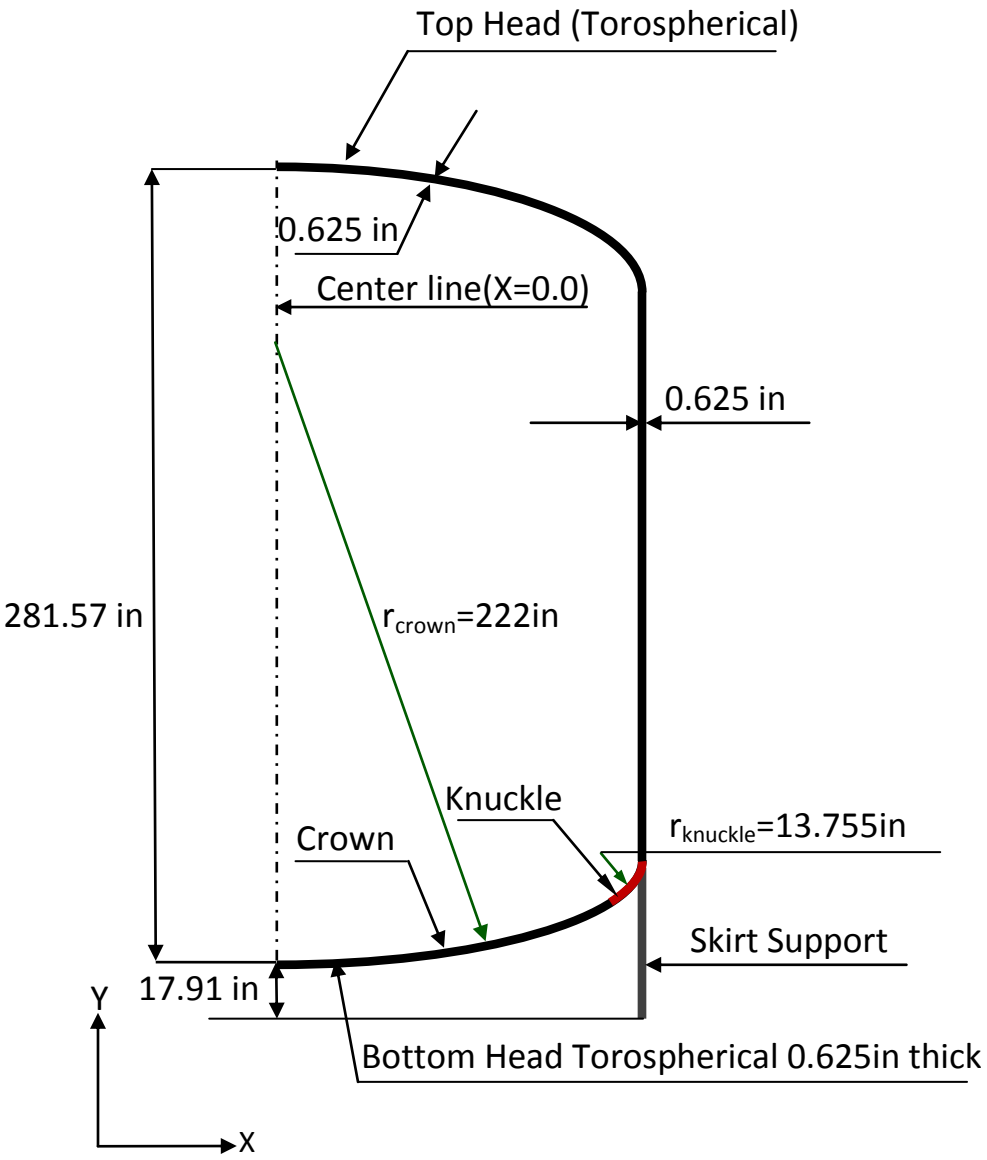

FIGURE 6.2: Axisymmetric Model Features of Empty Vessel

The bottom torospherical head nodes were created by using two different local cylindrical coordinate systems one each for crown and knuckle part respectively. The top head nodes were also created in a similar fashion. The vessel wall nodes were created in global Cartesian coordinates. Direct generation was used to create all the nodes and

elements. The nodal coordinate system was taken as parallel to the global cylindrical coordinate system. The displacement boundary conditions incorporate the fully anchored skirt attached to a rigid foundation on the ground. All the nodes at the base of skirt were restrained against displacement in all three orthogonal directions. Nodes at the vertical centerline (X=0.0) for the top and bottom head were restrained against displacement in the vertical direction.

6.2.1 Static Analysis of Empty Vessel

The empty vessel was analyzed for static loading condition by applying a ground acceleration of 0.5g in the horizontal direction. The acceleration in case of a static analysis is applied as an inertia (gravity) load. To get a resultant acceleration in the horizontal direction in case of axisymmetric harmonic elements, a combination of radial acceleration and the same magnitude of negative circumferential acceleration is applied as given by Eq. (4.6). The displacements, strains, reaction forces as well as stresses in the structure are then calculated by the FEA code, which can be viewed at any desired location around the circumference in the post-processing phase. Displacements in the vessel structure in the horizontal direction at the chosen location for response results, zero degrees, and forty five degrees around the circumference are shown in Fig. 6.3 and Fig. 6.4, respectively. A maximum displacement of 0.272×10^{-2} in. was observed at the top torospherical head of the vessel as shown in the contour plot represented by Fig.6.3 at a location of zero degrees around the circumference of vessel. The maximum horizontal displacement of 0.192×10^{-2} in. is observed at the same position on the top torospherical head but at a location of 45° around the circumference of the vessel as shown in Fig. 6.4.

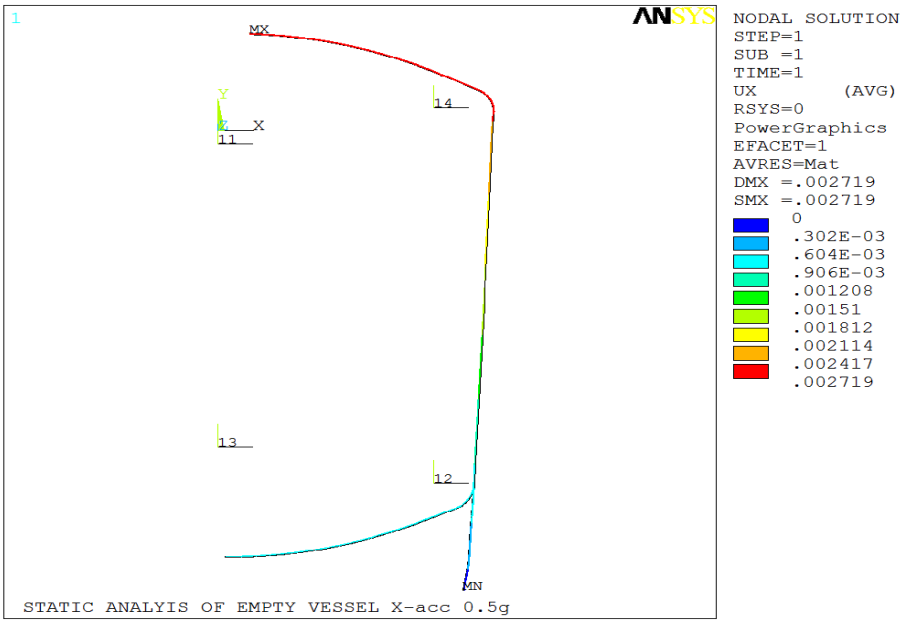

FIGURE 6.3: Horizontal Translations in Vessel Structure at **θ=0°**

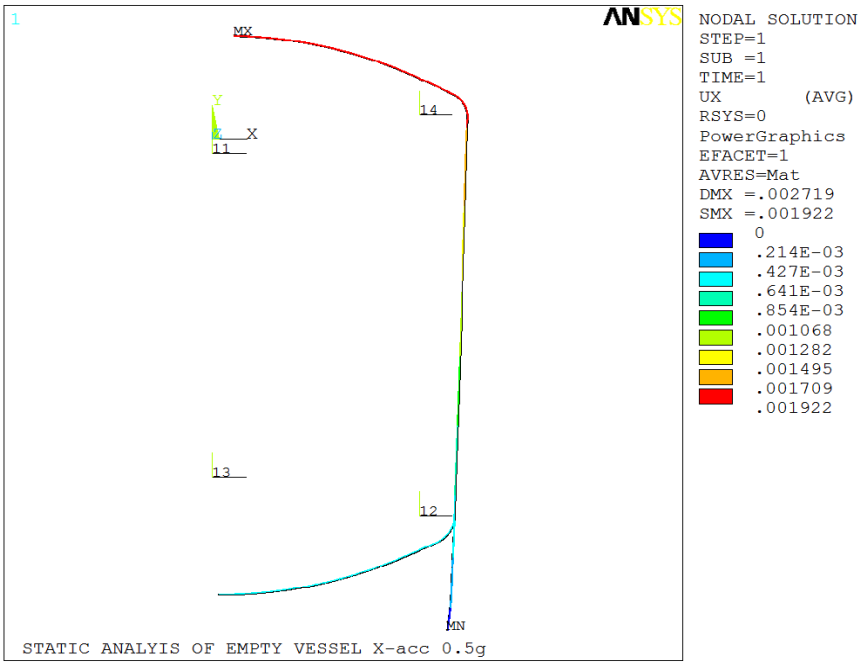

FIGURE 6.4: Horizontal Translations in Vessel Structure at **θ=45°**

It should be noted that the displacement at any angle around the circumference can be calculated by multiplying the calculated displacement at zero degrees location by

cosine of that angle by using the Fourier series given by the expression in Eq. (4.18). The results for vertical displacements, strains, stresses and reaction forces can also be obtained by plotting the respective contours or by listing the respective solution at all the nodes in the post-processing phase.

6.2.2 Modal Analysis of Empty Vessel

A dynamic analysis of the empty vessel was carried out by running a modal analysis. A "reduced" modal analysis was used to perform the mode frequency analysis to determine natural frequencies and mode-shapes of the empty vessel. A number of nodes were selected as master degrees of freedom based on the dynamic behavior of the vessel. A number of nodes on the vessel wall and vessel skirt were selected as master degrees of freedom (MDOF) in two horizontal directions and a number of nodes on the top head and bottom head of vessel were selected MDOF in the vertical direction. Few nodes on the vessel wall were selected MDOF in the vertical direction and a few nodes on the top and bottom torospherical heads were selected MDOF in two horizontal directions. Natural frequencies and Eigen vectors for the first fifty modes were calculated by the FEA code. The first ten calculated natural frequencies, participation factors, participation factor ratios and effective masses for the horizontal direction are shown in Table 6.1. The principal modes are determined by the participation factor ratio for a given direction. The highest participation factor ratio gives the first principle mode shape. Higher subsequent modes are identified based on successively decreasing participation factor ratios. The first principal mode shape in the horizontal direction is the first mode corresponding to the frequency of 49.189 Hertz and the second principal

mode shape in horizontal direction is the fourth mode corresponding to the frequency of 134.283 Hertz as shown in Table 6.1.

TABLE 6.1: Participation Factors in Horizontal Direction

Mode	Frequency (Hz)	Participation Factor ($lb_m^{1/2}$)	Participation Factor Ratio	Effective Mass (lb_m)
1	**49.189**	**6.904**	**1.000**	**47.661**
2	**103.190**	**1.710**	**0.248**	**2.925**
3	114.358	1.112	0.161	1.236
4	**134.283**	**-3.735**	**0.541**	**13.948**
5	138.043	0.157	0.227E-1	0.246E-01
6	138.312	0.953	0.138	0.908
7	144.992	-0.448	0.649E-1	0.201
8	145.422	-0.314	0.455E-1	0.987E-01
9	158.797	0.330	0.478E-1	0.109
10	159.865	0.845E-01	0.122E-1	0.714E-02

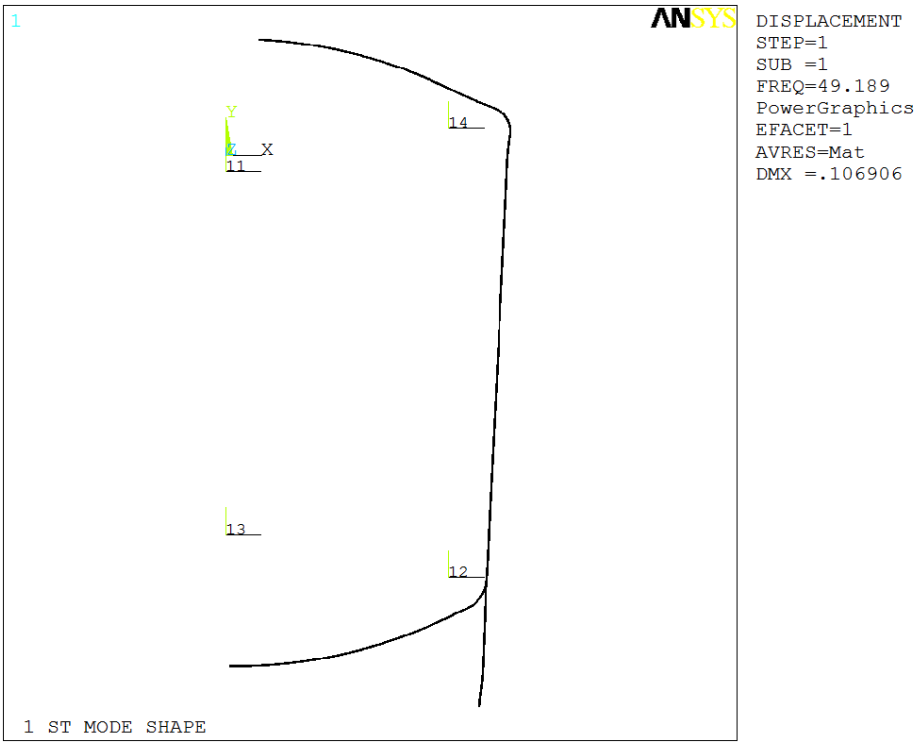

FIGURE 6.5: First Mode Shape for Empty Vessel

The mode shapes for the first two principal modes, i.e., the first mode and fourth mode shapes, in the horizontal direction are shown in Fig. 6.5 and Fig. 6.6, respectively.

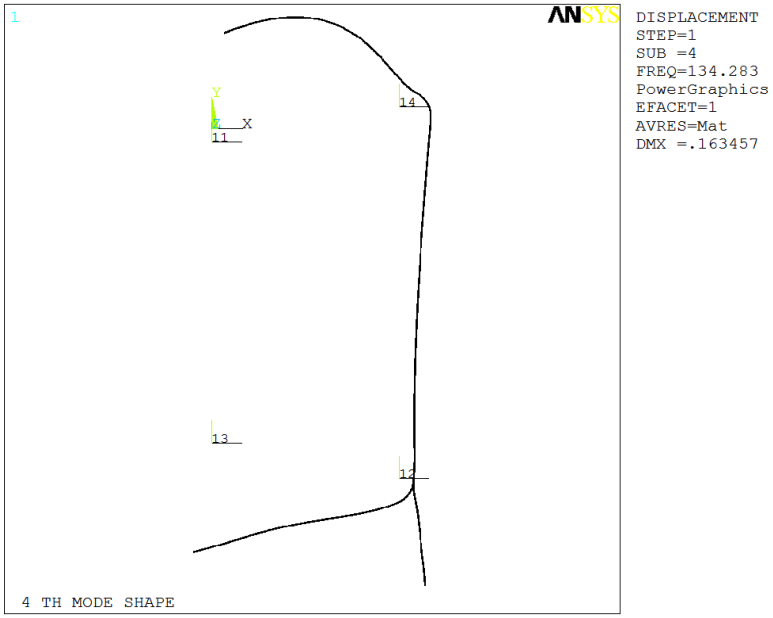

FIGURE 6.6: Second Mode Shape for Empty Vessel

6.2.3 Single Point Response Spectrum Analysis of Empty Vessel

A single point response spectrum (SPRS) analysis of the empty vessel was initiated to determine the mode coefficients and mode coefficient ratios. The mode coefficient ratios are used to determine the modes and number of modes to be combined to get the final response. The required mode coefficients and mode coefficient ratios can be obtained from the output file of the FEA code [27] used to analyze the subject vessel. The IEEE-693-2005 response spectrum curve [29] as shown in Fig. 4.7 was used to carry out the SPRS analysis. The first six calculated spectral acceleration values (SV) in base units and not multiples of g, mode coefficients, mode coefficient ratios along with natural frequencies, participation factors and effective mass are shown in Table 6.2. It can be observed for the data given in Table 6.2 that the fourth mode, i.e., the first principal mode

in the horizontal direction, having a mode coefficient ratio of one is the most dominant mode that contributes to the total response, followed by the fourth and second modes. The contribution to the total response for a particular mode is proportional to its mode coefficient and mode coefficient ratio. The higher the mode coefficient, the higher its contribution to the total response is as the contribution decreases as the mode coefficient decreases. It should be noted that as the frequency increases, the mode coefficient decreases as shown by Eq. (4.15), due to the squaring of the high frequency in the denominator of the equation.

TABLE 6.2: Mode Coefficients in Horizontal Direction

Mode	Frequency (Hz)	S.V. (in/s^2)	Participation Factor ($lb_m^{1/2}$)	Mode Coefficient ($in\text{-}lb_m^{1/2}$)	M.C. Ratio	Effective Mass (lb_m)
1	**49.189**	**193.20**	**6.904**	**0.139E-01**	**1.000**	**47.661**
2	**103.190**	**193.20**	**1.710**	**0.786E-03**	**0.562E-1**	**2.925**
3	114.358	193.20	1.112	0.416E-03	0.297E-1	1.236
4	**134.283**	**193.20**	**-3.735**	**-0.101E-02**	**0.725E-1**	**13.948**
5	138.043	193.20	0.157	0.403E-04	0.289E-2	0.246E-01
6	138.312	193.20	0.953	0.244E-03	0.174E-1	0.908

6.2.4 Combination of Modes for Empty Vessel

The participating modes were identified based on the respective mode coefficient ratios and were combined "manually" in the post-processing phase using the square root of the sum of the squares (SRSS) load case operator. Two locations around the circumference, zero degrees and forty five degrees were chosen as the desired location for response results to demonstrate the technique developed. The total response of the structural system can be obtained by combining only a few contributing modes as all the computed modes do not contribute to the final response. It was decided to combine modes having mode coefficient more than 0.024, i.e., for this case modes numbered one,

four, and two. Displacements of the structure in the horizontal direction at zero degrees and forty five degrees around the circumference (the chosen location for response results) were calculated and are shown in contour plots represented by Fig. 6.7 and Fig. 6.8, respectively.

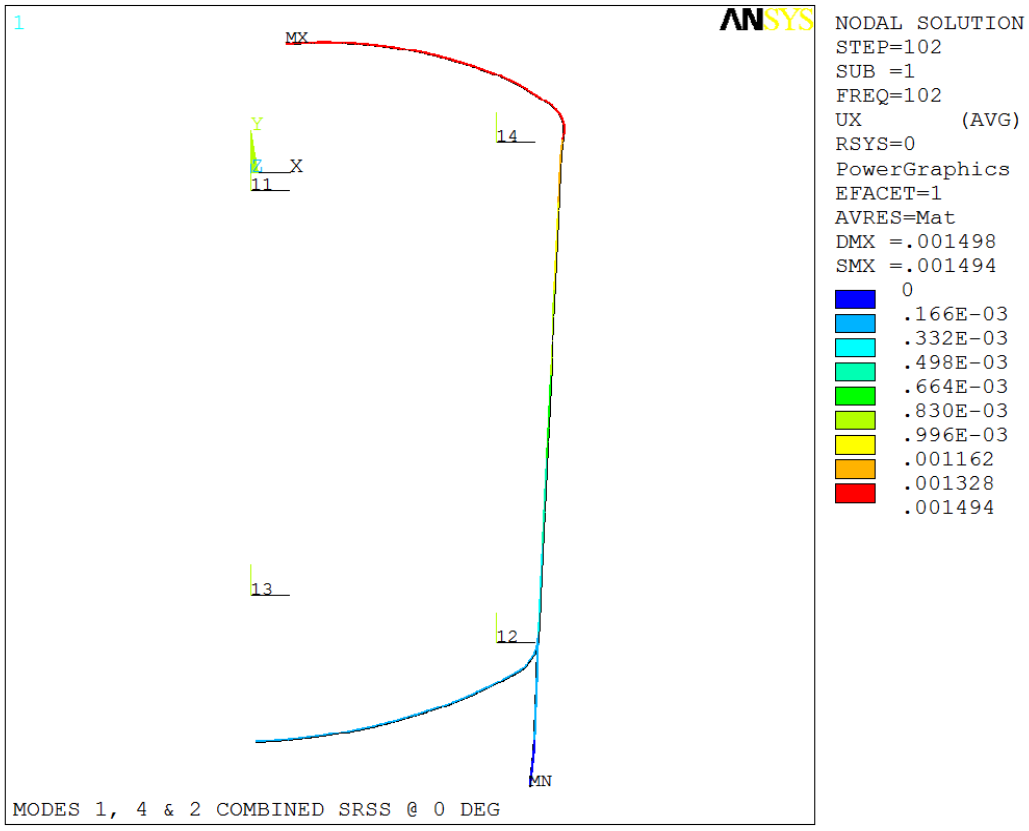

FIGURE 6.7: Horizontal Translations in Vessel Structure at **θ=0°**

It can be clearly concluded by comparing plots for displacement (response) in Fig. 6.7 and Fig. 6.8 and with the plots of mode shapes given by Fig. 6.5 and Fig. 6.6 that the first significant mode dominates the response results.

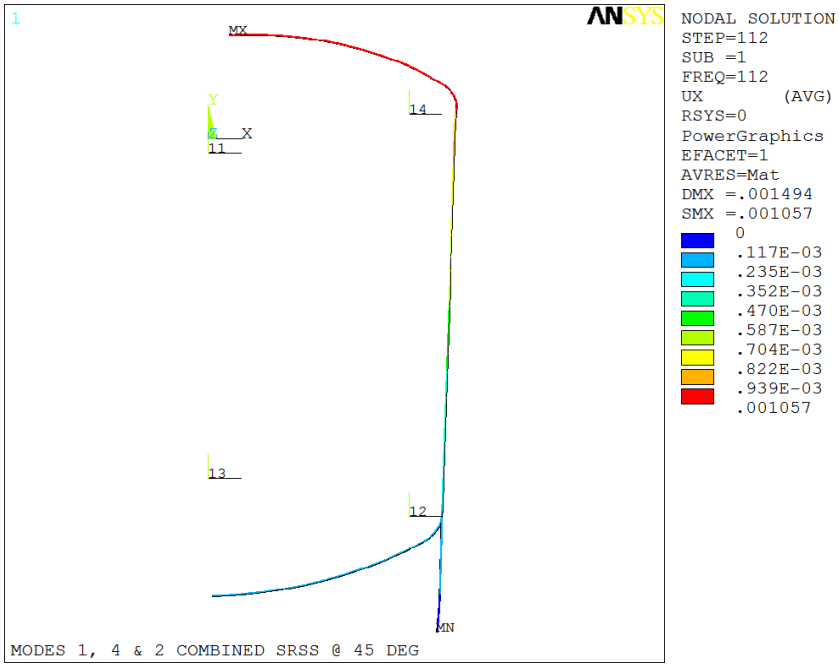

FIGURE 6.8: Horizontal Translations in Vessel Structure at **θ=45°**

6.3 Analysis of Water Filled Vessel

The empty vessel as analyzed in the previous section was filled with water and was analyzed for both static as well as dynamic loads. The geometric features of the axisymmetric model of the skirt supported, water filled vessel with torospherical heads are shown in Fig. 6.9. In addition to nodes and elements for the empty vessel, nodes and elements for the fluid were also created. The free surface of the liquid was modeled at Y= 0.0 with the positive Y-direction vertically upward. Coincident nodes were created at the fluid structure interface for the fluid and the vessel wall. The nodal coordinate system of the nodes was chosen parallel to global Cartesian coordinate system. The nodal coordinates of all nodes at the fluid structure interface (both structure and the fluid nodes) were then rotated in a direction parallel to the local coordinate system used to define the

structural nodes, such that the coincident nodes could be coupled only in a direction normal to the fluid-structure interface.

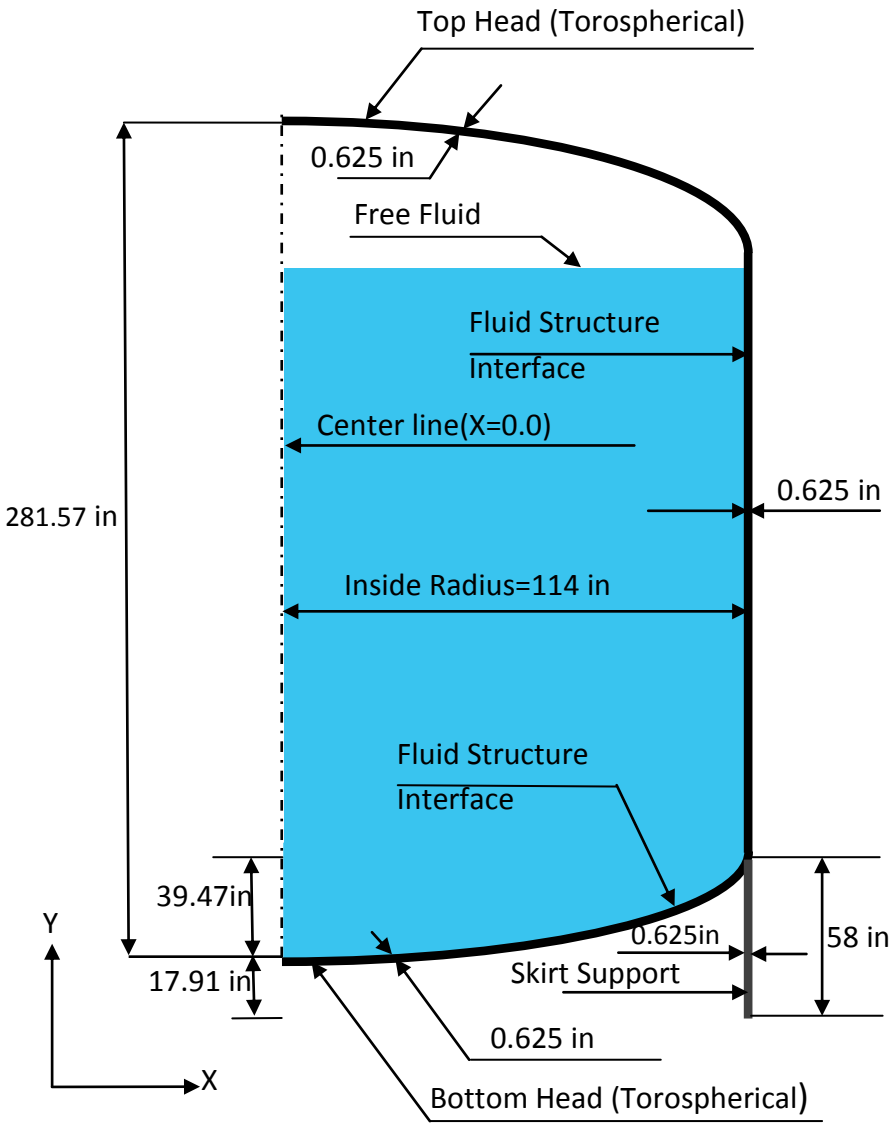

FIGURE 6.9: Axisymmetric Model Features of Fluid Filled Vessel

In addition to the boundary conditions for the structural elements, all fluid nodes along the vertical centerline were restrained against displacement in the vertical direction. All the fluid nodes along the vertical centerline at X=0.0 were made to take the same displacements in the two orthogonal horizontal directions by using displacement constraint equations. The four node axisymmetric fluid element shown in Fig. 4.5 was

used to model the contained fluid. The geometric aspect ratio of the fluid elements varied from 1:1 to 4:1 with the largest dimension of any fluid element not exceeding 0.625 in. Acceleration due to gravity in the vertical direction was applied to make the fluid springs effective, which are used to hold the free surface of fluid in place. The fluid filled vessel was analyzed for static loads as well as dynamic loads. The dynamic analysis is carried out in two phases; the modal analysis in the first phase to get the frequencies, mode shape and participation factors followed by the spectrum analysis to obtain the required mode coefficients and mode coefficient ratios.

6.3.1 Static Analysis of Water Filled Vessel

The vessel was analyzed for static loading by applying a ground acceleration of 0.500g in the horizontal direction as an inertia (gravity) load per Eq. (4.6). The displacements as well as stresses in the structure are then calculated by the FEA code. Displacements of the fluid in the vertical direction at two chosen locations, 0° and 45° around the circumference, are shown in Fig. 6.10 and Fig. 6.11, respectively. A maximum sloshing height of the fluid in the vertical direction at zero degrees (circumferential coordinate) is observed to be 56.947 in. as shown in Fig.6.10, whereas at forty five degrees, the sloshing height is calculated to be 40.268 in. as shown in Fig. 6.11. Similarly, results at other desired locations can be obtained by incorporating the Fourier series given by Eq. (4.18) into the response results. It may be noted that the fluid displacements as shown in the contour plots for the vessel are not plotted to the true scale. The fluid part having maximum sloshing height will definitely go out through the top torospherical head in case a true displacements scale is considered, as in the case of the fluid filled tank discussed in the previous chapter of this dissertation.

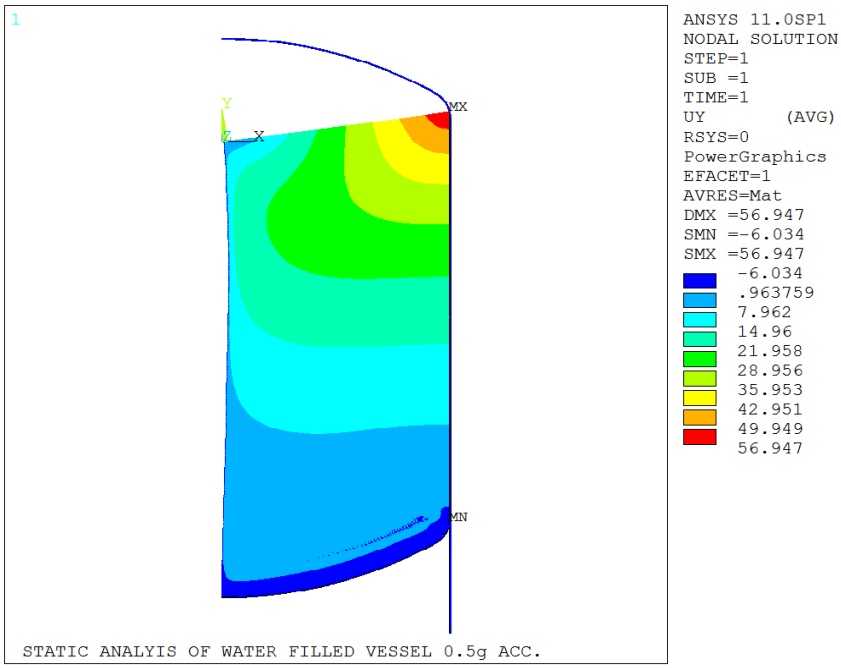

FIGURE 6.10: Vertical Translations in Fluid at **θ=0°**

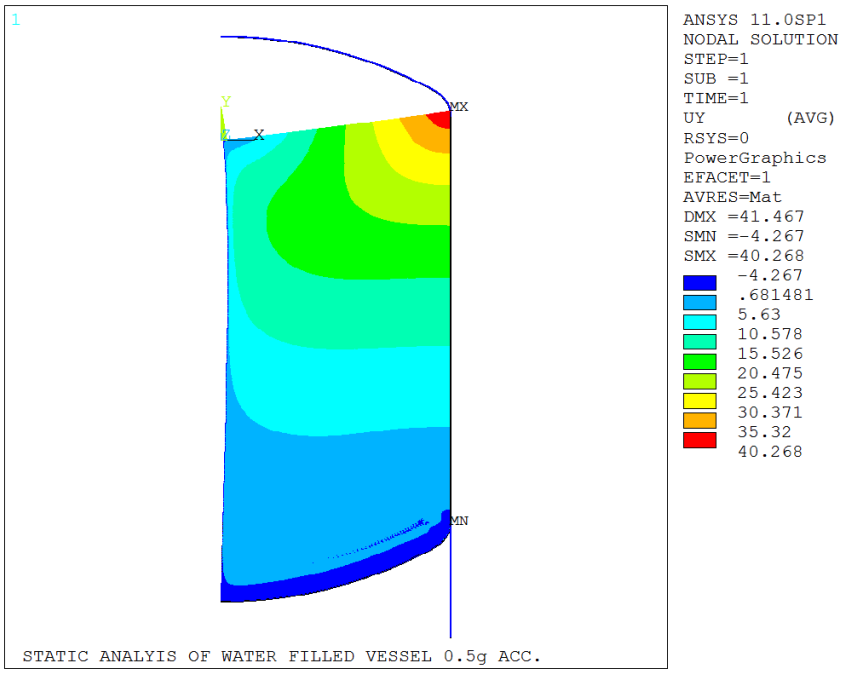

FIGURE 6.11: Vertical Translations in Fluid at **θ=45°**

The maximum calculated von Mises stress of 2103 psi is observed at the base of skirt fixed to the rigid foundation as shown in Fig. 6.12 whereas Fig. 6.13 depicts the

maximum calculated von Mises stress of 1675 psi as observed at the critical geometric juncture, i.e., at the skirt-vessel shell-bottom head juncture.

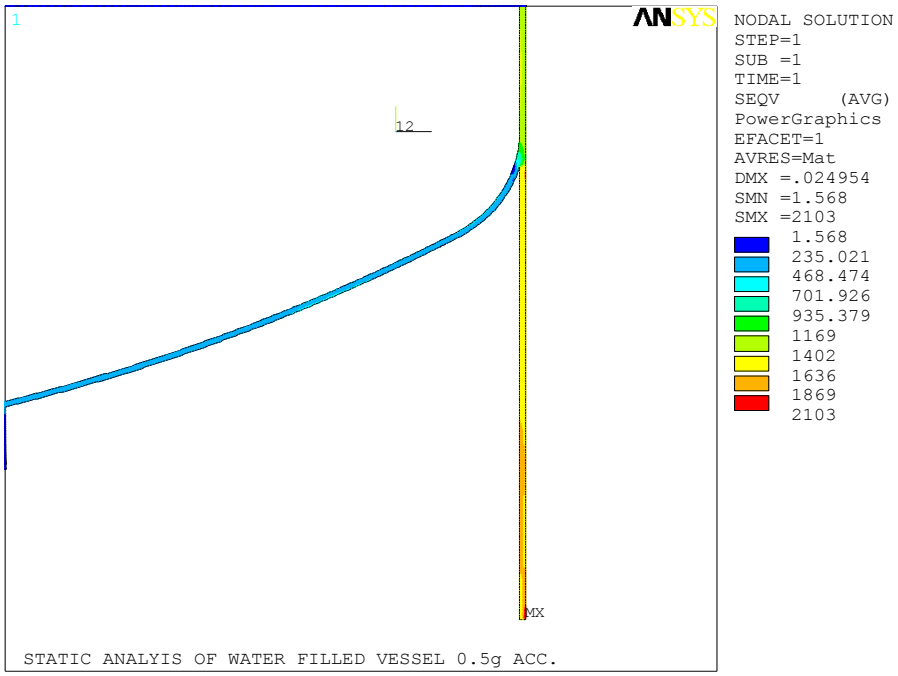

FIGURE 6.12: von Mises Stress in the Skirt Support

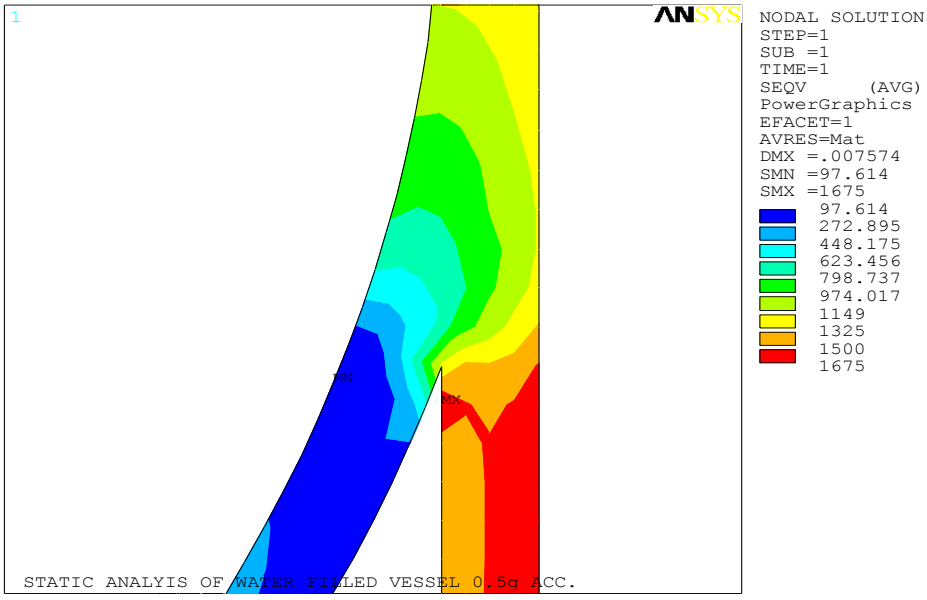

FIGURE 6.13: von Mises Stress at the Critical Juncture

6.3.2 Modal Analysis of Water Filled Vessel

The natural frequencies and mode-shapes of the fluid filled vessel were determined by initiating a modal analysis. A "reduced" modal analysis was used by defining master degrees of freedom based on dynamic behavior of the fluid filled vessel. In addition to selected master degrees of freedom (MDOF) for the empty vessel, supplementary MDOF were selected for the fluid nodes. All the fluid nodes at the free surface (Y=0.0) were selected as MDOF in the vertical direction as required by the FEA code [27]. The upper part of the fluid in the vessel, near the free surface, vibrated in low frequencies and independent of the vessel walls. This fluid portion (as discussed earlier) is termed the convective fluid. The remainder of the fluid, i.e., the part of fluid moving with the vessel walls and vibrating in higher frequencies, is termed the impulsive fluid.

TABLE 6.3: Convective Participation Factors in Horizontal Direction

Mode	Frequency (Hz)	Participation Factor ($lb_m^{1/2}$)	Participation Factor Ratio	Effective Mass (lb_m)
1	**0.346**	**17.215**	**0.486**	**296.356**
2	**0.618**	**-4.255**	**0.120**	**18.105**
3	**0.797**	**1.667**	**0.470**E-1	**2.780**
4	0.943	-1.234	0.348E-1	1.523
5	1.070	0.671	0.189E-1	0.450
6	1.183	-0.637	0.180E-1	0.406
7	1.287	0.379	0.107E-1	0.144
8	1.383	-0.405	0.114E-1	0.164
9	1.440	0.267	0.751E-2	0.712E-01
10	1.523	-0.308	0.869E-2	0.953E-01

The calculated convective and impulsive natural frequencies, participation factors, participation factor ratio and respective effective mass are shown in Table 6.3 and Table 6.4, respectively. The participation factor and effective mass as shown in Table 6.3 are for the horizontal direction, which is the direction of the ground acceleration to be

applied to the subject vessel. The first principal convective mode shape in the horizontal direction is the first mode corresponding to the frequency of 0.346 Hertz. The second convective mode shape in the horizontal direction is the second mode corresponding to the frequency of 0.618 Hertz as shown in Table 6.3.

TABLE 6.4: Impulsive Participation Factors in Horizontal Direction

Mode	Frequency (Hz)	Participation Factor ($lb_m^{1/2}$)	Participation Factor Ratio	Effective Mass (lb_m)
462	**22.298**	**35.404**	**1.000**	**1253.460**
475	**37.030**	**3.070**	**0. 867E-1**	**9.427**
481	**54.675**	**5.964**	**0.168**	**35.572**
482	65.540	5.459	0.154	29.808
483	73.540	3.521	0.994E-1	12.402
484	86.219	-0.450	0.127E-1	0.202
485	94.016	0.179	0.507E-2	0.322E-01
486	101.335	-2.112	0.596E-1	4.461
487	107.395	0.206	0.582E-2	0.424E-01
488	114.378	-2.649	0.748E-1	7.020

The first principal impulsive mode shape in the horizontal direction is mode number four hundred sixty two corresponding to the frequency of 22.298 Hertz.

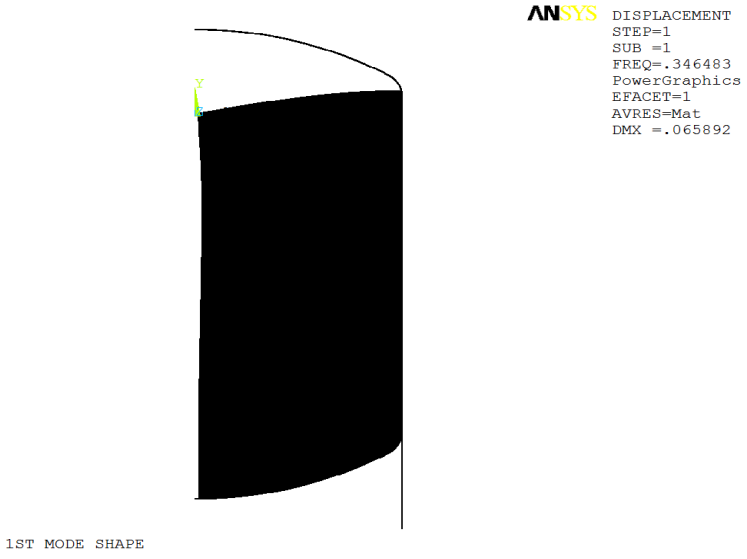

FIGURE 6.14: First Convective Mode Shape

The mode shapes for the first three convective modes corresponding to modes one, two and three in are shown in Fig. 6.14, Fig. 6.15 and Fig. 6.16 respectively.

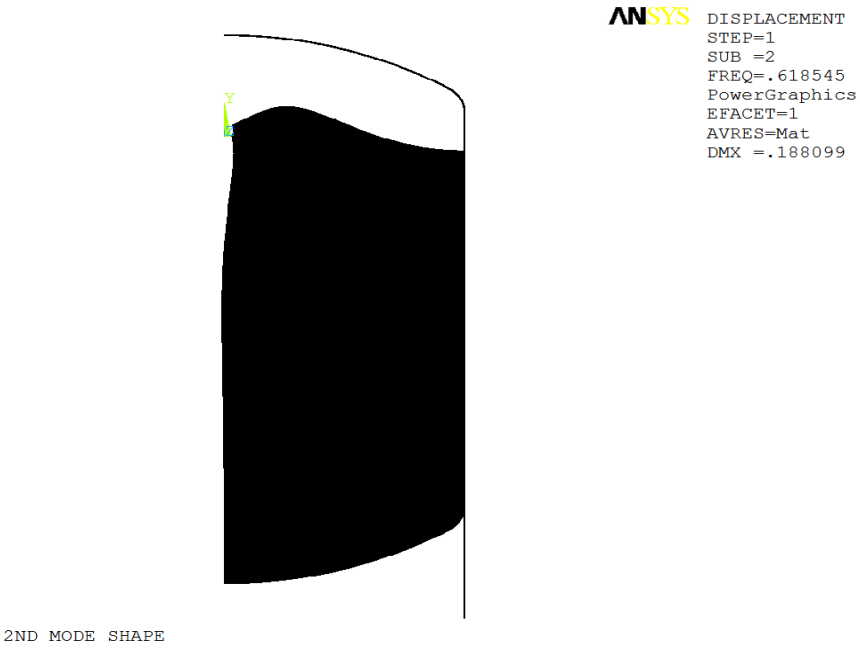

FIGURE 6.15: Second Convective Mode Shape

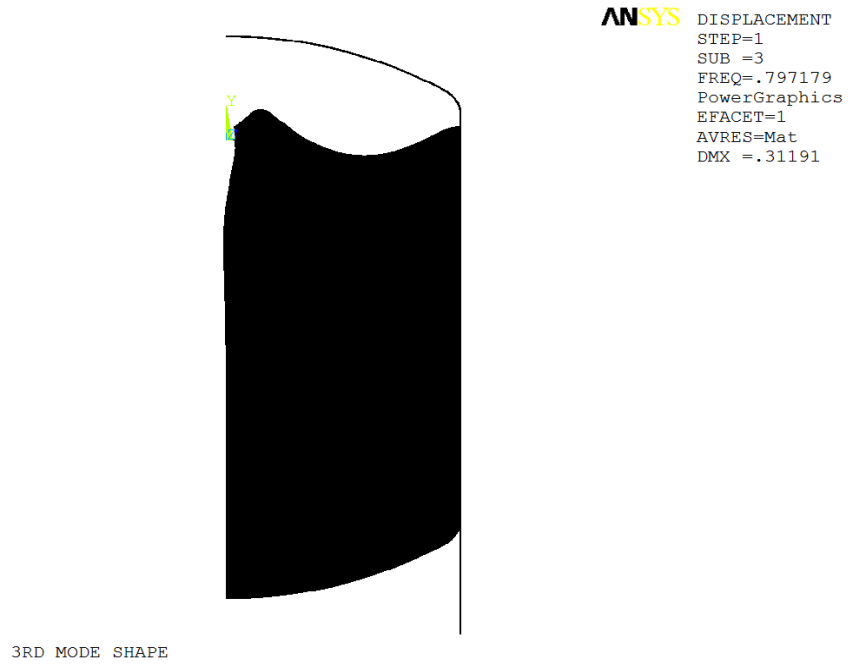

FIGURE 6.16: Third Convective Mode Shape

6.3.3 Single Point Response Spectrum Analysis of Water Filled Vessel

A single point response spectrum (SPRS) analysis of the fluid vessel was carried out to determine the mode coefficients and mode coefficient ratios. The IEEE-693-2005 response spectrum curve [29] was used to carry out the SPRS analysis. Alternatively, the mode coefficients and mode coefficient ratios can be determined by using the expression given by Eq. (4.15) and Eq. (4.17) in Chapter 4 of this dissertation. The calculated spectral acceleration values are in base units, not multiples of acceleration due to gravity. The mode coefficients, mode coefficient ratios along with natural frequencies, participation factors and effective mass for convective and impulsive modes are shown in Table 6.5 and Table 6.6 respectively. It can be observed for the data given in Table 6.5 that the first mode i.e., the first principal convective mode in horizontal direction, having a mode coefficient ratio of 1.000 is the most dominant mode contributing to the sloshing height of the fluid. The first principal impulsive mode corresponding to mode number four hundred sixty two and having a mode coefficient of one, as given in Table 6.6, is the most dominant for stresses in the structure, base shear, and overturning moment of the vessel.

TABLE 6.5: Convective Mode Coefficients in Horizontal Direction

Mode	Frequency (Hz)	S.V. (in/s^2)	Participation Factor ($lb_m^{1/2}$)	Mode Coefficient ($in\text{-}lb_m^{1/2}$)	M.C. Ratio	Effective Mass (lb_m)
1	**0.346**	**201.770**	**17.215**	**732.928**	**1.000**	**296.356**
2	**0.618**	**360.210**	**-4.255**	**-101.473**	**0.138**	**18.105**
3	**0.797**	**460.971**	**1.667**	**30.850**	**0.421E-1**	**2.780**
4	0.943	549.462	-1.234	-19.281	0.263E-1	1.523
5	1.070	623.262	0.671	9.248	0.126E-1	0.450
6	1.183	636.902	-0.637	-7.341	0.101E-1	0.406

It may be noted that the convective modes and impulsive modes were calculated by running two different load cases so as to avoid expanding insignificant modes that do not contribute to the total response in any manner.

TABLE 6.6: Impulsive Mode Coefficients in Horizontal Direction

Mode	Frequency (Hz)	S.V. (in/s^2)	Participation Factor ($lb_m^{1/2}$)	Mode Coefficient ($in\text{-}lb_m^{1/2}$)	M.C. Ratio	Effective Mass (lb_m)
462	**22.298**	**261.342**	**35.404**	**0.471**	**1.000**	**1253.460**
475	**37.030**	**193.200**	**3.0704**	**0.112E-1**	**0.230E-1**	**9.427**
481	**54.675**	**193.200**	**5.964**	**0.503E-2**	**0.110E-1**	**35.572**
482	65.540	193.200	5.459	0.679E-2	0.140E-1	29.808
483	73.540	193.200	3.521	0.319E-2	0.677E-2	12.402
484	86.219	193.200	-0.450	-0.100E-2	0.214E-1	0.202

6.3.4 Combination of Modes for Water Filled Vessel

A combination of the square root of the sum of the squares (SRSS) and algebraic sum rules was used to combine the participating modes in the post-processing phase. The first convective mode was combined with higher convective modes using SRSS. Next, the first impulsive mode was combined with higher impulsive modes using SRSS in a similar fashion. The resultant convective modes combined by SRSS and the resultant impulsive modes combined by SRSS were then combined using the algebraic sum method. The first three convective and first three impulsive modes were combined to obtain the total response. The higher modes were not combined as they do not contribute towards the total response or the contribution to total response was negligible. Response results for two chosen locations, zero degrees and forty five degrees around the circumference were calculated. Displacements of the fluid in the vertical and horizontal directions at zero degrees are shown in Fig. 6.17 and Fig. 6.18, respectively. The

calculated maximum sloshing height of 49.552 inches is observed at **θ=0°** around the circumference of the vessel.

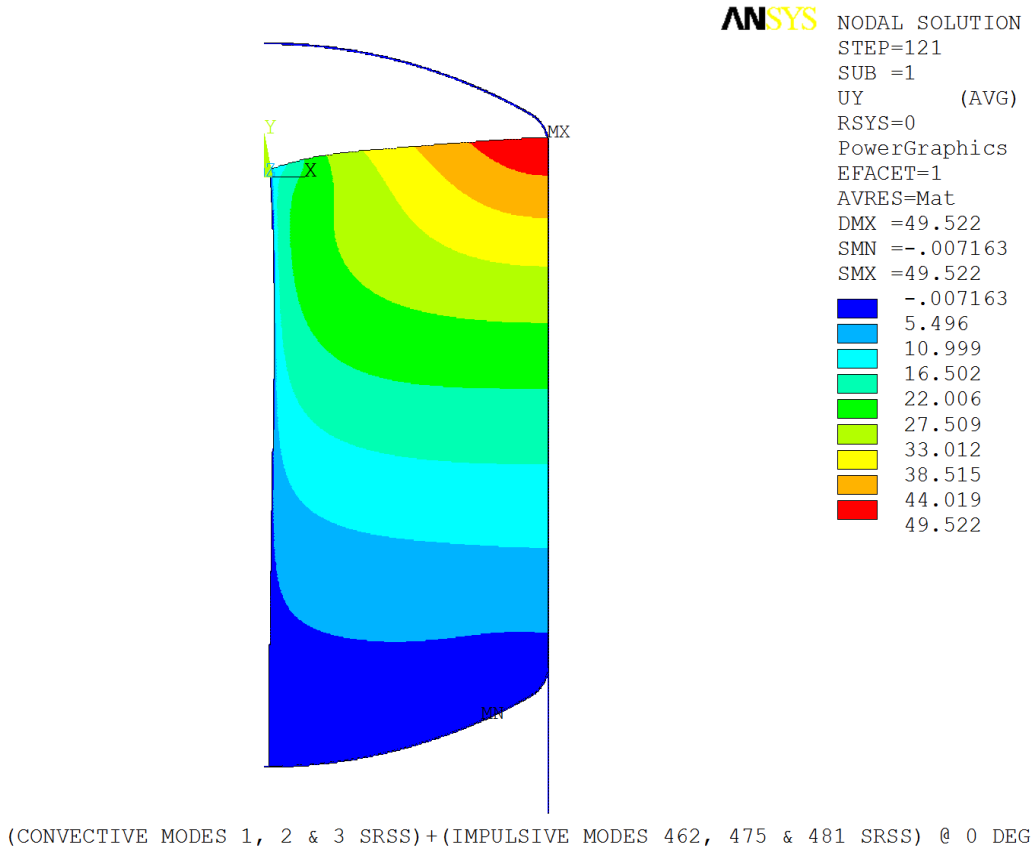

FIGURE 6.17: Vertical Translations in Fluid at **θ=0°**

Displacements of the fluid in the vertical and two horizontal directions at the second chosen location, i.e., at forty five degrees around the circumference are shown in Fig. 6.19, Fig. 6.20 and Fig. 6.21, respectively.

The von Misses stresses in the skirt and bottom head are shown in the contour plot represented by Fig. 6.22 for **θ=0°** around the circumference of the vessel. The maximum von Mises stress of 1825 psi was observed at the skirt-foundation juncture at **θ=0°**.

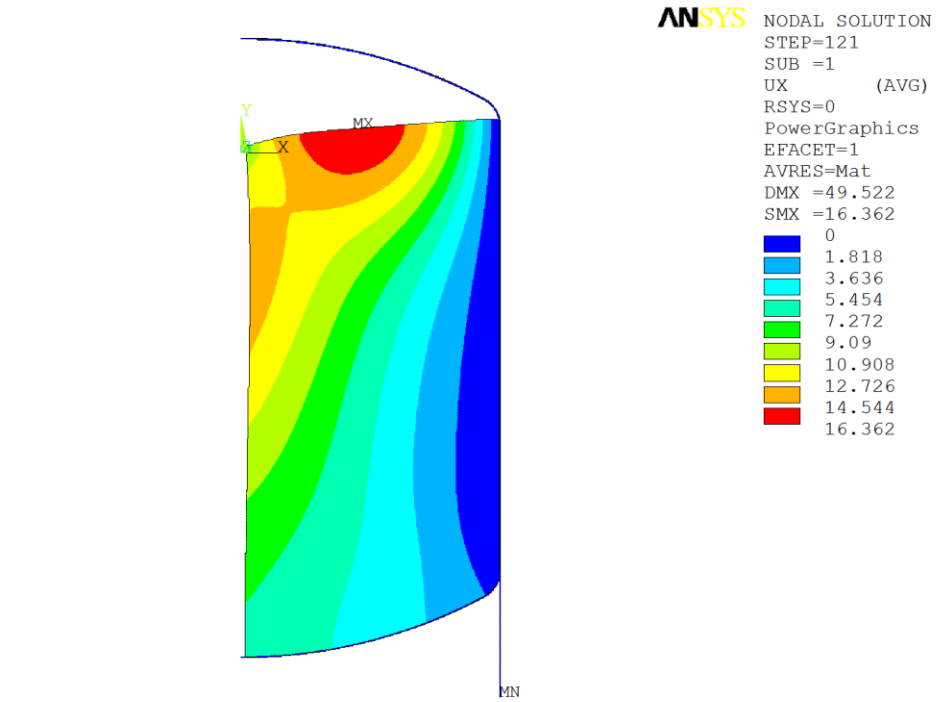

FIGURE 6.18: Horizontal Translations in Fluid UX at **θ=0°**

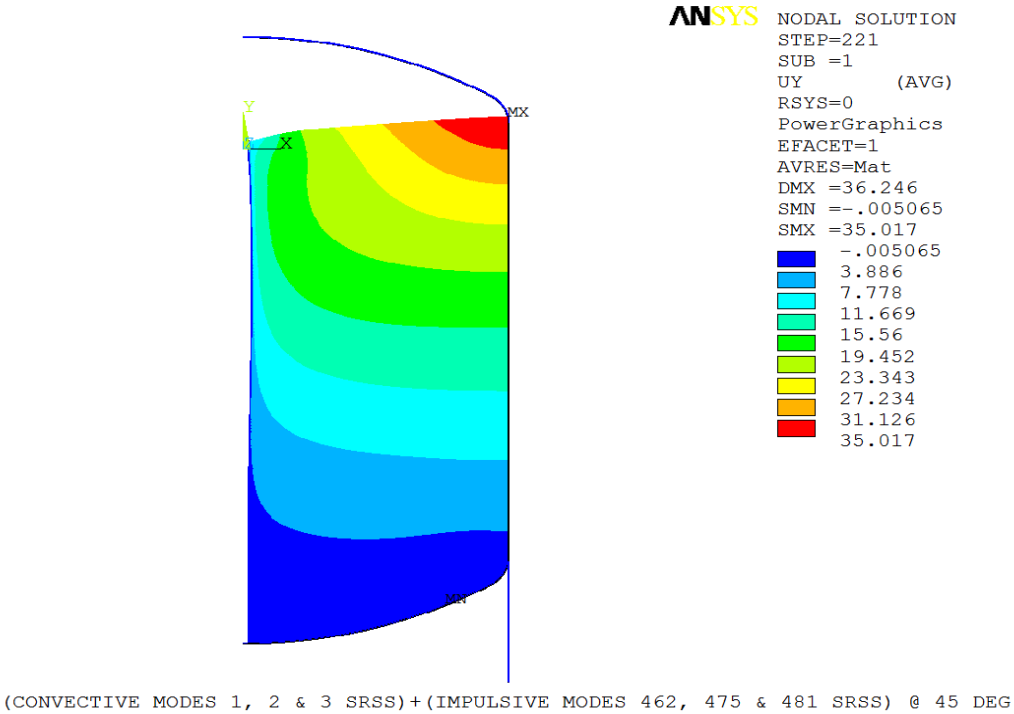

FIGURE 6.19: Vertical Translations in Fluid at **θ=45°**

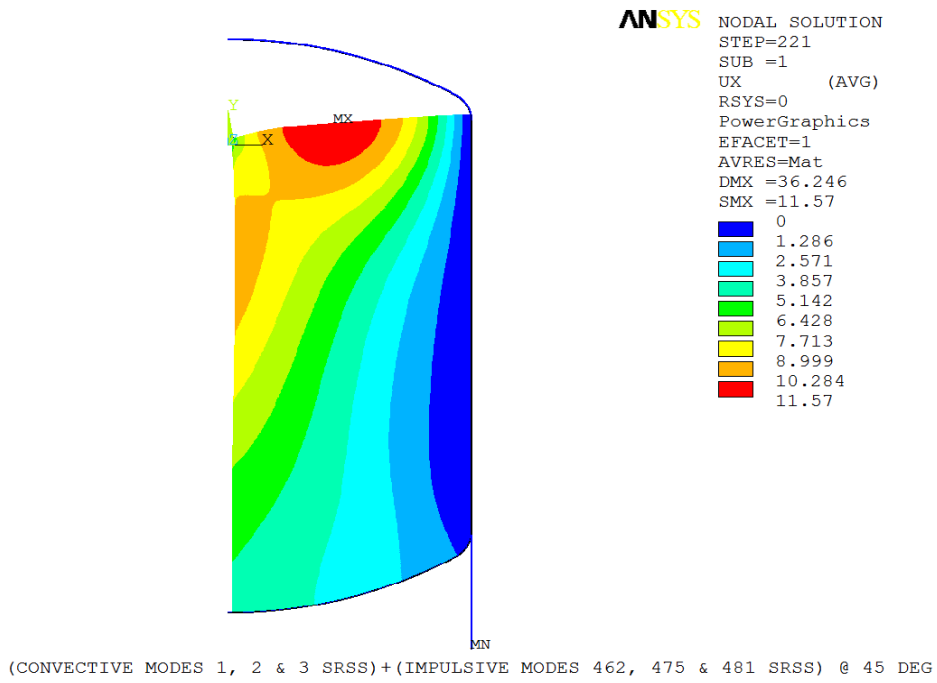

FIGURE 6.20: Horizontal Translations in Fluid UX at **θ=45°**

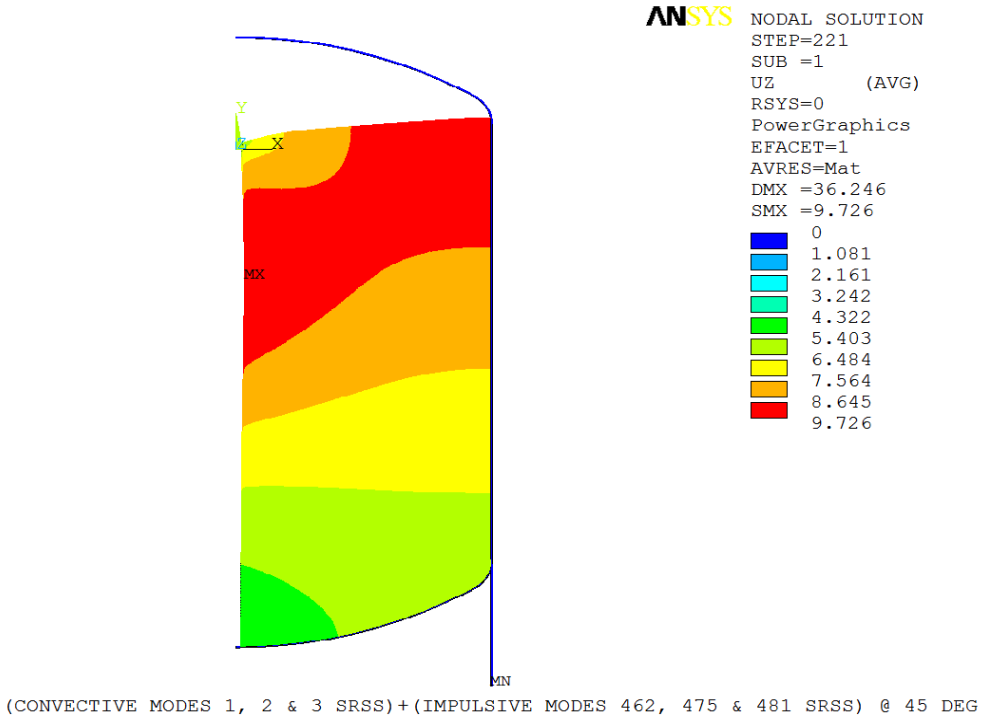

FIGURE 6.21: Horizontal Translations in Fluid UZ at **θ=45°**

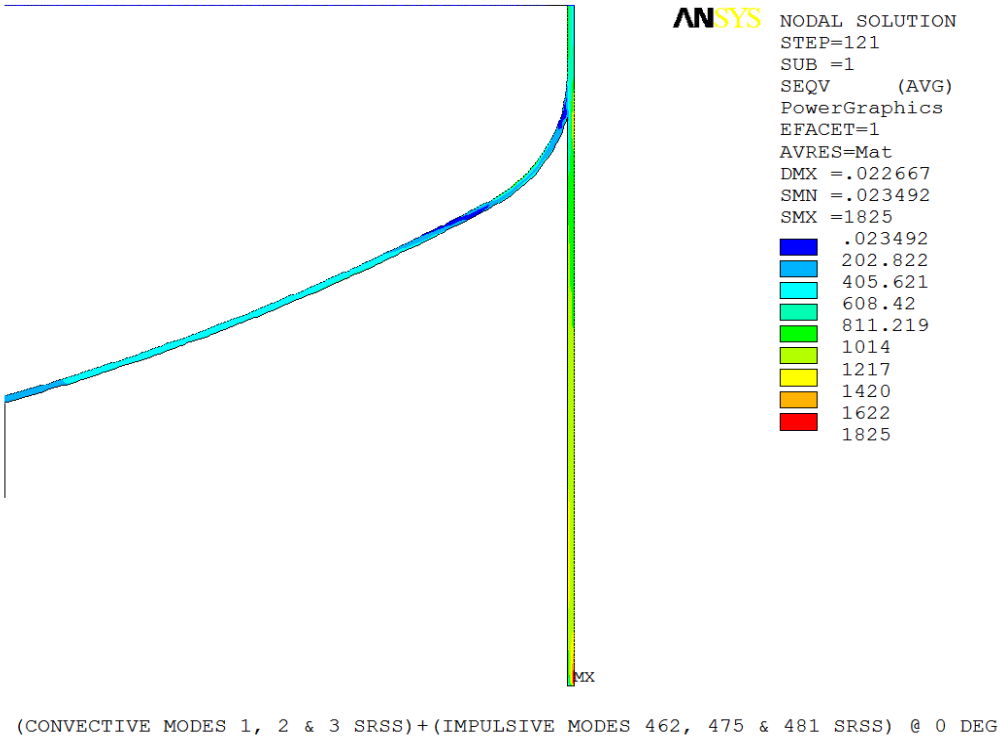

FIGURE 6.22: von Mises Stresses at Skirt Support at **θ=0°**

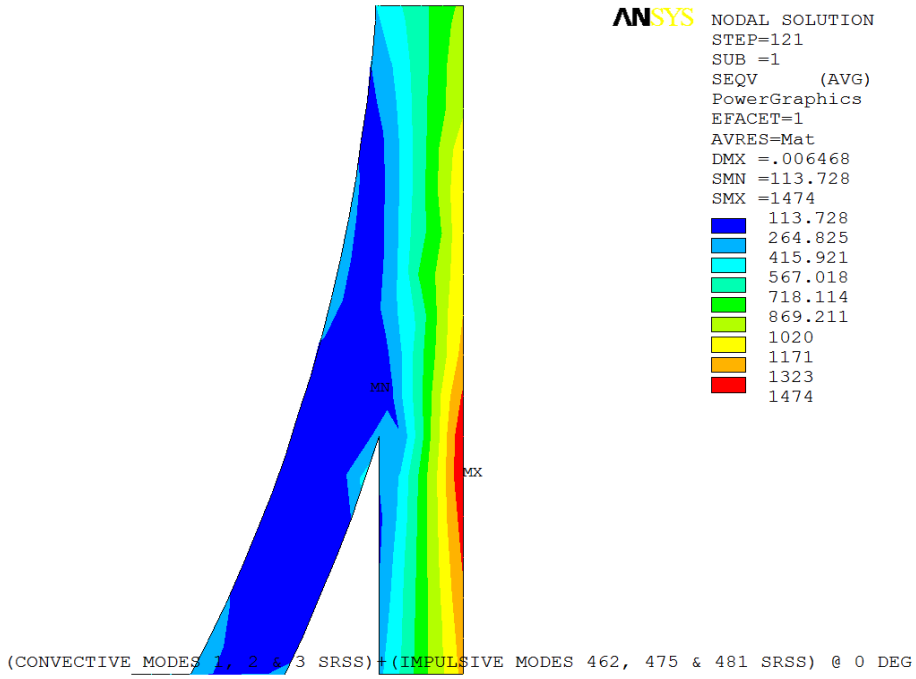

FIGURE 6.23: von Mises Stresses at Critical Juncture **θ=0°**

The von Mises stresses at the critical juncture of skirt, vessel wall and bottom torospherical head are given in Fig. 5.23 for **θ=0°**. The maximum von Mises stress of 1693 psi was observed at the skirt-foundation juncture at **θ=45°** by Fig. 6.24. For clarity it may be noted that all the stress plots are shown with the fluid elements removed.

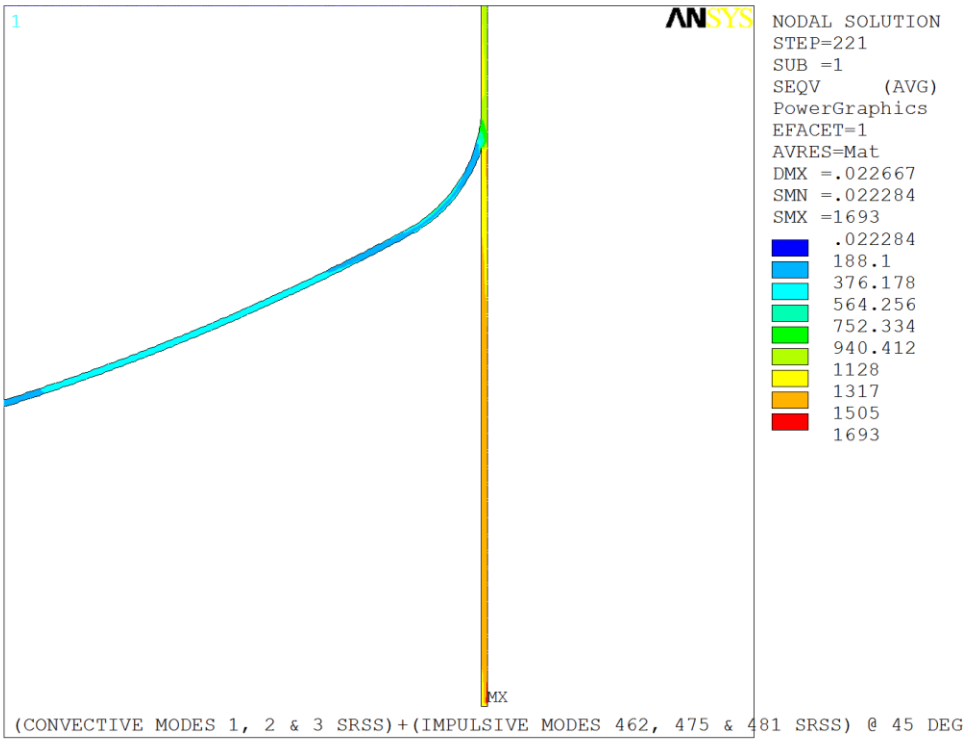

FIGURE 6.24: von Mises Stresses at Skirt Support at **θ =45°**

In addition to the calculated deflections in the fluid and the calculated stresses in the structure for the water filled vessel, the maximum base shear and maximum overturning moments were calculated by using the FEA code. The total base shear force at the base of the skirt was calculated to be 283340 lb_f. The net overturning moment was calculated by multiplying the base shear force by center of gravity of the mass of water filled vessel in vertical direction. The resulting net overturning moment was calculated to be 3.9891×10^7 in-lb_f.

CHAPTER 7: DISCUSSION OF SEISMIC ANALYSIS RESULTS

7.1 Comparison of Finite Element Results with Theoretical Results

The results of the fluid structure-interaction analysis utilizing the methodology developed in this dissertation were compared with results obtained from the works of Malhotra [5] and that defined in Eurocode 8 [25]. Results for both the fluid filled tank with flat heads and the fluid filled vessel with torospherical heads were compared with reference works [5] and [25]. The results for two different finite element analysis methods, i.e., static and dynamic analyses were also compared against one another. The fluid filled tank with flat heads as discussed in Chapter 5 and the fluid filled vessel with torospherical heads as discussed in Chapter 6 are of comparable geometric and material properties. Finally, the results for the fluid filled tank and the fluid filled vessel were compared at both zero degrees and forty five degrees around the circumference to the tank, because of the comparable geometries.

7.1.1 Comparison of Static Finite Element and Dynamic Finite Element Results

The response results for both the fluid filled tank and fluid filled vessel were compared for both the static and dynamic analyses (detailed modal analysis, i.e., the combination of modes). Table 7.1 shows comparison results between the two finite element analysis methods. It can be observed from the results in Table 7.1 that the static analysis yields higher response results for both displacements and stresses as compared to the dynamic analysis. The higher response results from the static analysis can be

attributed to the fact that the static analysis ignores the dynamic behavior of the fluid filled container. In addition, the static analysis applies a constant acceleration to the entire fluid and the fluid containing structure, whereas in the dynamic analysis, the mass of fluid is divided into impulsive and convective parts. Corresponding to the different natural frequencies associated with each constituent model element, respective spectral accelerations are applied to the impulsive fluid mass, convective fluid mass, and the tank structure proper.

TABLE 7.1: Static FEA Results Versus Dynamic FEA Results at **θ=0°**

	Static Analysis		Dynamic Analysis	
	Sloshing Height (in)	Stresses (psi)	Sloshing Height (in)	Stresses (psi)
Tank	59.645	1903	50.900	1827
Vessel	56.947	2103	49.552	1825

7.1.2 Comparison of Finite Element and Theoretical Results for Fluid Filled Tank

The natural frequencies and sloshing heights obtained from the detailed modal finite element analysis described herein were compared with results obtained from the work of Malhotra [5] and that defined in Eurocode 8 [25]. Table 7.2 shows comparison of the natural frequencies for the first convective mode and the first impulsive mode calculated by the finite element analysis and other analytical methods [5, 25]. The examination of FEA results shows good agreement with the those calculated by analytical expressions given by both Malhotra [5] and the Eurocode 8 [25]. The natural frequencies of only the first mode of vibration are compared with the theoretical results. The lower natural frequencies calculated by the FE method described herein may be attributed to the fact that the FEA takes into account the additional stiffness and associated mass of the top

head of tank, whereas the other methods given in references [5, 25] have no means to easily incorporate the top head into the respective models.

TABLE 7.2: Principal Natural Frequencies for Tank Calculated by FEA and Analytical Methods

	Convective Frequency (Hz)	Impulsive Frequency (Hz)
FEA	0.339	25.422
Eurocode 8	0.390	N/A
Malhotra [5]	0.390	27.488

Table 7.3 shows sloshing heights from the analytical expressions given by [5, 25] are in good agreement with the finite element result at circumferential location $\theta=0°$. The sloshing heights for all three methods posted in Table 7.3 were calculated using the same ground acceleration of 0.512g, the spectral acceleration corresponding to frequency of 0.339Hz from IEEE-693-2005 response spectrum curve [29], which is the first frequency of the sloshing fluid, regardless of the different natural frequencies given by the different methods.

TABLE 7.3: Sloshing Heights Calculated by FEA and Analytical Methods for Fluid Filled Tank

	Sloshing Height (in)
FEA	50.90
Eurocode 8	51.59
Malhotra [5]	61.42

Table 7.4 shows FEA results for the first convective mode, combination of first three convective modes, first impulsive mode, combination of first three impulsive modes, and finally, combination of first three convective and first three impulsive modes. It is clear from the data given in Table 7.4 that in order to calculate the total response, higher convective and impulsive modes should be combined with the principal

convective and impulsive modes, although the principal modes dominate the response but the higher modes have a small but significant contribution to the total response. The fluid filled tank analyzed is practically rigid. In the case of a more flexible structure, the higher modes may contribute much more significantly than the contribution of higher modes in the case of the analyzed tank. It can be further observed that the convective modes of the fluid are completely responsible for the vertical sloshing height of the fluid and the impulsive modes do not add appreciably to the fluid sloshing height. The impulsive modes are responsible for the stresses in the structure, whereas the convective modes play a secondary role in contributing towards the stresses in the structure.

TABLE 7.4: FEA Results for Different Modes and Mode Combinations for Tank

	Sloshing Height (in)	Stresses (psi)
First Convective Mode	49.69	345.22
Three Convective Modes Combined	50.85	348.25
First Impulsive Mode	0.041	1443
Three Impulsive Modes Combined	0.050	1502
Three Convective and Three Impulsive Modes Combined	50.90	1827

7.1.3 Comparison of Finite Element and Theoretical Results for Fluid Filled Vessel

The natural frequencies for the first convective and first impulsive modes calculated by the finite element analysis and analytical methods [5, 25] are shown in Table 7.5. The lower natural frequency calculated by the finite element method as shown in Table 7.5 may be attributed to two facts. First, the FEA takes into account the additional stiffness and associated mass of the top and bottom torospherical heads of the vessel, whereas the other methods given in references [5, 25] have no means to easily incorporate the top and bottom heads into the respective models. Second, Malhotra [5]

and Eurocode 8 [25] assume the vessel to be supported on the ground, whereas the subject vessel discussed herein is actually elevated and skirt supported.

TABLE 7.5: Principal Natural Frequencies for Fluid Filled Vessel Calculated by FEA and Analytical Methods

	Convective Frequency (Hz)	Impulsive Frequency (Hz)
FEA	0.346	22.298
Eurocode 8	0.401	N/A
Malhotra [5]	0.400	23.510

The summary of the fluid filled vessel sloshing height calculated by the finite element method at zero degrees around the circumference and by analytical expressions is shown in Table 7.6. The results of the finite element analysis and those calculated by both Malhotra [5] and the Eurocode 8 [25] are in excellent agreement with each other. It must be noted that the parameters used to calculate theoretical frequency and sloshing height using Malhotra [5] and Eurocode 8 [25] must first be converted to S.I. units. It must be further noted that sloshing heights for all three methods posted in Table 7.6 were calculated using the same ground acceleration of 0.522g, i.e., the spectral acceleration corresponding to a frequency of 0.346 Hz from IEEE-693-2005 response spectrum curve [29], regardless of the different natural frequencies given by the respective methods.

TABLE 7.6: Sloshing Heights Calculated by FEA and Analytical Methods for Fluid Filled Vessel

	Sloshing Height (in)
FEA	49.58
Eurocode 8	50.00
Malhotra [5]	59.52

The data given in Table 7.7 shows the FEA results for the first convective mode, combination of the first three convective modes, the first impulsive mode, the

combination of the first three impulsive modes, and finally, the combination of the first three convective and first three impulsive modes. It can again be concluded that the convective modes contribute toward sloshing height of the fluid, whereas the impulsive modes are mainly responsible for the stresses in the structure.

TABLE 7.7: FEA Results for Different Modes and Mode Combinations for Vessel

	Sloshing Height (in)	Stresses (psi)
First Convective Mode	48.29	334.92
Three Convective Modes Combined	49.46	339.68
First Impulsive Mode	0.071	1443
Three Impulsive Modes Combined	0.078	1486
Three Convective and Three Impulsive Modes Combined	49.58	1693

7.1.4 Comparison of Finite Element Results for Fluid Filled Tank and Fluid Filled Vessel

The fluid filled ground supported tank with flat heads as shown in Fig. 5.1 and the fluid filled elevated vessel with torospherical heads as shown in Fig 6.1 are of comparable size having a diameters of 20 ft. and 19 ft., respectively and comparable H/R ratio. The tank has a wall thickness of 0.500 in. whereas the vessel has a wall thickness of 0.625 in. The finite element analysis (dynamic analysis) results of the tank and vessel are given in Table 7.8 and table 7.9 for zero degrees and forty five degrees around the circumference, respectively. It may be noted by comparing results from Tables 7.8 and 7.9 that the sloshing height is a function of the circumferential position **θ**. Furthermore**,** the maximum sloshing height is at **θ=0°**, i.e., in the direction of the applied uniform lateral ground acceleration.

TABLE 7.8: FEA Results for Tank Versus Vessel at **θ=0°**

	Convective Frequency (Hz)	Impulsive Frequency (Hz)	Sloshing Height (in)	Stresses (psi)
Tank	0.3396	25.4216	50.90	1827
Vessel	0.3465	22.298	49.578	1825

TABLE 7.9: FEA Results for Tank Versus Vessel at **θ=45°**

	Convective Frequency (Hz)	Impulsive Frequency (Hz)	Sloshing Height (in)	Stresses (psi)
Tank	0.3396	25.4216	35.991	1736
Vessel	0.3465	22.298	35.017	1693

The von Mises stresses are also a function of circumferential angle, however, it must be remembered that von Mises stresses are the result of a non-linear combination of component stresses, which ultimately vary as a function of the circumferential position in the subject problems discussed herein. The fluid in the vessel vibrates at slightly higher frequencies (both convective and impulsive). This may be attributed to higher stiffness of vessel as its wall thickness is greater than that of the tank. Based upon the sloshing height results shown in Tables 7.8 and 7.9 herein and the published results of Antaal et al. [30], it can be observed that the torospherical head has little or no effect on the sloshing height as may also be observed for the tank's bottom flat head. Furthermore, the sloshing height is a function of diameter of the vessel and the applied convective acceleration. The lower stresses in the elevated vessel as compared to the ground supported tank can also be attributed to the greater wall and skirt thickness of the vessel as compared to the wall thickness of the tank.

CHAPTER 8: CONCLUSIONS

8.1 Conclusions

The seismic response method developed and discussed in the preceding paragraphs allows results to be obtained around the entire circumference of an axisymmetric model as is available in a full 3-D analysis, at much less costs. The benefits achieved through the use of the axisymmetric geometry reduced the total engineering effort and cost of modeling and analyzing a three dimension problem. Furthermore, the results of an axisymmetric analysis are better suited for a cylindrical geometry than a full 3-D analysis due to the use and availability of rectangular fluid elements for the entire geometric mesh, which in and of itself, is impossible in the case of a full 3-D model. This fact alone allows a more dense mesh to be utilized in the present method, which again may not be possible or certainly not practicable in a 3-D model.

The utilization of axisymmetric harmonic elements clearly takes full advantage of the ability to apply lateral accelerations associated with the single point spectrum analysis. The integrity of the seismic response analysis is maintained in combination with keeping the physical model size consistent with those of similar axisymmetric models. The results of the sloshing analysis utilized the methodology developed by the author and described in this dissertation were verified by the published analysis results and results of others as described in the open literature [5, 25]. In addition, based upon the calculated sloshing height from the tank with flat heads and vessel with torospherical

heads discussed herein, the torospherical head has little or no effect on the sloshing height as may also be observed for the tank's bottom flat head.

The techniques utilized in the Fourier series representations of the applied loads and employed in the harmonic axisymmetric elements for both the fluid and structure are well proven. The methodology can be utilized in more complex assemblies of axisymmetric structures whereby a requisite seismic response spectrum must be applied during the design and analysis phase of a project.

8.2 Recommendations for Further Study

While the finite element analysis software package utilized for the work described herein was one of the major commercial programs currently available, the technique could be utilized on any software package known to the author. Additional study utilizing other FEA packages could be conducted with the methodology incorporated as available options (at best) and simple macros (at worst). Understanding of the robust features available through the Fourier series representation of any of the loads or displacements opens the realm of further study to any application whereby the effects of an asymmetric parameter may be studied on an economical axisymmetric geometry. This would hold true whether that parameter is seismic or wind related or be another asymmetric application.

An additional computational fluid dynamics model of subject problem could be used to study the fluid-structure interactions while taking advantage of axisymmetric geometry of the cylindrical containers and the response results from computational fluid dynamics analysis can be compared with the methodology described herein.

REFERENCES

1. Malhotra, P. K., 2006, "Earthquake Induced Sloshing in Tanks with Insufficient Freeboard," *Structural Engineering International*, International Association for Bridge and Structural Engineering, Switzerland, pp. 222-225.

2. Haroun, M. A., Bhatia, H. A., and Zeiny, A., 1997, "Characterization of Observed Uplift and Buckling of an Unanchored Tank During the Northridge Earthquake," The Northridge Earthquake Research Conference, Los Angeles, CA.

3. Housner, G. W., 1963, "The Dynamic Behavior of Water Tanks," *Bulletin of the Seismological Society of America*, **53**, pp. 381-387.

4. Haroun, M. A., and Housner, G. W., 1981, "Earthquake Response of Deformable Liquid Storage Tanks," *Journal of Applied Mechanics*, **48**(2), ASME, New York, pp. 411-417.

5. Malhotra, P. K., Wenk, T., and Wieland M., 2000, "Simple Procedure for Seismic Analysis of Liquid Storage Tanks," *Structural Engineering International*, International Association for Bridge and Structural Engineering, Switzerland, pp. 197-201.

6. Fischer, F. D., and Rammerstorfer, F. G., 1999, "A Refined Analysis of Sloshing Effects in Seismically Excited Tanks, " *International Journal of Pressure Vessels and Piping*, **76**(10), Elsevier Science Ltd., London, pp. 693-709.

7. Shrimali M.K., Jangid R.S., 2003, "Earthquake Response of Isolated Elevated Liquid Storage Steel Tanks," *Journal of Constructional Steel Research,* **59** (10), Elsevier Science Ltd., London, pp. 1267-1288.

8. Livaoglu R., Dogangun A., 2006, "Simplified Seismic Analysis Procedures for Elevated Tanks Considering Fluid-Structure-Soil Interaction," *Journal of Fluids and Structures,* **22** (3), pp. 421–439.

9. Livaoglu R., Dogangun A., 2007, "Effect of Foundation Embedment on Seismic Behavior of Elevated Tanks Considering Fluid–Structure-Soil Interaction," *Journal of Soil Dynamics and Earthquake Engineering*, **27** (9), pp. 855–863.

10. Aquelet, N., Souli, M., Gabrys, J., and Olovson, L., 2003, "A New ALE Formulation for Sloshing Analysis," *Structural Engineering and Mechanics*, **16**(4), Techno Press, Korea, pp. 1-18.

11. Babu, S. S., and Bhattacharyya, S. K., 1996, "Finite Element Analysis of Fluid-Structure Interaction Effect on Liquid Retaining Structures Due to Sloshing," *Computers and Structures* , **59**(6), Elsevier Science Ltd., London, pp. 1165-1171.

12. Cho, J. R., Song, J. M., and Lee, J. K., 2001, "Finite Element Techniques for the Free-Vibration and Seismic Analysis of Liquid-Storage Tanks," *Finite Elements in Analysis and Design*, **37**(6-7), Elsevier Science Ltd., London, pp. 467-483.

13. Perov, S., Altstadt, E. and Werner, M., 2000, "Vibration Analysis of the Pressure Vessel Internals of WWER-1000 Type Reactors With Consideration of Fluid-Structure Interaction," *Annals of Nuclear Energy*, **27**(16), Elsevier Science Ltd., London, pp. 1441-1457.

14. Barron, R., and Chng, S. W Roy., 1989, "Dynamic Analysis and Measurement of Sloshing of Fluid in Containers," *Journal of Dynamic Systems, Measurement, and Control*, **111**(1), ASME, New York, pp. 83-90.

15. Austin, S. C., and Rhee, H., 1999, "A Method for Including Fluid Structure Interaction in an ANSYS Response Spectrum Seismic Analysis," *Transactions of the 15th International Conference on Structural Mechanics in Reactor Technology (SMiRT-15),* **VII**, Seoul, Korea, pp. 71-78.

16. Zeiny, A., 2003, "Factors Affecting the Nonlinear Seismic Response of Unanchored Tanks," *16th ASCE Engineering Mechanics Conference,* ASCE, New York.

17. Haroun, M. A., and Zeiny, A., 1996, "A Computational Technique for the Nonlinear Dynamic Analysis of Unanchored Liquid Storage Tanks," *Proceedings of the Third Asian-Pacific Conference on Computational Mechanics,* Seoul, Korea, pp. 1007-1012.

18. Haroun, M. A., and Zeiny, A., "Simulation of Dynamic Behavior of Unanchored Tanks," *Proceedings of the 13th International Conference on Structural Mechanics in Reactor Technology,* Porto Alegre, Brazil, pp. 341-346.

19. Hamdan, F.H., 2000, "Seismic Behavior of Cylindrical Steel Liquid Storage Tanks," *Journal of Constructional Steel Research*, **53**(3), Elsevier Science Ltd., London, pp. 307-333.

20. Jin, B., Chung, C., Jeon, S. J., Kim, J. H., Kim, K. H. Yoo, J.W., and Kim, H., 1996, "Preliminary Earthquake Response Analysis of 200,000kl Large Capacity Above-Ground LNG Storage Tank for the Basic Design Section," *Proceedings of the Third Asian-Pacific Conference on Computational Mechanic*, Seoul, Korea.

21. Papaprokopiou, D., and Karamanos, S. A., 2008, "Finite Element Analysis of Sloshing in Axisymmetric Vessels," PVP2008-61029, *ASME 2008 Pressure Vessels and Piping Division Conference*, ASME, New York.

22. Yun, C., Chang, S., and Watanabe, E., 2001, "Fluid-Structure-Soil Interaction Analysis of Cylindrical Liquid Storage Structures," *4th EqTAP Multilateral Workshop Proceedings*, Kamakura, Japan.

23. Jeong, K. H., 2003, "Free Vibration of Two Identical Circular Plates Coupled with Bounded Fluid," *Journal of Sound and Vibration*, **260**(4), Elsevier Science Ltd., London, pp. 653-670.

24. Antaal, B. S., Hari, Y., and Williams, D. K., 2010, "Implementation of Fourier Series in the Seismic Response Spectrum Analysis of Ground Supported Tanks," POWER2010-27257, *ASME 2010 Power Conference*, ASME, New York.

25. European Committee for Standardization, 1993, *Eurocode 8 Earthquake*, "Design of Structures for Earthquake Resistance, Part 4: Tanks, Silos and Pipelines", Brussels, Belgium.

26. Timoshenko, S.P., Weaver W., Jr., Young, D.H., 1990, *Vibration Problems in Engineering*, John Wiley & Sons, New York.

27. ANSYS, Inc., 2007, *Release 11.0 Documentation for ANSYS*, Canonsburg, PA.

28. Guyan, R. J., 1965, "Reduction of Stiffness and Mass Matrices," *AIAA Journal*, **3**(2), Reston, VA, p. 380.

29. IEEE, 2005, "IEEE Recommended Practice for Seismic Design of Substations," *IEEE-693-2005*, Institute of Electrical and Electronics Engineers, New York.

30. Antaal, B. S., Hari, Y., and Williams, D. K., 2010, "The Application of Harmonic Finite Elements in the Seismic Response Spectrum Analysis of a Skirt Supported Vessel," PVP2010-25886, *ASME 2010 Pressure Vessels and Piping Division Conference*, ASME, New York.